DECREASED JMJD3 EXPRESSION IN MESENCHYMAL STEM CELLS CONTRIBUTES TO LONG-TERM SUPPRESSION OF OSTEOBLAST DIFFERENTIATION IN MULTIPLE MYELOMA

Wei Zhao

Submitted to the faculty of the University Graduate School
in partial fulfillment of the requirements
for the degree
Doctor of Philosophy
in the Department of Biochemistry and Molecular Biology
Indiana University
June 2018

Accepted by the Graduate Faculty, Indiana University, in partial
fulfillment of the requirements for the degree of Doctor of Philosophy

_____
G. David Roodman, M.D., Ph.D., Chair

_____
Hal E. Broxmeyer, Ph.D.

Doctoral Committee

_____
Mervin C. Yoder, M.D.

April 5, 2018

_____
D. Wade Clapp, M.D.

_____
Theresa Guise, M.D.

ACKNOWLEDGEMENT

First and foremost, I would like to thank my mentor Dr. G. David Roodman for the undivided support throughout the pursuit of my Ph.D. Although I had initial difficulties adjusting to my studies in the U.S., I approached him with worries of getting rejected, yet he believed in me and allowed me to join the lab as the only student. Further, he not only fully respected my research interest in epigenetic regulation, but also gathered all resources to help me develop my interest into an independent project. He challenged me with tough scientific questions and instilled in me the ability to think critically and independently, which I came to realize is crucial for being successful as a researcher as well as a person. He also unconditionally supported my career decision to become a doctor in U.S. after my graduation. For all his unparalleled dedication as a mentor, I feel grateful forever.

I would also like to thank my committee members Dr. Hal E. Broxmeyer, Dr. Mervin C. Yoder, Dr. D. Wade Clapp, Dr. Theresa Guise and Dr. Rebecca Silbermann. They provided invaluable insights to steer my project around potential problems and inspired me to move forward strongly in the face of difficulties. Despite that they are fully occupied as the leaders in biomedical research at Indiana University, they more than often changed their own schedules to better support me. I would like to give my special gratitude to Dr. Rebecca Silbermann for her kindness and resourcefulness. She communicates with me like a close friend, and offers help both scientifically and emotionally. She resigned from my committee in my fifth year of Ph.D. research due to

her move to the University of Oregon, but she remains an important advisor in my entire journey as a graduate student.

Finally, I would like to thank all the staff from the Graduate Division for protecting their students against any unfair treatment and establishing a nurturing environment for future scientists. More importantly, I want to thank my wife Pin Li, who has always been a great and patient listener to my struggles and a firm supporter of the decisions I've made. She witnesses my ups and downs. It's highly doubtful that I could make this far without her trust and sacrifice.

Wei Zhao

DECREASED JMJD3 EXPRESSION IN MESENCHYMAL STEM CELLS CONTRIBUTES TO LONG-TERM SUPPRESSION OF OSTEOBLAST DIFFERENTIATION IN MULTIPLE MYELOMA

Multiple myeloma (MM) is the most frequent cancer to involve the skeleton, with over 80% of myeloma patients developing lytic bone disease (MMBD). Importantly, MM-associated bone lesions rarely heal even when patients are in complete remission. Bone marrow stromal cells (BMSCs) isolated from MM patients have a distinct genetic profile and an impaired osteoblast (OB) differentiation capacity when compared to BMSCs from healthy donors. Utilizing an *in vivo* model of MMBD and patient samples, we showed that BMSCs from tumor-bearing bones failed to differentiate into OBs weeks after removal of MM cells. Both Runx2 and Osterix, the master transcription factors for OB differentiation, remained suppressed in these BMSCs. However, the molecular mechanisms for MM-induced long-term OB suppression are poorly understood.

We characterized both Runx2 and Osterix promoters in murine pre-osteoblast MC4 cells by chromatin immunoprecipitation (ChIP). The transcriptional start sites (TSSs) of Runx2 and Osterix in untreated MC4 cells were co-occupied by transcriptionally active histone 3 lysine 4 tri-methylation (H3K4me3) and transcriptionally repressive histone 3 lysine 27 tri-methylation (H3K27me3), termed the “bivalent domain”. These bivalent domains became transcriptionally silent with increasing H3K27me3 levels when MC4 cells were co-cultured with MM cells or treated with TNF-α, an inflammatory cytokine increased in MM bone marrow microenvironment. The increasing H3K27me3 levels

induced by MM cells or TNF-α were associated with the downregulation of the H3K27 demethylase JMJD3 in MC4 cells and murine BMSCs. Knockdown of JMJD3 in MC4 cells was sufficient to inhibit OB differentiation. Further, ectopic overexpression of JMJD3 in MC4 cells partially rescued the suppression of osteoblast differentiation induced by TNF-α. We also found that pre-incubation of MC4 cells with the NF-κB inhibitor quinazoline (QNZ) before TNF-α treatment prevented the downregulation of JMJD3. In agreement with our *in vitro* findings, BMSCs from MM patients had persistently decreased JMJD3 expression compared to healthy BMSCs.

Our findings together demonstrate that decreased JMJD3 expression in BMSCs contributes to the long-term OB suppression in MMBD by remodeling histone landscapes at the Runx2 and Osterix TSSs. Thus, developing strategies to restore JMJD3 expression in BMSCs should increase bone formation and possibly decrease tumor burden in MM.

G. David Roodman, M.D., Ph.D., Chair

TABLE OF CONTENTS

LIST OF FIGURES

LIST OF ABBREVIATIONS

α-MEM:	α-modified Eagle medium
APRIL:	A proliferation-inducing ligand
ATCC:	American Type Culture Collection
BAFF:	B-cell activating factor
BMSC:	Bone marrow stromal cells
ChIP:	Chromatin immunoprecipitation
CMV:	Cytomegalovirus
DD:	Death domain
DMEM:	Dulbecco's modified Eagle's Minimum Essential Medium
DXA:	Dual-energy X-ray absorptiometry
EHMT2:	Euchromatin histone-lysine N-methyltransferase 2
ESC:	Embryonic stem cell
EV:	Empty pcDNA3.1 vector
FDA:	US Food and Drug Administration
Gfi1:	Growth factor independence 1
Gfi1 o/e:	Flag-tagged Gfi1-overexpressing pcDNA3.1
GFP:	Green fluorescence protein
GLP:	G9a-like protein
GPS 3.0:	Group-based Prediction System 3.0
H3K4me3:	Histone 3 lysine 4 tri-methylation
H3K9me3:	Histone 3 lysine 9 tri-methylation
H3K27me3:	Histone 3 lysine 27 tri-methylation
HAT:	Histone acetyltransferase
HDAC:	Histone deacetylase
HP1:	Heterochromatin protein 1
HSC:	Hematopoietic stem cell
IC50:	Half-maximum inhibitory concentration
IGF-1:	Insulin-like growth factor I
IHC:	Immunohistochemistry
IMDM:	Iscove’s Modified Dulbecco’s Medium
iPSC:	Induced pluripotent stem cell
LTR:	Long-terminal repeat
MC4:	MC3T3-E1 subclone 4
MC14:	MC3T3-E1 subclone 14
MCS:	Multiple cloning site
MDS:	Myelodysplastic syndrome
MEF:	Mouse embryonic fibroblast
MM:	Multiple myeloma
MMBD:	Multiple myeloma bone disease

MM-BMSC:	BMSCs isolated from MM patients
MS:	Mass spectrometry
mTOR:	Mammalian target of rapamycin
MTT:	3-(4, 5-Dimethyl-2-thiazolyl)-2, 5-diphenyl-2H-tetrazolium Bromide
ND-BMSC:	BMSCs isolated from normal donors
NFATc1:	Nuclear factor of activated T cells
NO66:	Nuclear protein 66
OAF:	Osteoclastogenic activating factors
OB:	Osteoblast
ONG:	Osteonecrosis of the jaw
QNZ:	Quinazoline
ORR:	Overall response rate
OPG:	Osteoprotegerin
ORF:	Open reading frame
PcG:	Polycomb group
PRC1:	Polycomb repressive complex 1
PRC2:	Polycomb repressive complex 2
Prx1:	Paired related homeobox protein
PTM:	Posttranslational modification
Pol II:	RNA polymerase II
R^2:	Coefficient of determination
RANK:	Receptor activator of NF-κB
RANKL:	Receptor activator of NF-κB ligand
RBP2:	Retinoblastoma binding protein 2
RIPA:	Radioimmunoprecipitation assay
RLU:	Relative luciferase unit
SCN:	Severe congenital neutropenia
SODD:	Silencer of death domain
TBE:	Tris-borate-EDTA
TBST:	Tris-buffered saline with Tween 20
TK:	Thymidine kinase
TNF-R1:	TNF receptor type 1
TNF-R2:	TNF receptor type 2
TRADD:	Receptor type 1-associated death domain protein
trxG:	Trithorax group
TSS:	Transcriptional start site
vControl:	Empty plasmid
vJMJD3:	JMJD3-overexpressing plasmid

CHAPTER 1

INTRODUCTION

1.1 Current Understanding of MMBD

MM is the most common cancer that involves skeleton. 70% of newly diagnosed MM patients are found to have bone lesions, which eventually affect an additional 20% of patients as the disease progresses[1]. Symptomatic patients frequently complain of debilitating bone pain in the back or chest, although pain in extremities is also seen. Bone pain can be triggered by any movement and is characteristically absent during sleep. Pathologic fractures can occur in up to 60% of MM patients with no apparent trauma history and cause loss of vertebral height if vertebrae are involved or neurovascular damage if long bones are involved[2]. Also, as the largest calcium reservoir in the body, bone destruction can increase blood calcium levels beyond physiological range. MM patients with hypercalcemia suffer from anorexia, nausea, vomiting, confusion, fatigue, constipation, renal stones, depression and/or polyuria. Thus, MMBD severely impairs the patients' quality of life and more importantly increases the mortality rate by 20%[3].

Bone is maintained by constantly undergoing formation and resorption, a lifelong process called bone remodeling[4-6]. In adults, 10% of skeleton is replaced each year. Bone remodeling is necessary to repair accumulating micro-damage and to transform the woven bone into lamellar structures during the fracture healing process. At the microscopic level, bone remodeling is mediated by the coupled function of two types of bone cells: the osteoblast that produces bone and the osteoclast that resorbs bone. Bone formation by osteoblasts and resorption by osteoclasts are delicately

balanced by cytokines and cell-to-cell interactions so that no more or less bone is formed[7]. One of the mechanisms by which osteoblasts and osteoclasts communicate with each other is the bidirectional signaling between the surface receptor EphB4 on osteoblasts and its membrane-bound ligand Ephrin B2 on osteoclasts. The forward signaling following EphB4 activation promotes osteoblast differentiation, and the reverse signaling following Ephrin B2 activation simultaneously suppresses osteoclast differentiation[8,9]. Another established mechanism involves expression of receptor activator of NF-κB ligand (RANKL) and its soluble decoy receptor osteoprotegerin (OPG) by BMSCs and osteoblasts. Upon binding to receptor activator NF-κB (RANK) on osteoclast precursors, RANKL potently stimulates osteoclast differentiation, activation and survival by activating NF-κB, MAPKs and calcineurin/nuclear factor of activated T cells (NFATc1), the master transcription factor of osteoclastogenesis[10,11]. Neutralizing RANKL with the monoclonal antibody Denosumab effectively blocks osteoclastogenesis[12]. Similar to Denosumab, OPG, an endogenous RANKL decoy receptor, also plays a major role in negatively regulating osteoclasts[13]. These results demonstrate that BMSCs and osteoblasts either promote or inhibit osteoclast differentiation depending on the RANKL/OPG ratio, which varies in response to a variety of hormones, such as vitamin D3[14], PTH[15], and prostaglandins[16]. The balanced coupling between osteoblasts and osteoclasts, however, can be severely disturbed in inflammatory and neoplastic bone diseases.

MM has unique features compared to other cancers frequently metastasizing to bones, such as breast and prostate cancer. Like those cancers, myeloma activates

osteoclasts by directly secreting osteoclastogenic activating factors (OAFs) and inducing other cells in bone marrow microenvironment to secrete OAFs (Figure 1). Cytokines identified as OAFs in MM include RANKL, TNF-α, MIP-1α, IL1, IL-6[17], Activin A[18] and Annexin II[19]. RANKL as discussed already is a critical factor for osteoclast differentiation, activation and survival. TNF-α synergizes with RANKL to accelerate osteoclast differentiation mainly by increasing the expression of downstream mediators c-Src, TRAF2, TRAF6, and MEKK1[20]. Also, TNF-α increases RANKL expression in BMSCs and osteoblasts. Although elevated quantities of TNF-α have been reported in serum and bone marrow of MM patients, it's still unclear whether myeloma cells themselves make a major contribution to the elevated TNF-α levels[21]. MIP-1α, produced by myeloma cells, belongs to the CC chemokine family and plays an important role in attracting osteoclast precursors and differentiating them into mature osteoclasts independent of RANKL[22-25]. Serum levels of MIP-1α correlate with the severity of bone lesions and survival of MM patients[26]. IL-1β is another important factor that regulates different stages of osteoclast differentiation. Since osteoclast precursors don't initially express its receptor IL-1R1, the promoting effects of IL-1β depends on RANK/RANKL signaling which creates a permissive environment by upregulating IL-1R1 on osteoclast precursors[27]. Importantly, the overactive osteoclasts destroy bones, releasing growth factors buried in the bone osteoid matrix to support myeloma growth. The reciprocity between MM cell-induced osteoclast formation and osteoclasts releasing growth factors from bone to increase MM cell growth is known as "vicious cycle" and underlines the importance of controlling MMBD to reduce tumor burden.

Unlike other cancers, myeloma markedly suppresses osteoblast differentiation and functionality by producing or inducing osteoblast inhibitory factors, including DKK1, sclerostin, TNF-α, IL-1β and IL-7, or by direct cell adhesion with BMSCs which activates NF-κB and p38 signaling in BMSCs (Figure 1). Wnts are soluble glycoproteins in bone marrow microenvironment that play a pivotal role in osteoblastogenesis by engaging their membrane-bound receptor complexes Frizzled/LRP5/6[28-30]. Of three well characterized pathways activated by Wnts, the canonical pathway involving β-catanin stabilization and transcriptional activation is responsible for most of its effects on osteoblasts[31]. Derangement of Wnt signaling has been reported to result in skeletal abnormality. For example, a loss of function mutation of LRP5 causes osteoporosis-pseudoglioma syndrome. Patients with this syndrome suffer from vision problems and osteoporotic fractures with an early onset[32]. DKK1 and sclerostin are natural antagonists of Wnt signaling that sequester LRP5/6. Elevated production of DKK1 in myeloma cells, as shown by immunohistochemistry (IHC) of bone marrow in MM patients, correlates with the presence of bone lesions[33]. In further support of DKK1's involvement in MMBD, treating SCID mice engrafted with primary MM cells with DKK1 neutralizing antibodies prevents progressive bone loss[34]. Similar to DKK1, Sclerostin which is predominantly produced by mature osteocytes also contributes to the pathogenesis of MMBD[35-37]. Secretion of Sclerostin from osteocytes is greatly enhanced by contact with myeloma cells[38]. Blockade of sclerostin by either genetic deletion or neutralizing antibodies in mouse models of MMBD inhibits the development of lytic lesions and increases circulating levels of osteoblast activity markers[39]. TNF-α is another well recognized

inhibitor of osteoblast differentiation through mechanisms independent of disrupting Wnt signaling. Upon binding to its receptor TNFR1, TNF-α triggers trimerization of the receptor, subsequently recruits tumor necrosis factor receptor type 1-associated death domain protein (TRADD) as the initiating event, and eventually culminates in the activation of NF-κB, JNK, p38, ERK, and caspases. Nevertheless, the molecular map of TNF-α signaling hasn't been conclusively defined[40]. It has been reported that inhibition of NF-κB or JNK activation in osteoblast precursors partially restores the suppression of osteoblast differentiation by TNF-α[41,42]. Regardless of the individual signaling pathways involved, TNF-α rapidly downregulates the expression of both Runx2 and Osterix in osteoblast precursors, which are the master transcription factors indispensable for normal osteoblastogenesis. Of note, MM patients have higher serum levels of TNF-α compared to normal donors.

Current pharmacologic treatments for MMBD target the elevated activity of osteoclasts in patients. Bisphosphonate therapy is the mainstay for treating MMBD[43-45]. Their anti-catabolic effects result from enhanced osteoclast apoptosis partly due to the inhibition of the mevalonate pathway[46]. Bisphosphonate therapy may also have direct cytotoxic effects on tumor cells and alter tumor-stromal cell interactions[47]. However, bisphosphonate therapy only decreases skeletal-related events by 50% and is associated with a low incidence of serious adverse effects, including renal impairment and osteonecrosis of the jaw (ONJ)[48]. Another drug option currently under investigation in MM is denosumab[49], which binds receptor activator of nuclear factor kappa-B ligand (RANKL) with high affinity and disrupts RANKL-RANK interaction on osteoclasts,

preventing their maturation. Denosumab is also associated with ONJ and can also result in increased infections because of RANKL's role in the immune system[50,51]. In addition to unfavorable side effects of anti-catabolic therapy, effective anabolic agents targeting suppressed osteoblasts are generally lacking. Growing knowledge of the molecular mechanisms responsible for MMBD should provide more treatment options hopefully in the near future. As a result, targeting MMBD using a combination of anabolic and anticatabolic medication should also improve MM patient 5-year survival rates.

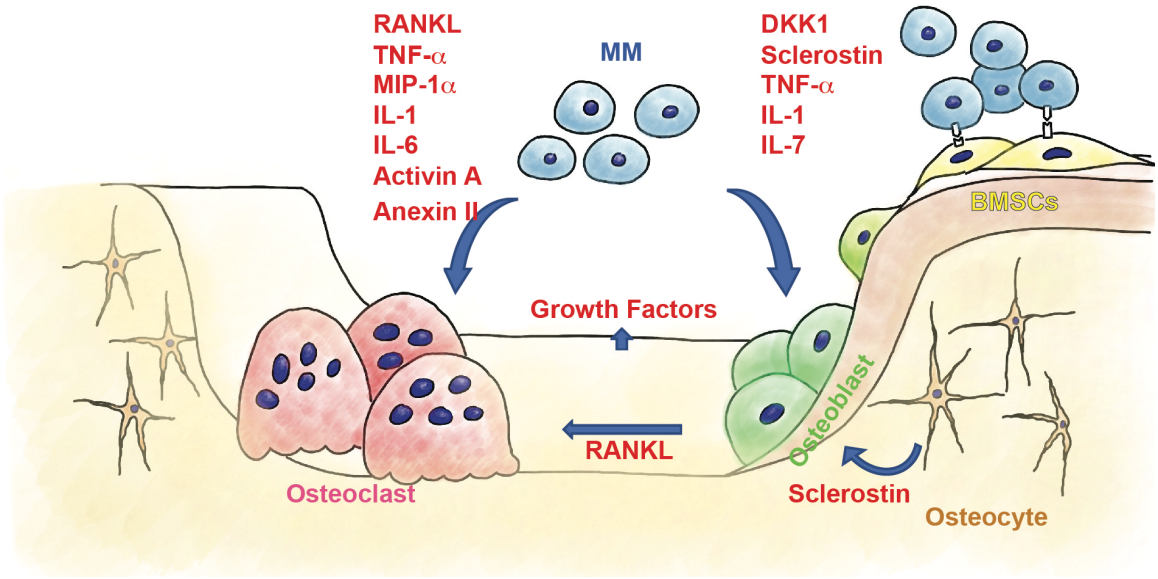

Figure 1: Mechanisms of MMBD

Myeloma cells disrupt the delicate equilibrium of osteoblast activity and osteoclast activity by direct cell-cell interaction and inducing a variety of cytokines. The OAFs, including RANKL, TNF-α, MIP-1α, IL-1, IL-6, Activin A, Anexin II and others, stimulate osteoclast activity, whereas the osteoblast inhibitory factors, including DKK1, Sclerostin, TNF-α, IL-1, IL-7 and others, suppress osteoblast activity. Thus, bone resorption by osteoclasts is favored over bone formation by osteoblasts, resulting in lytic bone lesions in MM patients.

1.2 The Role of Gfi1 in Mediating Persistent Suppression of Osteoblast Differentiation in MM

Bone lesions in MM patients persist even when patients are in complete remission. Several independent studies have shown that BMSCs isolated from MM patients (MM-BMSCs) are selectively refractory to potent osteogenic stimuli *in vitro* in the absence of MM cells compared to BMSCs from normal donors (ND-BMSCs), while their capacities to differentiate into adipocytes and chondrocytes are not affected[52-55]. Those studies used the plastic adhesion technique to enrich BMSCs, which have to be continuously cultured for more than a month until other cell populations die out. Considering the time required to obtain homogenous BMSCs, the defects present in MM-BMSCs that block their differentiation into osteoblasts are not transient in nature. Further, MM-BMSCs have been reported to show other distinct phenotypes from their healthy counterparts[56-60]. Myeloma cells induce MM-BMSCs to secrete increased levels of IL-1β, IL-3, IL-6, IL-10, BAFF, GDF15, TNF-α, TGFβ1, DKK1, RANKL and AREG. These cytokines create a permissive niche for myeloma growth as well as increase bone destruction. In addition, MM-BMSCs had lower expression of Runx2, Osterix and TAZ than ND-BMSCs[61,62]. Loss of these master transcription factors of osteoblast differentiation may explain the defective osteoblastogenesis in MM-BMSCs. However, it is unclear how MM-BMSCs maintain their persistent inability to differentiate into osteoblasts. Garayoa and colleagues found several non-recurrent chromosomal gains and losses (>1 Mb size) in MM-BMSCs, which hardly explain the anomaly shared by MM-

BMSCs[63]. This knowledge gap encouraged us to investigate the underlying molecular mechanism(s) mediating long-term suppression of osteoblast differentiation in MM.

In 2011, Dr. D'Souza from our group identified the transcription factor, growth factor independence 1 (Gfi1), as a potential target involved in the protracted inability of MM-BMSCs to differentiate into functional osteoblasts[64]. The human Gfi1 gene encodes a 422 amino-acid protein composed of N-terminal SNAG domain, an intermediate domain and C-terminal zinc finger domain. While both the SNAG domain and intermediate domain are responsible for protein-protein interaction, the zinc finger domain binds to the consensus DNA sequence TAAATCAC(A/T)GCA[65,66]. Being a transcriptional repressor, Gfi1 recruits euchromatin histone-lysine N-methyltransferase 2 (EHMT2) to specific genomic region, which mono- and dimethylates H3K9[67]. The newly created H3K9me marks lead to transformation of transcriptionally active euchromatin to transcriptionally silent heterochromatin by interacting with heterochromatin protein 1 (HP1)[68]. In addition to its role in H3K9 modification, EHMT2 weakly methylates unmodified H3K27 into H3K27me[69]. This triggers the initial events that progressively lead to epigenetic silencing with subsequent participation of the Polycomb Repressive Complex 2 (PRC2). Other identified Gfi1 binding partners include histone deacetylases (HDACs) that reduce the accessibility of the transcriptional machinery[67], the adaptor protein Ajuba that assembles Gfi1 into protein complexes[67,70] and p53 that dictates cell survival. In line with its interaction with multiple biologically important proteins, Gfi1 plays a crucial role in regulating hematopoietic stem cell (HSC) quiescence[71,72], and B and T lymphocyte differentiation[73-75]. Mutations in Gfi1 cause autosomal dominant

severe congenital neutropenia (SCN), which subjects affected patients to recurrent infection[76,77]. However, no group had ever attempted to investigate the biological function of Gfi1 in BMSCs and osteoblasts until Dr. D' Souza.

Dr. D'Souza first used an *in vivo* model of MMBD where mice were injected intratibially with saline as control or the murine myeloma cell line 5TGM1 cells that stably expressed thymidine kinase (TK) for negative selection and green fluorescence protein (GFP) for positive selection. Progressive bone destruction occurs in this model over the course of 4 weeks. Compared to BMSCs isolated from saline-injected tibiae, BMSCs from MM-bearing tibiae showed persistent defects in osteoblast differentiation in absence of myeloma cells for more than one month, as proven by lack of induction of osteoblast marker genes and impaired Alizarin Red staining that reflects osteoblast mineralization activity by osteoblast differentiating factors. BMSCs isolated from bone marrow of mouse models and MM patients had decreased osteoblast differentiation with increased expression of Gfi1. To further delineate the molecular mechanisms, a plasmid encoding wild-type mouse Gfi1 was co-transfected with the luciferase reporter plasmid regulated by mouse Runx2 promoter (-992/+111) into osteoblast precursor MC4 cells. The relative luciferase unit (RLU) was inhibited dose-dependently by overexpression of wild-type Gfi1, which was also observed by overexpression of mutated Gfi1 (N382S) that was thought to abolish DNA binding, suggesting a novel binding site of Gfi1 on the Runx2 promoter. Importantly, knockdown of Gfi1 in BMSCs from MM patients restored their osteoblast differentiation capacity, implicating Gfi1 in establishing and maintaining the defective osteoblastogenesis in MM.

Building upon Dr. D'Souza's work, our collaborator Dr. Adamik found significantly decreased levels of transcriptionally active histone marks H3K9ac and H3K4me3, increased levels of transcriptionally repressive histone mark H3K27me3, and unproductive RNA polymerase II (Pol II) elongation on the Runx2 promoter in MC4 cells exposed to myeloma cells[78]. He localized the -37/-7 region on the Runx2 promoter as the predominant binding site of Gfi1. Binding of Gfi1 to this region was sufficient to recruit HDAC1 and EZH2, the H3K27 methyltransferase in PRC2. Consistently, stable knockdown of Gfi1 in MC4 cells effectively prevented the aggregation of those histone modifiers at -37/-7 region and, more importantly, helped MC4 cells escape the prolonged epigenetic silencing of Runx2 expression induced by myeloma cells. Similarly, antagonizing Gfi1 using specific inhibitors against HDAC1 (MC1294) and EZH2 (GSK126) restored Runx2 gene expression in MC4 cells as well as BMSCs from MM patients, thereby reversing MM-mediated suppression of osteoblast differentiation. Further supporting Gfi1's role in the pathogenesis of MMBD, Dr. Silbermann in our group, using a novel inhibitor XRK3F2 that targeted the ZZ domain of sequestosome 1/p62 which serves as a platform for formation of signaling complexes, found that p62-ZZ domain mediated Gfi1 induction in BMSCs exposed to myeloma cells[79]. MicroCT analysis showed that XRK3F2 treatment induced dramatic cortical bone formation in MM-bearing tibiae in mouse models of MMBD described above in this chapter. These results collectively demonstrate that epigenetic alteration rather than genetic mutation in MM-BMSCs could mediate the protracted suppression of osteoblast differentiation in MM. They further suggested that targeting histone modifiers could provide new therapeutic

options to treat MMBD, although there could be a potential “off-target” effects with these treatments.

1.3 “Bivalent Domains” and Epigenetic Memory

Runx2 and Osterix are the master transcription factors that regulate osteoblast differentiation. Knockout of either Runx2[80] or Osterix[81] in mice leads to a complete loss of both endochondral and intramembranous ossification. They, however, are not the only regulators. It’s been suggested that osteoblast differentiation also requires concomitant epigenetic remodeling of chromatin landscapes. Histones are repeating protein units that organize eukaryotic DNA. Their N-terminal tails are subject to distinct modifications, including methylation, acetylation, phosphorylation, ubiquitination and sumoylation, which actively control gene transcription by either directly changing the interaction of DNA with nucleosomes or recruiting “reader” proteins to modulate the accessibility of transcription factors to genomes[82]. Histone acetylation catalyzed by histone acetyltransferases (HATs), for example, neutralizes the positive charge of lysine residues, thereby relaxing the interaction between histones and negatively charged DNA[83]. This epigenetic change provides an easier access of transcription machinery to the promoter region of associated genes and greatly enhances transcription without altering genetic information. Conversely, histone deacetylation catalyzed by histone deacetylases (HDACs) shuts down gene transcription[84]. Unlike histone acetylation, other histone modifications that don’t cause net change in charge also affect gene expression by recruiting or repelling “reader proteins” in a histone- and sequence-specific manner. The chromodomain of heterochromatin protein 1 (HP1) recognizes trimethyl-histone 3 lysine 9 (H3K9me3) marks via aromatic cage pockets and compacts transcriptionally

active euchromatin into transcriptionally silent heterochromatin[85]. Other protein domains that bind histone modifications include Tudor, PWWP, PHD fingers, BAH, and ADD[86]. Interestingly, different combination of adjacent or distant histone modifications preferentially recruits certain reader proteins that require complex interaction with histone tails. Therefore, studying multiple histone modifications instead of focusing on one should provide more insights into the epigenetic landscape.

The long-lasting regulation of histone modifications on gene expression relies on their inheritability across generations, although a certain degree of plasticity is allowed. Current models suggest that each daughter cell randomly inherits parental histones, which subsequently act as a template to spread the same post-transcriptional modification pattern to neighboring native histones[82,87]. Recycling, splitting and redistributing parental histones are facilitated by histone chaperones accumulated at the replication fork[88-92]. This model works flawlessly on long stretches of nucleosomes carrying the same marks. However, the epigenetic information may be accidentally lost if certain histone modifications exist only in a few nucleosomes. The specific histone modification marks that fit into this model have to meet two conditions. First, this histone modification is relatively stable to merit its role in “epigenetic memory”. The histone modifications that are easily erased in daughter cells don’t present a consistent inheritance pattern. A number of studies have shown that histone methylation has a significantly longer half-life compared to histone acetylation and phosphorylation, indicating the capacity of histone methylation to pass on parental epigenetic information in a noise-resistant manner. In contrast, histone acetylation and

phosphorylation are short-lived and thus not strictly viewed as true epigenetic marks[93]. Second, this histone modification has the ability to propagate to adjacent unmodified histones by directly and indirectly recruiting histone modifiers that write the same type of histone modification. As a well-studied example, H3K27me3 marks attract EED, which is one of the core components of Polycomb repressive complex 2 (PRC2) responsible for H3K27 trimethylation[94]. Considering the stability and self-enforcement of histone methylation, we investigated the effects of multiple histone methylation on osteoblast differentiation in MM patients as well as normal donors.

The "Bivalent domain" discovered by Bernstein et al. in 2006 is a region on the genome harboring both the transcriptionally active H3K4me3 marks and the transcriptionally repressive H3K27 marks[95]. Although the opposing functions of H3K4me3 and H3K27me3 in the same genome appear to be contradictory at the first look, this epigenetic pattern allows fine-tuning of associated gene expression. By analogy, H3K4me3 functions as the "gas pedal" and H3K27me3 as the "brake pedal" in the scenario of gene expression. Genes with bivalent domains at their transcriptional start sites (TSSs), which are prevalent in embryonic stem cells (ESCs) and multipotent cells, are expressed at minimal levels[95]. Intriguingly, most of bivalent genes are transcription factors that dictate cell fates. Depending on the specific developmental cue, a bivalent domain may resolve to either a transcriptionally active domain by losing H3K27me3 or a transcriptionally silent domain by losing H3K4me3[95]. Bernstein et al. also showed in a separate study that when mouse ESCs were induced to differentiate into neuronal progenitor cells (NPCs), 46% of bivalent domains resolved to H3K4me3

exclusively with induction of related genes. 16% of bivalent domains resolved to H3K27me3 exclusively and 32% lost both marks with silencing of related genes. The remaining 8% were unchanged[96]. Resolution of bivalent domains to monovalent domains was also observed during differentiation of mouse ESCs into mouse embryonic fibroblasts (MEFs)[96]. From the viewpoint of bivalent domains, a series of dichotomous decision commits ESCs to terminal differentiated lineages.

The existence of a bivalent domain was equivocal since some argued that the detection by ChIP of both H3K4me3 and H3K27me3 at the same genomic region merely reflected cellular heterogeneity - a mixture of one population with H3K4me3 only and another with H3K27me3 only. These doubts were subsequently resolved thanks to the pioneering studies that utilized homogenous cell population[97], single-cell technique[98], or sequential ChIP[99-102]. In attempts to uncover "true" bivalency in certain genes, investigators had to take the necessary measures to minimize cellular heterogeneity. Further, mass spectrometry (MS) data suggest the coexistence of H3K4me3 and H3K27me3 in different H3 copies of the same nucleosome, with each mark occupying one H3 tail[103,104]. This asymmetric modification results from the ability of H3K4me3 or H3K27me3 to prevent methylation of the competing type on the same H3. Specifically, the presence of H3K27me3 destabilizes the interaction between H3 and H3K4 methyltransferase complexes, thereby preventing establishment of new H3K4me3 marks[105]. The existing H3K4me3 can be further removed from genes by KDM5A which is an H3K4me2/3 demethylase recruited by PRC2[106]. Similarly, H3K4me3 inhibits PRC2 activity by abolishing the interaction of RbAp46/48 with H3[107]. MLL3/4 complexes,

which catalyze methylation of H3K4, contains the H3K27 demethylase UTX[108,109]. It's interesting to see that a histone methyltransferase complex of one type generally associates with a histone demethylase of the competing type. In addition, active gene transcription facilitated by high levels of H3K4me3 removes H3K27me3 along the gene body as the elongating form of RNA Pol II binds the H3K27 demethylase JMJD3 and paves the way for productive transcription[110].

The antagonism between H3K4me3 and H3K27me3 delicately maintains the equilibrium between them in a bivalent domain until it's severely disturbed in response to appropriate differentiation signals. Resolution of a bivalent domain to a monovalent domain is physiologically difficult to reverse since the accumulation of one type of methyl histone marks actively excludes the other type as discussed above. One exception involves induced pluripotent stem cells (iPSCs) where ectopic overexpression of the pluripotent transcription factors Oct4, Sox2, c-Myc and Klf4 restores bivalency that closely resembles ESCs[111-113]. Nevertheless, it doesn't naturally occur *in vivo*. The relative irreversibility of a monovalent domain is consistent with the observation that ESCs progressively lose bivalent domains as they undergo terminal differentiation, although a few novel bivalent domains occasionally form.

1.4 Model Justification

A. Osteoblast precursor model:

MC4 cells together with other subclones were originally isolated by diluting phenotypically heterogeneous MC3T3-E1 cells at a density of 100 cells/100 mm dish and culturing them for 2 to 3 weeks until separate clones were well formed[114]. Compared to other subclones, MC4 cells show a strong potential to differentiate into mature osteoblasts *in vitro* after exposure to ascorbic acid for 12 days and inorganic phosphate for the last 2 days. They also produced woven bones over six weeks in Collagraft sponges implanted subcutaneously in immunodeficient mice. Some subclones able to mineralize *in vitro* nevertheless fail to form bones *in vivo*[114]. Alternatively, MC3T3-E1 subclone 14 (MC14) displays a similar phenotype and can be used interchangeably with MC4 cells[114]. The close resemblance of MC4 cells to primary osteoblast precursors makes them an ideal candidate to study the molecular mechanisms of osteoblast differentiation under normal and pathological circumstances. Further, certain research questions can be answered using MC4 cells instead of primary BMSCs due to homogeneity of MC4 cells. In this study, investigating bivalent genes in MC4 cells maximally minimizes “apparent” bivalency simply generated by cellular heterogeneity. In contrast, investigating bivalent genes in primary BMSCs, the majority of which are nondifferentiating fibroblast-like cells[115], inevitably makes the results difficult to interpret. In addition, examining changes in gene expression is more reliable in MC4 cells since they aren’t masked by the presence of changes in other populations.

B. I*n vivo* mouse model of MM:

Aging C57BL/KalwRij mice spontaneously develop neoplasms of plasma cells, namely Waldenstrom macroglobulinemia and MM[116-118]. This unique feature provides a valuable reservoir of MM cells, known as the 5TMM series, to study MM and generate *in vivo* MM mouse models. Of the 5TMM series, 5T2MM and its more aggressive variant 5T33MM lines have been extensively characterized[119]. The *in vivo* 5TMM models were successfully created by transplanting spontaneously developed myeloma cells in C57BL/KalwRij mice to syngeneic recipients, and propagated by continuously transplanting purified myeloma cells to mice. The 5TMM model shows homing of myeloma cells specifically to bone marrow and the mice develop progressive bone destruction. The high similarity of the 5TMM model to MM patients allows it to be widely used in studies investigating homing and proliferation of myeloma cells[117,120]. However, it's not an efficient model to study MMBD due to the extensive time (12-14 weeks) required to develop bone lesions. The 5TGM1 model developed from the 5TMM model is better suited for research efforts investigating MMBD. 5TGM1 cells, derived from 5T33MM cells, cause severe bone destruction within 4 to 5 weeks *in vivo*[121]. In addition, we engineered 5TGM1 cells to stably express a fusion protein comprised of GFP and thymidine kinase (TK). GFP is used to monitor tumor burden and separate myeloma cells from other populations[122]. Since Ganciclovir, a guanine analog to treat cytomegalovirus (CMV) infection, is specifically phosphorylated by TK to form toxic metabolites, treating 5TGM1 cells with appropriate concentrations of GCV eliminates the MM without affecting other population[123]. In the 5TGM1 model, 5TGM1 cells are

injected into tibiae of C57BL/KalwRij mice to induce localized bone destruction. Comparable to the 5TMM model, the 5TGM1 model has tumor infiltration restricted to bone marrow and spleen when the cells are administrated intraveneously. What makes this model most appropriate is the rapidity of the development of lytic bone lesions and ability to isolate myeloma cells or BMSCs from inoculated bones. Other animal models of myeloma exist, including the Pristane-induced plasmacytoma in BALB/c mice, the SCID xenograft model and the SCID-hu model[124]. These models, however, present different characteristics from MM patients or are immunocompromised. As a result, we selected the 5TGM1 model to investigate the molecular mechanism(s) responsible for the long-term suppression of osteoblast differentiation in MM.

1.5 Rationale and Central Focus

Studies characterizing MM-BMSCs have focused on their differences from those of normal donors, including microRNA profiles, gene profiles and biological phenotypes, and have provided important insights in how distinct gene profiles in MM-BMSCs contribute to their unique phenotype. Importantly, identification of these dysregulated microRNAs and genes provide valuable directions for future studies to understand the molecular mechanisms of OB differentiation. However, how ND-BMSCs gradually change into MM-BMSCs in MM patients and how this phenotype is maintained in the absence of myeloma cells is unclear. To address this research question, our studies could provide the evidence that epigenetic changes are implicated in the development of MM-BMSCs and long-term suppression of bone formation in MM.

Activation of signaling cascades fade and allow cells to return to their previous states without continuous stimuli. However, development and adaption to the surrounding environment usually requires an organism to convert an ephemeral environmental signal into long-lived phenotypic changes. Epigenetic changes that control gene transcription independent of genetic sequence and are inheritable across generations act as a platform integrating all transient stimuli from outside of cells and establishing a stable phenotype accordingly[125]. Furthermore, the role of epigenetic changes in the pathogenesis of MMBD has not been clearly defined. In this study, we were interested in one particular epigenetic landscape known as bivalent domains. Besides its capacity of generating long-lasting epigenetic memory as discussed in the

previous section, emerging evidence provides hints of the possible involvement of bivalent domains in regulating osteoblast differentiation. The H3K4me3 demethylase nucleolar protein 66 (NO66)[126] and retinoblastoma binding protein 2 (RBP2)[127] exert inhibitory effects on osteoblast differentiation. Ectopic expression of EZH2, which mediates H3K27 tri-methylation, impairs osteogenesis while enhancing lipogenesis[128]. Based on these findings, we hypothesized that bivalent domains dictate the expression of genes essential for osteoblast differentiation and that resolution of bivalent domains into transcriptionally silent domains mediates the long-term suppression of osteoblast differentiation in MM by silencing the expression of these key regulators. Understanding the molecular mechanism(s) should help identify targets to reverse MMBD and possibly decrease tumor burden. The proposed mechanism may also be generalizable to other biological phenomena where an ephemeral microenvironment persistently changes phenotypes of cells, such as hematopoietic stem cell (HSC) development in different organs during embryogenesis and the establishment of latent viral infection in host cells.

CHAPTER 2

MATERIALS AND METHODS

2.1 Chemicals and Antibodies

JNK inhibitor SP600125 (Cat # S5567), p38 inhibitor SB203580 (Cat # S8307) and MEK1 inhibitor PD98059 (Cat # S215) were purchased from Sigma. Antibodies to JMJD3 (1:250), H3K27me3 (1:3000) and NF-κB inhibitor (Cat # 481406) were purchased from Millipore. Runx2 (1:1000,), phospho-c-Jun (1:1000), c-Jun (1:1000), IκBα (1:1000) were obtained from Cell Signaling, and β-actin (1:3000) from Santa Cruz.

2.2 Plasmids

Cumate-pLenti-Cloning-SV40-GFP (Cat: # iCu007, Abmgood) (Figure 2-1); MGC premier cDNA clone for JMJD3 (Cat: # TCMS1004, Transomic); psRSV-Rev (Cat: # 12253, Addgene); pMDLg-RRE (Cat: # 12251, Addgene); pCMV-VSVG (Cat: # 8454, Addgene); Gfi1-overexpressing pcDNA 3.1 was constructed by former lab member.

2.3 Buffers

Radioimmunoprecipitation assay (RIPA) buffer: 150 mM sodium chloride, 1.0% NP-40, 0.5% sodium deoxycholate, 0.1% SDS and 50 mM Tris (pH 8.0); 2x Laemmli buffer: 10% β-mercaptoethanol, 20% glycerol, 0.004% bromophenol blue, 4% SDS and 0.125 M Tris-HCl; Running Buffer for Western blot: 190 mM glycine, 25 mM Tris and 0.1% SDS; Transfer buffer for Western blot: 192mM glycine, 20% methanol, 25 mM Tris and 0.1%

SDS; Tris-buffered saline with Tween 20 (TBST) buffer: 150 mM sodium chloride, 0.1% Tween 20 and 20 mM Tris (pH 7.5); Stripping Buffer: 25 mM glycine and 2% SDS (pH 2.0); Tris-borate-EDTA (TBE) buffer: 89mM boric acid, 2mM EDTA and 89 mM Tris (pH 7.6).

2.4 Cell Line Culture

Mouse MC3T3-E1 subclone-4 (MC4) pre-osteoblasts were purchased from American Type Culture Collection (ATCC) and maintained in ascorbic acid-free α-modified Eagle medium (α-MEM) (Cat: # A1049001, GIBCO) supplemented with 10% FCS and 1% pen/strep. MC4 cells were continuously sub-cultured twice a week in a ratio of 1:6 using trypsin-EDTA solution (Cat: # T4049, Sigma) until they reached passage 20. Osteoblast differentiation was induced by culturing confluent MC4 cells in α-MEM containing 10% FCS, 50 μg/ml ascorbic acid and 10 mM β-glycerophosphate.

The mouse myeloma cell line 5TGM1 was kindly provided by Dr. Bobatunde O. Oyajobi (University of Texas at San Antonio) and the late Gregory R. Mundy (Vanderbilt University, Nashville, TN). These MM cells can be propagated *in vitro*, home to the BM to induce osteolytic lesions, secrete IgG2b, and produce the same panel of cytokines associated with MM bone disease in patients. 5TGM1 cells were stably transfected with a lentiviral construct containing a fusion gene encoding GFP for positive selection and thymidine kinase (TK) for negative selection. The construct to produce these engineered 5TGM1 cells (5TGM1-GFP-TK) was kindly provided by Dr. Hee-Yong Chung (Hanyang University, Seoul, Korea). 5TGM1 cells were maintained in RPMI 1640 (Cat: # GIBCO)

with 10% FCS and 1% pen/strep, and sub-cultured twice a week in a ratio of 1: 10. Co-cultures of 5TGM1 and MC4 cells (10:1) were performed in a 1:1 (v/v) mix of α-MEM and RPMI 1640 with 10% FCS.

The human embryonic kidney cell line (293TF) was purchased from Invitrogen and maintained in Dulbecco's modified Eagle's Minimum Essential Medium (DMEM) (Cat: # 12200-017, GIBCO) with 10% FBS and 1% pen/strep. 293TF cells were sub-cultured three times a week in a ratio of 1:8 to avoid any confluency. Alternatively, 293TF cells were cultured in DMEM with 10% FBS only for any transfection experiments.

2.5 Primary Human BMSC Culture

After obtaining informed consent in accordance with the Declaration of Helsinki and approval by Indiana University Institutional Review Board, BM aspirates were collected in heparin from 4 healthy donors and 7 myeloma patients. Marrow mononuclear cells were separated by Ficoll-Hypaque density sedimentation and cultured in for 3 weeks to obtain stromal cells as follows. Briefly, BM cells were incubated in Iscove's Modified Dulbecco's Medium (IMDM) (Cat: # 12200-036, GIBCO) with 10% FCS and 1% pen/strep overnight, and the nonadherent cells were removed the next day. The cultures were then continued for 21 days with media changes every 4 days. Cells were subsequently detached with trypsin-EDTA solution at subconfluence and replated (10^5 cells/10 cm dish) for use at passages 2 and 3.

2.6 Mouse Model of MMBD

Specific-pathogen-free C57BL/KaLwRij mice (6–12 weeks of age) were obtained from Dr. Jolene Windle at Virginia Commonwealth University. The knees of mice were bent over to expose the epiphysis of tibiae, where a needle was inserted along the long axis of tibiae to inject 20 μL of saline with or without 10^5 5TGM1 cells. Blood samples were collected once a week for ELISA assay of monoclonal IgG2b secreted by MM cells. Mice were sacrificed 21 days after tumor inoculation. The severity of bone destruction was initially assessed by X-ray radiography and subsequently quantified by microCT. All research protocols were approved by the Veterans Administration Indianapolis Healthcare System and IUSM Institutional Animal Care and Use Committee.

Primary BM cells were flushed out of tibiae using 1 ml of IMEM with 1% pen/strep. The cells were centrifuged, resuspended and plated in 100 mm culture dishes in 10 mL IMEM supplemented with 10% FCS and 1% pen/strep. Nonadherent cells were removed the next day and the media replaced every other day. Cell cultures were treated with 20 μg/ml ganciclovir for 3 days to remove residual 5TGM1-GFP-TK cells. Adherent BMSCs were cultured at 37°C for 21 days and then sub-cultured to passage 2 and 3 using trypsin-EDTA before their expression profile and differentiation potential were assessed.

2.7 JMJD3 siRNA Transfection of MC4 Cells

Each transfection experiment included scrambled siRNA (Cat: # D-001810-10-05, Dharmacon) as a negative control, mouse GAPDH siRNA (D-001830-02-05, Dharmacon) as a positive control and two different sets of mouse JMJD3 siRNAs (Cat: # J-063799-09-0002 and J-063799-10-0002, Dharmacon). These mouse JMJD3 siRNAs were modified to minimize off-target effects and specifically targeted two different open reading frames (ORFs) of JMJD3. MC4 cells were seeded in 6-well plates at a density of 8 X 10^4 cells/well in the afternoon so that they reached desired 80% confluency after overnight culture. For each well, one tube with 200 μl of reduced serum medium Opti-MEM I (Cat: # 31985-062, Thermofisher Scientific) containing 0.5 μl of 100 μM siRNA and another tube with 200 μl of serum-free Opti-MEM containing 3 μl of DharmaFECT^{tm} 1 transfection reagent (T-2001-02) were prepared. Depending on the number of wells to be transfected and the number of siRNAs to be used, the volume of each component was accordingly scaled up. Each tube was incubated at room temperature for 5 minutes. The two tubes were then mixed together and incubated for additional 20 minutes. 1.6 ml of antibiotic-free complete medium was then added to the mix for a final volume of 2 ml transfection medium and a final siRNA concentration of 25 nM. The culture media in 6-well plates were replaced by the freshly made transfection medium, which was removed 6 hours later to avoid the cytotoxicity of the DharmaFECT^{tm} 1 transfection reagent to MC4 cells. RNA and protein levels were examined 48 hours later to determine knockdown efficiency by qPCR and Western blot, respectively.

2.8 Transient Transfection

Cells were seeded in 6-well plates in a density of 8 X 10^4 cells/well for MC4 cells and 1 X 10^6 cells/well for 293TF cells in the afternoon so that they reached desired 80% confluency after overnight culture. For each well, 6 ul of Fugene 6 transfection reagent (Cat: # E2691, Promega) was gently diluted in 94 ul of Opti-MEM and incubated in room temperature for 5 minutes. 1 μg plasmid DNA was added to obtain the transfection reagent / DNA mix, which was incubated for additional 20 minutes and then added in a drop-wise manner to each well containing complete culture medium. Depending on the number of wells to be transfected and the number of plasmids to be used, the volume of each component was accordingly scaled up. The medium was replaced 6 hours later to avoid any cytotoxicity of Fugene 6 transfection reagent to MC4 cells. Cells were visualized under a fluorescent microscope to assess transfection efficiency, if transfected with plasmids that express GFP or RFP. RNA and protein levels were examined 48 hours later by qPCR and Western, respectively.

2.9 Generation of a Stable JMJD3-Overexpressing Cell Line

A third-generation lentiviral system was used to package a self-constructed mouse JMJD3-overexpressing plasmid (vJMJD3) or empty plasmid (vControl) since 5' long-terminal repeat (LTR) of its backbone is hybrid with a CMV promoter, which doesn't require Tat to transcriptionally activate the gene of interest. Further, splitting of

the lentiviral products into three different vectors maximally prevents generation of replication-competent lentiviruses. To produce the viral soup, 293TF cells were seeded in 10 cm dishes at a density of 6 X 10^6 cells/dish in the afternoon so that they reached the desired 80% confluency the following morning. Transient transfection was performed as described above except multiple plasmid DNAs were transfected simultaneously. Briefly, the transfection reagent / plasmid DNA mix containing 534 μl of Opti-MEM I, 66 μl of Fugene 6, 6.5 μg pMDLg-RRE, 3.5 μg psRSV-Rev, 2.5 μg pCMV-VSVG, and 10 μg vJMJD3 or vControl were added in a drop-wise manner to 293TF cells with 10 ml complete medium. The medium was then replaced 6 hours later. The viral soup was collected 48 hours later and centrifuged at 1500 RPM to collect the supernatant, which was immediately stored in a -80 °C freezer for future use.

MC4 cells were seeded in 6-well plates at a density of 8 X 10^4 cells/well in the afternoon so that they reached desired 80% confluency the following morning. The complete medium was replaced by viral soup containing 2 μg/ml polybrene that facilitated the attachment of viral particles to cell surface. The viral soup was then replaced by complete medium 24 hours later. 48 hours after infection, stable JMJD3-overexpressing MC4 cells (MC4/JMJD3) or their empty vector control counterparts (MC4/EV) were selected by consecutive 3-week culture in complete medium containing 2 μg/ml puromycin, the concentration of which was experimentally determined by killing curves. The success of generating MC4/JMJD3 and MC4/EV cells was validated by comparing JMJD3 mRNA and protein levels.

2.10 Full-length Mouse JMJD3 cDNA Synthesis

In a total reaction volume of 25 μl, 12.5 of μl Q5 High-Fidelity 2X Master Mix (Cat: #M0492S, NEB), 10 mM mouse JMJD3 forward primer (Appendix), 10 mM mouse JMJD3 reverse primer (Appendix), 1 ng MGC premier cDNA clone for JMJD3 and variable volume of nuclease-free water were gently mixed and prepared on ice. Routine PCR was subsequently performed using the following thermocycling conditions: 1 cycle at 98 °C for 30 seconds, followed by 30 cycles of 98 °C for 10 seconds and 78 °C for 3 minutes, and finally 1 cycle at 72 °C for 2 minutes. The correct size of PCR products was validated by DNA electrophoresis.

2.11 Purification of cDNA and Plasmids

JMJD3 cDNA products and endonuclease-digested plasmids were purified using QIAquick PCR purification Kit (Cat: # 28104, Qiagen) according to the manufacturer's instructions. Briefly, 1 volume of each sample and 5 volumes of Buffer PB were gently mixed and transferred to a QIAquick column. The QIAquick column was centrifuged at 12000 RPM and the flow-through discarded after every procedure. The DNA retained on the column membrane was then washed once with 750 μl of Buffer PE, followed by elution using 30 μl of nuclease-free water.

2.12 Cloning of Mouse JMJD3 cDNA into Cumate-pLenti-Cloning-SV40-GFP Lentiviral Plasmid

Purified mouse JMJD3 cDNA and Cumate-pLenti-Cloning-SV40-GFP plasmid were digested by MfeI (Cat: # R0589S, NEB) and BamHI (Cat: # R0136T, NEB). The reaction mix of 50 μl containing 1 μg DNA, 10 units of MfeI, 10 units of BamHI, 5 μl of 10X CutSmart Buffer, and variable volumes of nuclease-free water was incubated at 37 °C for 3 hours. The desired DNA fragments were isolated by subjecting digested DNA samples to DNA electrophoresis and cutting out the bands of correct size. These DNA fragments were then purified using a QIAquick Gel Extraction Kit (Cat: # 28704, Qiagen) according to the manufacturer's instructions. Mouse JMJD3 cDNA fragments and the Cumate-pLenti-Cloning-SV40-GFP backbone were ligated at room temperature for 10 minutes in a reaction volume of 20 μl containing 2 μl of T4 DNA ligase Buffer (10X), 84.67 ng mouse JMJD3 cDNA, 50 ng vector, 1 μl of T4 DNA Ligase (Cat: # M0202, NEB) and variable volume of nuclease-free water.

2.13 Transformation into 5-alpha Competent *E. coli*

100 ng of plasmid DNA was gently mixed with 50 μl of freshly thawed 5-alpha competent E. coli (Cat: # C2987H, NEB). The mix was incubated on ice for 30 minutes, followed by heat shock at 42 °C for 30 seconds. 950 μl of room temperature LB medium was then added. The transformed bacteria were then vigorously shaken at 37 °C for 60

minutes and 50 μl was spread on a neomycin-containing LB plate for overnight culture. The desired clone was subsequently validated based on DNA electrophoresis and plasmid sequencing results.

2.14 Minipreparation of Plasmids

Minipreparation of plasmids was done using a QIAprep Spin Miniprep Kit (Cat: # 27104, Qiagen) according to the manufacturer's instructions. The obtained plasmids were mainly used for cloning and validation. Briefly, 2.5 ml of bacteria in LB medium were pelleted by centrifugation at 8000 RPM for 3 minutes at room temperature and resuspended in 250 μl of prechilled Buffer P1 by vigorous vortex. 250 μl of Buffer P2 was mixed with the resuspended bacteria by inverting microcentrifuge tubes several times until the solution becomes blue. 350 μl of Buffer N3 was then added with solution turning colorless and white precipitates forming. Following centrifugation at 13000 RPM for 10 minutes, the supernatant was transferred to the QIAprep 2.0 spin column. Columns were centrifuged at 13000 RPM for 30 seconds and flow-through discarded after each procedure. The plasmids retained on the columns were washed with 750 μl of Buffer PE and subsequently eluted with 50 μl of Buffer EB. Plasmids were immediately used or stored at -20 °C.

2.15 Maxipreparation of Plasmids

Minipreparation of plasmids was done using QIAfilter Plasmid Maxi Kit (Cat: # 12262, Qiagen) according to the manufacturer's instructions. The obtained plasmids were mainly used for transient and stable transfections. Briefly, 250 ml of bacteria in LB medium were pelleted by centrifugation at 6000 x g for 15 minutes at 4 °C and resuspended in 10 ml of prechilled Buffer P1 by a combination of repetitive pipetting and vigorous vortex. 10 ml of Buffer P2 was mixed with the resuspended bacteria by inverting the microcentrifuge tubes 4 to 6 times until the solution becomes blue. 10 ml of Buffer N3 was then added with solution turning colorless and white precipitates forming. The bacterial lysate was then transferred to the QIAfilter Cartridge and filtered through the membrane of the cartridge into the equilibrated QIAGEN-tip with precipitates left behind. The bacterial lysate went through the resin of QIAGEN-tip by gravity. The QIAGEN-tip was then washed with 30 ml of Buffer QC twice. Plasmids were eluted into 15 ml of Buffer QF, and, after thoroughly being mixed with 10.5 ml of room-temperature isopropanol, were centrifuged at 15000 x g for 30 minutes at 4 °C. Obtained plasmid precipitates were rinsed with 5 ml of room-temperature 70% ethanol, air-dried for 10 minutes, and dissolved into TE buffer.

2.16 DNA Electrophoresis

12 μl of DNA samples were thoroughly mixed with 3 μl of GelPilot Loading Dye

(5X) (Cat: # 239901, Qiagen) and loaded onto 0.8% of agarose gel. 6 μl of GelPilot 1kb Ladder (Cat: # 239085, Qiagen) was also used to determine band sizes. DNA electrophoresis was conducted at 80 V for 40 minutes, followed by imaging under UV light.

2.17 RNA Extraction, RNA Quantification, cDNA Synthesis and qPCR

RNA extraction was performed using an RNeasy Mini Kit (Cat: # 74104, Qiagen) according to the manufacturer's instructions. Briefly, cells were washed with cold PBS twice to remove any residual medium before they were lysed by adding 350 μl of Buffer RLT Lysis buffer to each sample and homogenized by pipetting up and down. Cell lysates were then transferred to columns that have silicon membranes to selectively bind RNA. Columns were centrifuged at 12000 RPM at room temperature and flow-through discarded after each procedure. The columns were washed with 750 μl of Buffer RW1 once followed by 500 μl of Buffer RPE twice. The RNA retained in the column was then eluted with 50 μl of nuclease-free water.

The concentration and quality of RNA were determined using a NanoDrop 2000 Spectrophotometer after RNA extraction. All RNA samples were kept on ice the entire time. 1 μl of nuclease-free water was first assessed as blank before 1 μl of each RNA sample was quantified. Only RNA samples with A260/A230 and A260/A280 ratios above 1.8 were used in subsequent application. After obtaining their concentration, RNA samples were immediately used for cDNA synthesis or stored at -80 °C.

cDNA synthesis was performed using the two-step method. All reactions were assembled on an ice-cold plate. In the first reaction volume of 2.5 μl, 300 ng RNA, 0.25 μg random primers (Cat: # C118A, Promega) and nuclease-free water were thoroughly mixed, heated at 70 °C for 5 minutes and immediately chilled on ice. 7.5 μl of reverse transcription reaction mix per sample was prepared at the same time. Depending on the number of samples, the volume of each ingredient was accordingly scaled up. For each sample, the reverse transcription reaction mix contained 2 μl of GoScript 5X Reaction Buffer (Cat: # A500D, Promega), 1.5 μl of 25 mM $MgCl_2$ (Cat: # A351H, Promega), 0.5 μl of 10 mM PCR Nucleotide Mix (Cat: # U151B, Promega), 0.5 μl of GoScript Reverse Transcriptase (Cat: # A501D) and variable amount of nuclease-free water. 2.5 μl of RNA/primer mix and 7.5 μl of reverse transcription mix were combined and incubated in a T100 Thermal Cycler (Biorad) using the following thermocycling conditions: 25 °C for 5 minutes, 42 °C for 1 hour and 70 °C for 15 minutes. cDNA samples were diluted by 10 folds. They were then immediately used for qPCR quantification or stored at -20 °C.

CFX96 Touch System (Biorad) was utilized for qPCR operation. For each reaction, 5 μl of SsoAdvanced universal SYBR Green supermix (Cat: # 1725274, Biorad) containing 500 nM of forward and reverse primers, and 5 μl of diluted cDNA sample were mixed thoroughly. Technical triplicates were carried for each gene/cDNA sample combination to minimize variability. The reaction conditions were as follows: 1 cycle of 95 °C for 30 seconds, followed by 35 cycles of 95 °C for 10 seconds and 60 °C for 30 seconds, and finally the melting-curve analysis embedded in the program. The DNA sequences of mouse and human primers used for qPCR are listed in Appendix. Relative expression

was calculated using the comparative $2^{-\Delta\Delta Ct}$ method. The geometric means of CT values of β-actin, GAPDH and HMBS were used as the internal control since a combinational application of these three genes provide the most reliable control in osteoblasts based on the geNorm algorithm.

2.18 Protein Extraction and Quantification

Cells were washed with cold PBS twice to remove any residual medium before adding an appropriate volume of RIPA buffer freshly supplemented with 1 mM PMSF (Cat: # 329-98-6, Sigma) and protease inhibitor cocktail (Cat: # P8340, Sigma). Cell lysates were collected into 1.7 ml microcentrifuge tubes using cell scrapers, incubated on ice for 30 minutes and centrifuged at 12000 RPM for 20 minutes at 4 °C. The supernatants, which were the protein sample free from any cellular debris, were then transferred to new 1.7 ml microcentrifuge tubes.

Protein concentrations were determined using a Pierce BCA Protein Assay Kit (Cat: # 23225, ThermoFisher Scientific) according to the manufacturer's instructions. Briefly, protein standards were prepared by serial dilution of BSA. Final BSA concentrations of protein standards included 0 μg/μl, 0.33 μg/μl, 0.5 μg/μl, 0.66 μg/μl, 0.83 μg/μl, 1 μg/μl and 2 μg/μl. 15 μl of each protein standard were added in order to a 96-well plate based on their concentrations. 2.5 μl of protein samples diluted with 12.5 μl of MilliQ water were added to the same 96-well plate. Protein concentrations were measured using SpectraMax 250. The coefficient of determination (R^2) of protein

standards was also checked to ensure accuracy. After obtaining protein concentrations, protein samples were immediately denatured for Western blot or stored at -80 °C.

2.19 Western Blot and Analysis

15 μg of protein thoroughly mixed with 4X Laemmli Sample Buffer were heated at 95 °C for 5 minutes before being loaded into wells of 4-20 % Mini-PROTEAN TGX precast protein gels (Cat: # 4561095, Biorad). Precision Plus Protein Standards (Cat: # 1610375, Biorad) were used to indicate band size. The gel was run at 80 V for 10 minutes and 100 V for approximately 90 minutes.

Protein transfer was performed using the semi-dry method. From bottom (anode) to top (cathode) were a thick filter paper, a PVSF membrane having been activated by methanol for 1 minute, the gel and a thick filter paper. The protein transfer conditions were 12 V for 20 to 30 minutes, depending on the size of the protein of interest. 17 kD histone proteins require shorter transfer time to prevent any penetration through the PVSF membrane. 178 kD JMJD3 requires a longer time for complete transfer.

The PVSF membrane was then blocked in 5% (w/v) skim milk in TBST at room temperature for 1 hour, followed by overnight incubation with primary antibodies in their proper blocking solution at 4 °C. On the following day, the PVSF membrane was rinsed with TBST 3 times for 10 minutes each. HRP-conjugated secondary antibodies diluted in 2% skim milk in TBST were incubated with the PVSF membrane for 1 hour at room temperature. The PVSF membrane again was rinsed with TBST 3 times. Protein

signals were visualized using chemiluminescent substrates (Cat: # RPN2232, GE Healthcare). The ratio of protein of the interest to the internal control was semi-quantitatively determined by ImageJ software.

2.20 Chromatin Immunoprecipitation

ChIP assay was performed using the SimpleChIP Enzymatic Chromatin IP Kit (Cat: #9003, Cell Signaling) according to manufacturer's instruction. The kit utilized micrococcal nuclease digestion instead of sonication to generate DNA fragments of approximately 150-900 bp. 8 X 10^6 treated or untreated MC4 cells were lysed for each cross-linked chromatin preparation that sufficed for 5 separate immunoprecipitations.

Protein and DNA were cross-linked by incubating the cells in 1% (v/v) formalin for 10 minutes. The cross-linking was subsequently stopped by addition of 1/10 volume of 10X glycine. Cells were washed with ice-cold PBS twice, transferred into a 15 ml conical tube in ice-cold PBS plus PMSF, and centrifuged at 1500 RPM at 4 °C for 5 minutes to obtain the cell pellets. To selectively lyse plasma membranes, the pellets were incubated in 10 ml of ice-cold Buffer A supplemented with DTT, protease inhibitor cocktail and PMSF on ice for 10 minutes. Nuclei were then centrifuged and resuspended in 1 ml Buffer B plus DTT, which provided chemical conditions for micrococcal nuclease to subsequently digest DNA at 37 °C for 20 minutes. The volume of micrococcal nuclease used was experimentally optimized by visualizing DNA fragments on agarose gel following DNA electrophoresis. Nuclear pellets were then sonicated by three 20-second

pulses on ice to break the nuclear membrane. The resulting lysates were centrifuged at 10000 RPM for 10 minutes at 4 °C to obtain the supernatants, which were the cross-linked chromatin preparation that could be stored at -80 °C for future use.

For each immunoprecipitation, 400 μl of 1X ChIP Buffer freshly supplemented with 2 μl of protease inhibitor cocktail were thoroughly mixed with 100 μl of the cross-linked chromatin preparation. The volume of each component was scaled up accordingly depending on the number of immunoprecipitaions to be done. 10 μl of the mix was set aside as 2% input, while the rest was incubated with 10 μl of H3 antibody (Cat: # 4620S, Cell Signaling) as a positive control, 2 μl of normal rabbit IgG (Cat: # 2729, Cell Signaling) as a negative control, 2 μl of H3K27me3 antibody (Cat: # 07-449, Millipore), or 2 μl of H3K4me3 antibody (Cat: # ab8580, Abcam) overnight at 4 °C.

The following day, each immunoprecipitation preparation was incubated with 30 μl of ChIP-Grade Protein G Agarose Beads for 2 hours at 4 °C with rotation. The agarose beads having sequestered the DNA-protein complexes were pelleted at 6000 RPM for 1 minute and supernatant discarded. They were rinsed with 1 ml of Low Salt Wash Buffer (300 μl 10X ChIP buffer + 2.7 ml water) at 4 °C for 5 minutes three times followed by 1 ml of High Salt Wash Buffer (100 μl 10X ChIP Buffer + 900 μl water + 70 μl 5M NaCl) at 4 °C for 5 minutes once. DNA-protein complexes were eluted by incubating agarose beads in 150 μl 1X ChIP Elution Buffer for 30 minutes at 65 °C with gentle vortexing. After the agarose beads were removed by brief centrifugation at 6000 RPM for 1 minute, the cross-linking of DNA-protein complexes was reversed by adding 6 μl 5M NaCl and 2 μl Proteinase K to the supernatant, and incubating for 2 hour at 65 °C. The spared 2%

input was also diluted with 150 μl of 1X ChIP Elution Buffer and treated identically with 6 μl 5M NaCl and 2 μl Proteinase K as described above to reverse DNA-protein crosslinking.

Eluted DNA was purified using the provided DNA purification spin columns. Briefly, 150 μl of DNA sample thoroughly mixed with 600 μl of DNA Binding Reagent A was transferred to the columns and centrifuged at 14000 RPM for 30 seconds. The DNA retained in the column was subsequently washed with 700 μl of DNA Wash Reagent B and eluted into 1.7 ml microcentrifuge tubes with 50 μl of DNA Elution Reagent C. Purified DNA from immunoprecipitation preparations and 2% input was then analyzed by qPCR using primers that specifically targeted the mouse Runx2 and Osterix promoters (Appendix). The reagents and thermocycling conditions were the same as those for standard qPCR. The immunoprecipitation efficiency was calculated using the following formula: Percent Input = $2\% \times 2^{(CT\ 2\%\ Input\ Sample - CT\ IP\ Sample)}$

2.21 ALP Staining

One BCIP/NBT tablet (Cat: # B5655, Sigma) was dissolved in 10 ml of distilled water to prepare the substrate solution. Cells were then washed with ice-cold PBS twice to remove any residual medium, followed by short incubation in 10% neutral buffered formalin (v/v) for 30 seconds. Longer fixation led to irreversible inactivation of ALP. Cells were washed with ice-cold PBS freshly supplemented with 0.05% Tween 20 twice before incubation in the substrate solution in the dark for 10 to 20 minutes. The staining

process was checked every 5 minutes to prevent saturation. Staining was stopped by removing the substrate solution and rinsing the cells with ice-cold PBS supplemented with 0.05% Tween 20.

2.22 Alizarin Red Staining

To prepare the Alizarin Red S solution, 2 g Alizarin Red S (Cat: # A5533, Sigma) was dissolved in 100 ml of distilled water with the pH adjusted to 4.1 to 4.3 using HCl or NH_4OH. The solution was filtered and stored in the dark at room temperature. The pH was checked every time before staining. Cells were washed with ice-cold PBS twice to remove any residual medium, followed by incubation in 70% ethanol overnight. Cells were washed with distilled water twice before being incubated in the Alizarin Red S solution at room temperature in the dark for 45 minutes. The staining process was stopped by removing the Alizarin Red S solution and rinsing the cells with distilled water four times.

2.23 MTT Assay

10 μl of 5 mg/ml MTT (3-(4, 5-Dimethyl-2-thiazolyl)-2, 5-diphenyl-2H-tetrazolium Bromide) (Cat: # M2128, Sigma) dissolved in distilled water was added to only 100 μl of complete medium as control or cells in 100 μl of complete medium in a 96-well plate. After incubation of the plate at 37 °C for 4 hours, 100 μl of MTT lysis buffer (10% SDS

plus 0.01 M HCl) was added to each well. On the following day, the plate was read using the SpectraMax 250 at a wavelength of 570 nm.

2.24 Statistics

Each experiment was repeated at least 3 times, and all quantitative data are presented as mean ± SD. Statistical significance was determined by unpaired two-tailed Student t test if two groups were compared or one-way ANOVA if more than two groups were involved. Results were considered significantly different for $p < .05$. The number of * marks was used in the figures to indicate the p value range with * < 0.05, ** < 0.01, *** < 0.001.

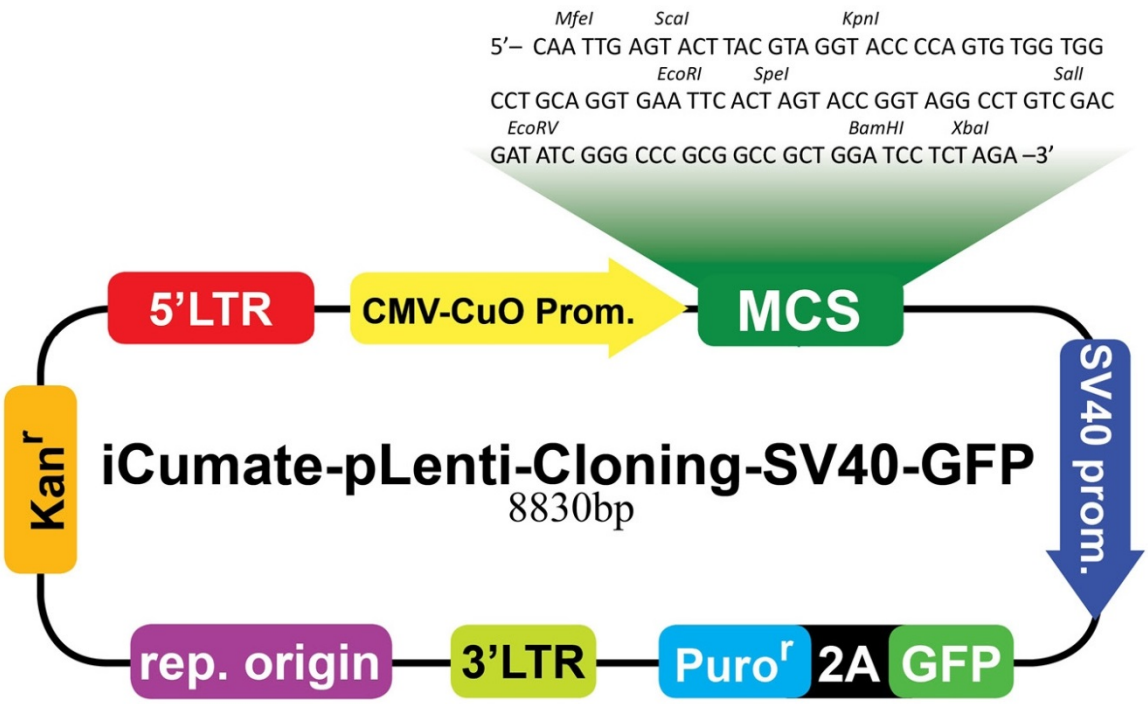

Figure 2: Plasmid Map of iCumate-pLenti-Cloning-SV40-GFP Backbone

MfeI and *BamHI* multiple cloning sites (MCSs) were selected for insertion of the full-length mouse JMJD3 due to the absence of these recognized restriction sites in the JMJD3 sequence. The expression of JMJD3 is driven by a hybrid CMV promoter (yellow box). A kanamycin resistance gene (orange box) is expressed for positive selection of bacterial clones cultured on LB plates containing 50 μg/ml kanamycin. Puromycin resistance gene (light blue box) is expressed under a SV40 promoter (dark blue box) for positive selection of MC4 cell clones cultured in complete medium containing 2 μg/ml puromycin. GFP is expressed for visual assessment of infection efficiency and positive selection by FACS.

CHAPTER 3

DOWNREGULATION OF THE H3K27ME3 DEMETHYLASE JMJD3 ALLOWS RESOLUTION OF THE BIVALENT DOMAINS ON THE RUNX2 AND OSTERIX PROMOTERS AND CONTRIBUTES TO THE INHIBITION OF OSTEOBLAST DIFFERENTIATION IN MM

3.1 Introduction

Multipotent BMSCs possess the capacity to differentiate into osteoblasts, chondrocytes, adipocytes, and myoblasts in response to appropriate stimuli. The differentiation process is initiated by induction of a set of pivotal transcription factors that activate the expression of lineage-specific genes and suppress the expression of transcription factors essential for other differentiation processes. Runx2 and Osterix direct BMSCs to osteoblast differentiation[80,81,129]; Sox5/6/9 regulates chondrocyte differentiation[130,131]; PPARγ[132], C/EBPα[133] and KLF15[134] dictate adipocyte differentiation; and MyoD5[135], Myf5[135] and myogenin[136] drive myogenesis. Dysregulation of these transcription factors have been reported in a variety of diseases.

Runx2 belongs to the Runx family of transcription factors that share a DNA-binding runx domain and, when forming a heterodimer with Cbfβ, binds to its consensus sequence 5'-PYGPYGGT-3'[137]. Runx2 induces the expression of Osterix, ALP, COL1α1, SPP1, BGLAP, and IBSP[81,138]. These target genes either play an important role in osteoblastogenesis or are integral components of the bone mineralized matrix. Compared to wild-type mouse embryos, homozygous Runx2 -/- embryos manifest a complete lack of skeletal ossification due to defective endochondral and intramembranous ossification. Cartilage development, however, is unaffected[80,129]. Consistent with *in vivo* studies, calvarial cells isolated from Runx2 -/- mice fail to differentiate into osteoblasts in response to BMP2 treatment. They retain the capacity to differentiate into mature adipocytes and chondrocytes[139]. Osterix is equally

important as Runx2 and is another master transcription factor of osteoblast differentiation. Osterix -/- mouse embryos closely resemble the phenotype of Runx2 -/- mouse embryos with absent mineralization, even though Runx2 is normally expressed in osterix -/- mice[81].

In addition to transcription factors, normal osteoblast differentiation requires ongoing epigenetic remodeling of the chromatin landscape[140-144]. Epigenetic mechanisms modulate the accessibility of osteoblast-specific genes to transcriptional activators and repressors, thereby regulating gene expression independent of DNA sequences. Considering the longevity and inheritability of "true" epigenetic marks, any anomaly of epigenetic modifiers that write or erase these marks may fundamentally disrupt osteoblast differentiation long term, as occurs in MM. MM patients present with lytic bone lesions that persist even after they are in complete remission following treatment. Further, BMSCs isolated from MM patients show an impaired capacity to differentiate into functional osteoblasts compared to those from normal donors[52-55]. These defects persist after myeloma cells are removed. Chromosomal alterations and genetic mutations have been sporadically described in BMSCs from MM patients, and these alterations/mutations have failed to explain the persistent blockade of osteoblast differentiation[63]. Therefore, it's reasonable to infer that epigenetic changes are potentially involved in the long-term suppression of osteoblast differentiation in MM. In our studies, we focused on histone methylations, H3K4me3 and H3K27me3, to explain osteoblast suppression in MM due to their role in generating epigenetic memory as discussed in details in Chapter 1.4. In support of this notion, bivalent domains, defined

by co-occupancy of both H3K4me3 and H3K27me3 marks at the same loci, are enriched on promoters of developmentally important genes in ESCs and cells of limited potency[95]. Resolution of bivalent domains into either transcriptionally active or repressive domains determines lineage specification[96]. Emerging evidence has shown that the histone modifiers of H3K4me3 or H3K27me3 regulate osteoblast differentiation. However, which osteobastogenic genes are occupied by bivalent domains at their TSSs has not been identified. Due to the essential role of Runx2 and Osterix in osteoblast differentiation, we first investigated the histone methylation pattern of their promoters by ChIP.

Trithorax group (trxG) and Polycomb group (PcG) proteins are two antagonistic systems involved in establishing and maintaining bivalency[145]. They were initially discovered as a heterogeneous collection of proteins whose mutations disrupt Hox gene expression pattern and proper body segmentation in drosophila. A subset of trxG proteins assist gene transcription by spreading H3K4me3 marks in the vicinity of promoters. One of the mechanisms involves the interaction between H3K4me3 marks and the PHD domain of the basal transcription factor TFIID, suggesting a role of H3K4me3 marks in the assembly of the preinitiation complex[146,147]. These trxG proteins each contain a SET domain responsible for methyltransferase enzymatic activity. They are enzymatically active only when complexing with accessory proteins[148-150]. The core components of the methyltransferase complexes show evolutional conservation in yeasts, drosophila and mammals, although the number of these complexes differs. The mammalian counterparts include SET1A/B and MLL1-4. The SET1A/B complexes are

major players that contribute to bulk H3K4me3[151]. Deletion of CFP1, a subunit of SET1A/B complexes that target complexes to unmethylated CpG islands and H3K4me1/2/3-rich regions, causes global reduction in H3K4me3 levels[152]. In contrast, the MLL1-4 complexes assume a more gene-specific role[151]. To oppose the promoting effects of trxG proteins on gene transcription, PcG proteins form multiprotein Polycomb-repressive complex 1 and 2 (PRC1/2) that silence productive gene transcription via several mechanisms. PRC1 is capable of compacting chromatin independent of its ubiquitin ligase activity, thereby limiting the accessibility of the transcriptional machinery to promoters[153]. PRC2 catalyzes H3K27 di- or tri-methylation through its core subunit EZH1 or EZH2. Other subunits, including SUZ12, EED and RbAp46/48, are indispensable for the function of PRC2[154,155]. EED allosterically activates the methyltransferase activity of PRC2 after interacting with PRC2's own product H3K27me3 marks. Deletion of EED leads to global reduction in H3K27me3 levels[156]. The histone chaperones RbAP46 and 48 also contribute to chromatin binding by interacting with H3 and H4[157]. It's intriguing that H3K4 and H3K27 methyltransferases all require accessory proteins to fulfil their enzymatic activity. Involvement of multiple proteins may provide additional levels of regulation.

As noted above, depending on lineage commitment, bivalent domains resolve into transcriptionally active or silent domains by removing H3K27me3 or H3K4me3 marks, respectively. This predicts the existence of tri-methyl histone demethylases[158]. Discovery of JMJD2 in 2006 by several groups, a specific H3K9me2/3 and H3K36me2/3 demethylase, first refuted the concept that tri-methyl histone marks are generally

irreversible due to the high thermodynamic stability of N-CH_3 bonds[159-161]. JMJD2 belongs the Jumonji protein family, the members of which all contain the conserved JmjC domain capable of demethylating histone methyl-groups in a Fe(II) and α-ketoglutarate-dependent manner. The Jumonji proteins that specifically demethylate H3K4me3 include NO66, JARID1A, JARID1B, JARID1C and JARID1D[162]. In line with their function in reducing the transcriptionally active mark H3K4me3, they act as transcriptional repressors to silence gene expression. The more recently discovered H3K27me3-specific demethylases are UTX and JMJD3[108,109,163,164]. UTX, but not JMJD3, contains tetratricopeptide repeats that mediate protein-protein interaction. UTX and JMJD3 erasure of transcriptionally repressive mark H3K27me3 to induce gene expression has been extensively reported. These demethylases are essential players in resolving bivalency by countering the effects of trG and PcG proteins. An elegant example is the robust induction of JMJD3 in LPS-activated macrophages, which decreases the H3K27me3 levels on the bivalently marked BMP2 promoter[163]. These results suggested that JMJD3 may contribute to the long-term osteoblast suppression in MM.

3.2 Results

3.2.1 TNF-α and myeloma cells inhibit Runx2 and Osterix expression in BMSCs by resolving the bivalent domains at the TSSs into transcriptionally silent domains

Myeloma cells have been reported to inhibit osteoblast differentiation by direct contact with BMSCs or inducing cytokines (DKK1, sclerostin, IL-1β, IL-7, TNF-α et al) in bone marrow microenvironment of MM patients. We utilized direct co-culture of the 5TGM1 murine myeloma cells and the murine early pre-osteoblast cell line MC4 cells as one of our *in vitro* models. Because floating 5TGM1 cells are readily removed from adherent MC4 cells by thorough washing with PBS, the expression profile in MC4 cells can be selectively examined without concerns of potential contamination. Another *in vitro* model in our study involves 2-day treatment of MC4 cells with 10 ng/ml TNF-α, a cytokine that is markedly elevated in sera and marrow aspirates of MM patients. The concentration and duration of TNF-α treatment we used was based on previous studies that most commonly used this regimen to show inhibition of osteoblast differentiation without causing significant cell apoptosis. As expected, MC4 cells treated with 10 ng/ml TNF-α or co-cultured with 5TGM1 cells for 2 days showed decreased mRNA levels of Runx2 and Osterix (Figure 3-1A). Similar results were also obtained with primary mouse BMSCs isolated from tibiae (Figure 3-1B). Consistent with the qPCR results, TNF-α and 5TGM1 cells decreased protein levels of Runx2 and Osterix in MC4 cells at day 2 and day 4, respectively (Figure 3-1C).

BMSCs from MM patients have been reported to maintain distinct gene profiles and persistent defects of osteoblast differentiation. This long-lasting genotype and phenotype encouraged us to investigate if epigenetic changes in Runx2 and Osterix were involved in the suppression of osteoblast differentiation in MM. As discussed in the introduction of this chapter, bivalent domains might be a previously uncharacterized mechanism by which the expression of osteoblastogenic genes is regulated. Therefore, we characterized the Runx2 and Osterix TSSs by ChIP using antibodies against H3K4me3 and H3K27me3 in undifferentiated MC4 cells. These studies revealed bivalency at both TSSs, which were co-occupied by the transcriptionally active mark, H3K4me3, and the transcriptionally repressive mark H3K27me3 (Figure 3-2A and B). As a negative control, the intronic region of Runx2 (+33130) was solely occupied by H3K27me3. Using the monoclonal cell line MC4 cells instead of isolated mouse BMSCs excluded the possibility of "apparent" bivalent domains generated merely by BMSC heterogeneity.

Resolution of bivalent domains into monovalent domains during lineage commitment is not a readily reversible process due to self-enforcement of the same type of methyl marks and repellency of different types of marks. Bivalent domains in mESCs cannot be restored physiologically during embryogenesis unless ectopic overexpression of Yamanaka factors Oct4, Sox2, c-Myc and Klf4 is induced. Therefore, we investigated the bivalency at the Runx2 and Osterix TSSs in MC4 cells by ChIP, during normal osteoblast differentiation or after the cells were exposed to TNF-α or myeloma cells. Compared to the basal levels in untreated MC4 cells at Day 0, H3K4me3 levels were increased and H3K27me3 levels were decreased at the Runx2 and Osterix TSSs in

MC4 cells that had been cultured in osteogenic medium for 2 days. These epigenetic changes paralleled the reduction in Runx2 and Osterix mRNA levels, suggesting the ongoing resolution of bivalent domains into transcriptionally active domains. In contrast, TNF-α treatment or co-culture of MC4 cells with 5TGM1 cells for 2 days resolved the bivalent domains at Runx2 and Osterix TSSs in MC4 cells into transcriptionally silent domains. These domains contained decreased H3K4me3 levels and increased H3K27me3 levels, resulting in a decreased H3K4me3 to H3K27me3 ratio (Figure 3-3).

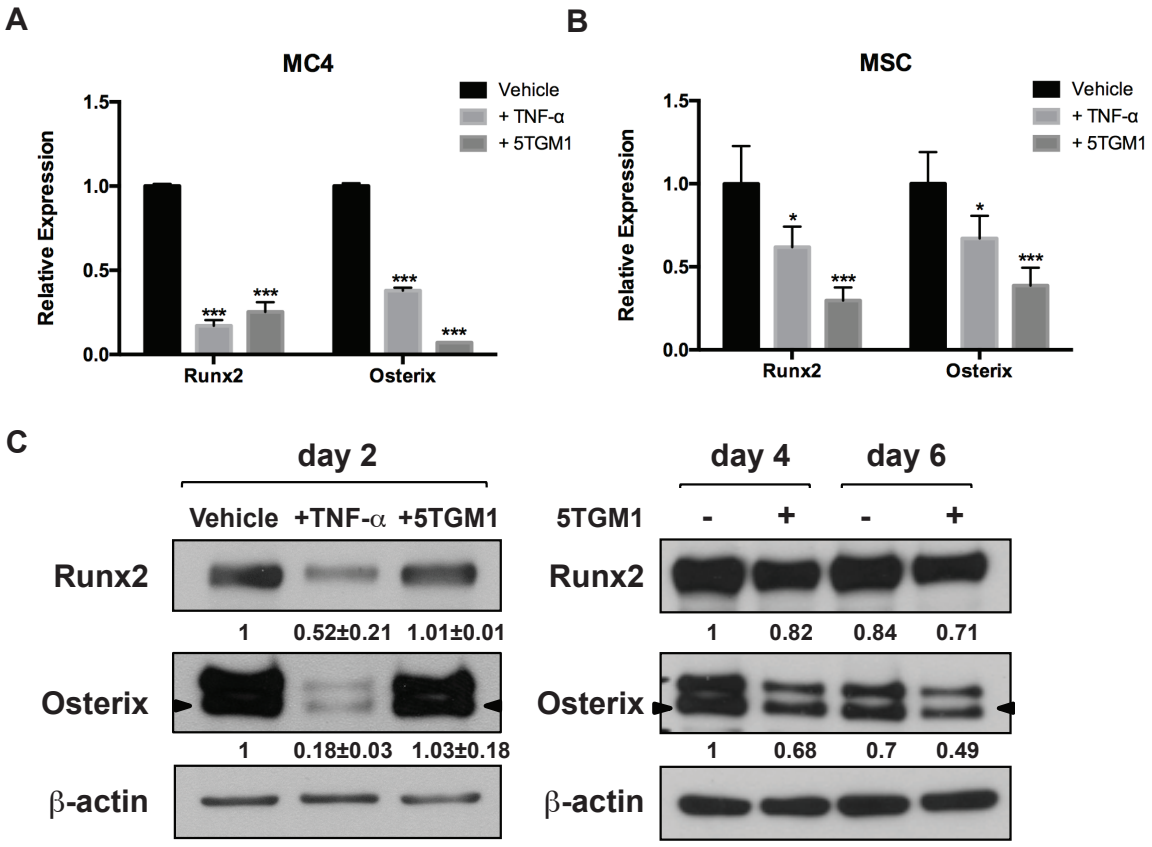

Figure 3-1: TNF-α and Myeloma Cells Decrease the Expression of Runx2 and Osterix in MC4 cells and Mouse BMSCs.

MC4 cells **(A)** or mouse BMSCs **(B)** were directly co-cultured with 5TGM1 cells or treated with 10 ng/ml TNF-α for 2 days. Relative Runx2 and Osterix mRNA levels in MC4 cells were measured by qPCR with the geometric mean of the CT values of β-actin, GAPDH and HMBS as the internal control. **(C)** MC4 cells were treated with 10 ng/ml TNF-α for 2 days or co-cultured with 5TGM1 cells for 2, 4 and 6 days. Runx2 and osterix protein levels in MC4 cells were measured by Western blot with β-actin as the internal control. Error bars in each column graph represent SD of three biological replicates. * $p < 0.05$; ** $p < 0.01$; ***$p < 0.001$ compared with the black bar in individual group. The numbers shown in the Western blot indicate normalized densitometry values.

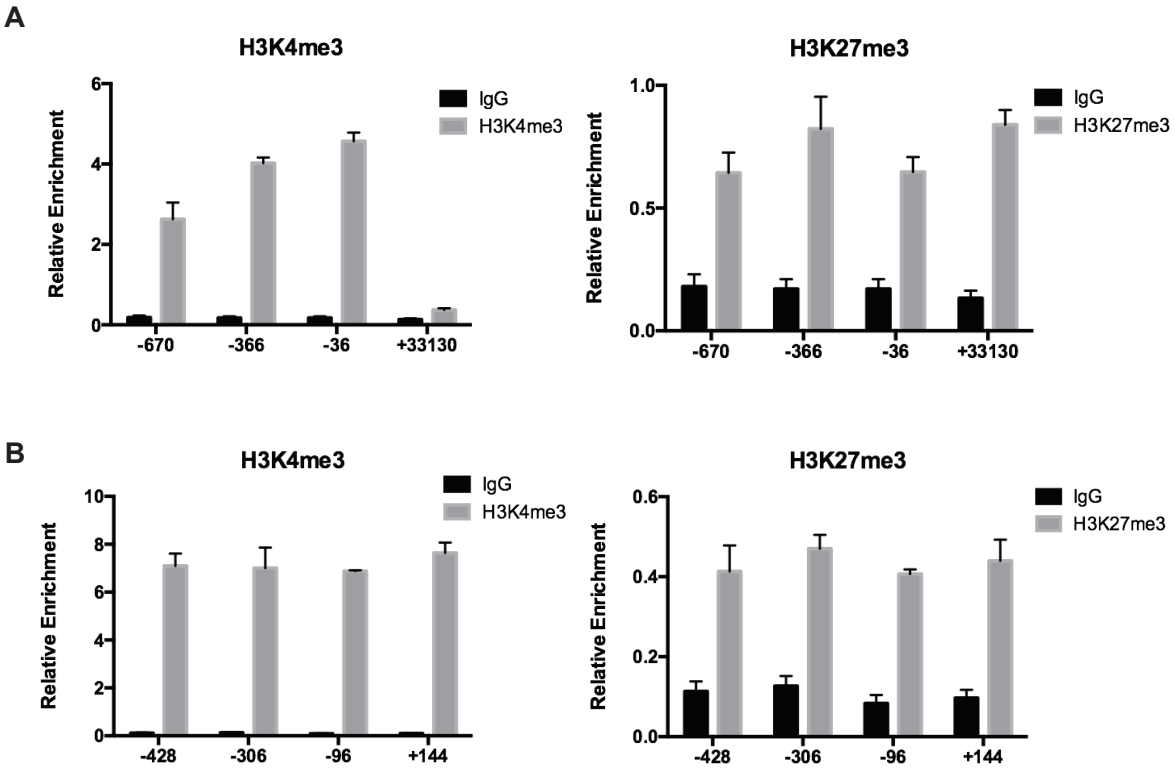

Figure 3-2: Bivalent Domains Occupy the TSSs of Runx2 and Osterix in MC4 Cells.

ChIP was performed in undifferentiated MC4 cells using antibodies against H3K4me3 and H3K27me3. The numbers on x-axis indicate the positions on the Runx2 **(A)** or Osterix **(B)** promoter with +1 as the first transcribed nucleotide. Error bars in each column graph represent SD of three biological replicates.

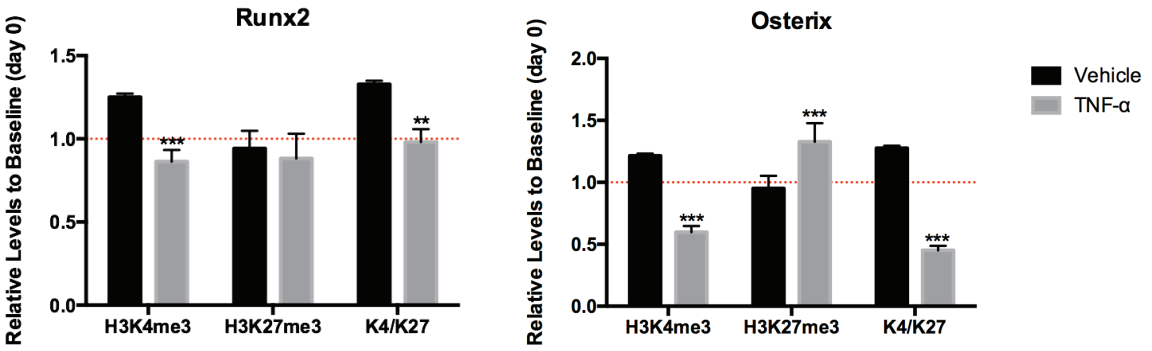

Figure 3-3: Bivalent Domains are Resolved into Transcriptionally Silent Domains at the Runx2 and Osterix TSSs in BMSCs by TNF-α.

MC4 cells were cultured in α-MEM medium with or without 10 ng/ml TNF-α for 2 days. ChIP was performed using antibodies against H3K4me3 and H3K27me3. The red line indicates the basal level of each epigenetic mark in untreated MC4 cells at Day 0. The epigenetic changes represent a total of three different sites at the Runx2 TSS and four different sites at the Osterix TSS. Error bars in each column graph represent SD of three biological replicates. * $p < 0.05$; ** $p < 0.01$; ***$p < 0.001$ compared with the black bar in individual group.

3.2.2 The H3K27me3-specific demethylase JMJD3 is downregulated in BMSCs from MM patients

Resolution of bivalent domains at TSSs into transcriptionally silent domains requires simultaneous propagation of H3K27me3 marks and removal of H3K4me3 marks. To avoid potential conflicts with our colleagues who are studying H3K4me3 alterations in osteoblast differentiation in MM, we mainly focused on the deregulation of H3K27me3 levels in BMSCs from MM patients. In addition, EZH2, which catalyzes H3K27 tri-methylation, has been reported to be overexpressed in a subset of myeloma cells. Blocking its enzymatic activity using EZH2-specific inhibitors (E7438, CPI169, GSK126 and GSK343) causes global reduction of H3K27me3 levels and relieves the suppression of multiple tumor suppressor genes in myeloma cells. In agreement with the change in their gene profile, EZH2-specific inhibitor-treated myeloma cells become less proliferative and more differentiated compared to untreated cells. Therefore, targeting H3K27me3 marks in MM might not only restore the capacity of BMSCs to differentiate into mature osteoblasts, but also efficaciously eliminate myeloma cells in combination with other chemotherapies.

To determine if H3K27me3 levels were increased locally at the Runx2 and Osterix TSSs or globally in the whole chromatin, we treated MC4 cells or mouse BMSCs with 10 ng/ml TNF-α or co-cultured them with 5TGM1 cells for 2 days. Western blot analysis of whole cell lysates showed that TNF-α treatment and co-culture with 5TGM1 cells increased global H3K27me3 levels in both MC4 cells and mouse BMSCs (Figure 3-4A and B). This suggests either activation of the H3K27 methyltransferase complex PRC2 or

inhibition of the H3K27 demethylases, namely JMJD3 and UTX. Changes in expression levels, posttranscriptional modifications (PTMs) or recruiting measures of these histone modifiers as well as associated proteins might be the underlying mechanism(s) for the increased H3K27me3 marks. Therefore, we first measured by qPCR the expression levels of key mediators that control H3K27me3 levels in BMSCs. TNF-α treatment didn't affect the gene expression of PRC2 core components EZH2 or SUZ12, although it slightly decreased EED gene expression (Figure 3-5A). We found that JMJD3 was the predominant H3K27me2/3 demethylase in both MC4 cells and mouse BMSCs since its gene expression was 40 to 80 fold greater than that of UTX (Figure 3-5B). Both TNF-α treatment and co-culture with 5TGM1 cells decreased JMJD3 mRNA and protein levels in MC4 cells (Figures 3-5C). Similar changes were also found in mouse BMSCs (Figure 3-5D).

To correlate our *in vitro* findings with what actually occurs in MMBD, we isolated human BMSCs from marrow aspirates of age-matched healthy donors and MM patients. P0 BMSCs were obtained by culturing BM mononuclear cells in IMDM medium for 3 weeks. Only P2 and P3 BMSCs were used in the following experiments. Importantly, Western blot analysis showed that BMSCs from MM patients had markedly decreased JMJD3 protein levels compared to healthy donor BMSCs, even in the absence of myeloma cells for more than one month (Figure 3-6A). Densitometry analysis of Western blots by ImageJ further demonstrated the downregulation of JMJD3 in BMSCs from MM patients (Figure 3-6B). These data collectively suggest the potential

contribution of JMJD3 to the pathogenesis of lytic bone lesions in MM. Identifying negative regulators of JMJD3 may open novel therapeutic options to treat MMBD.

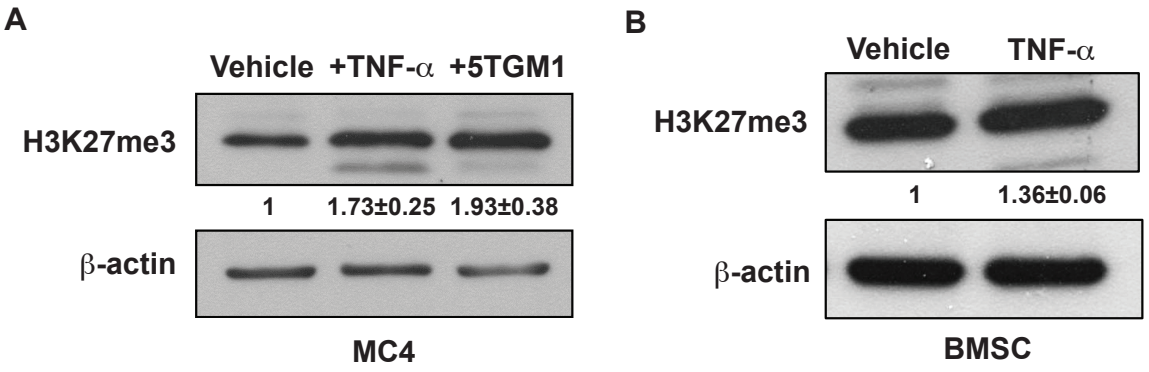

Figure 3-4: TNF-α and Myeloma Cells Increase Global H3K27me3 Levels in Stromal Cells.

MC4 cells **(A)** or mouse BMSCs **(B)** were treated with 10 ng/ml TNF-α or co-cultured with 5TGM1 cells for 2 days. Global H3K27me3 protein levels were measured by Western blot with β-actin as the internal control. The numbers shown in the Western blot indicate normalized densitometry values.

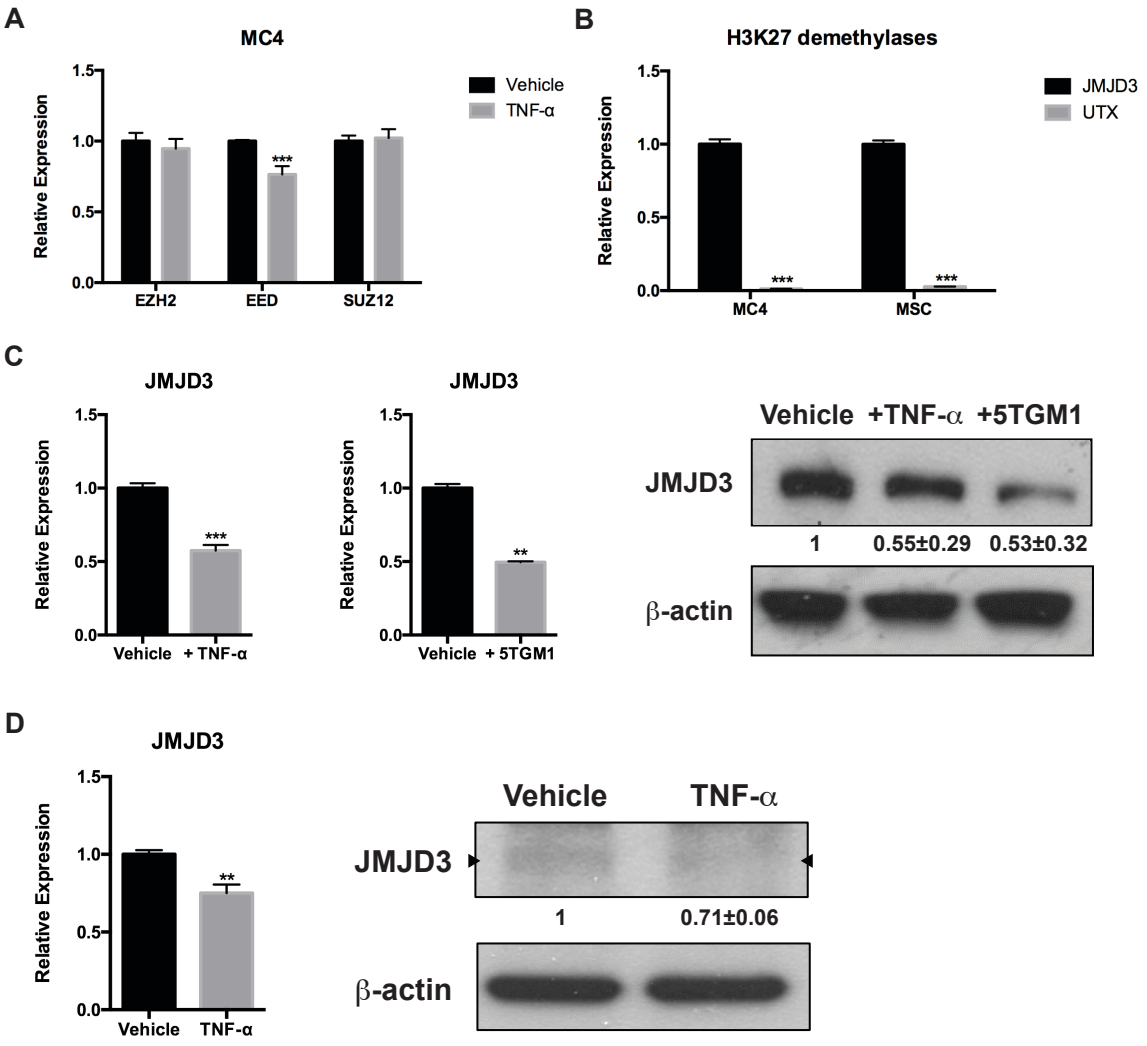

Figure 3-5: TNF-α and Myeloma Cells Decrease the Expression of the H3K27me2/3 Demethylase JMJD3 in Stromal Cells.

(A) MC4 cells were treated with 10 ng/ml TNF-α for 2 days. Relative mRNA levels of Ezh2, Eed, and Suz12 in MC4 cells were measured by qPCR with the geometric mean of the CT values of β-actin, GAPDH and HMBS as the internal control. **(B)** Relative mRNA levels of JMJD3 and UTX in untreated MC4 cells and mouse BMSCs were measured by qPCR with the geometric mean of the CT values of β-actin, GAPDH and HMBS as the internal control. MC4 cells **(C)** or mouse BMSCs **(D)** were treated with 10 ng/ml TNF-α or co-cultured with 5TGM1 cells for 2 days. JMJD3 mRNA level was measured using qPCR with the geometric mean of the CT values of β-actin, GAPDH and HMBS as the internal control. JMJD3 protein levels were measured by western with β-actin as the internal control. Error bars in each column graph represent SD of three biological replicates. * $p < 0.05$; ** $p < 0.01$; ***$p < 0.001$ compared with the black bar in individual group. The numbers shown in the Western blot indicate normalized densitometry values.

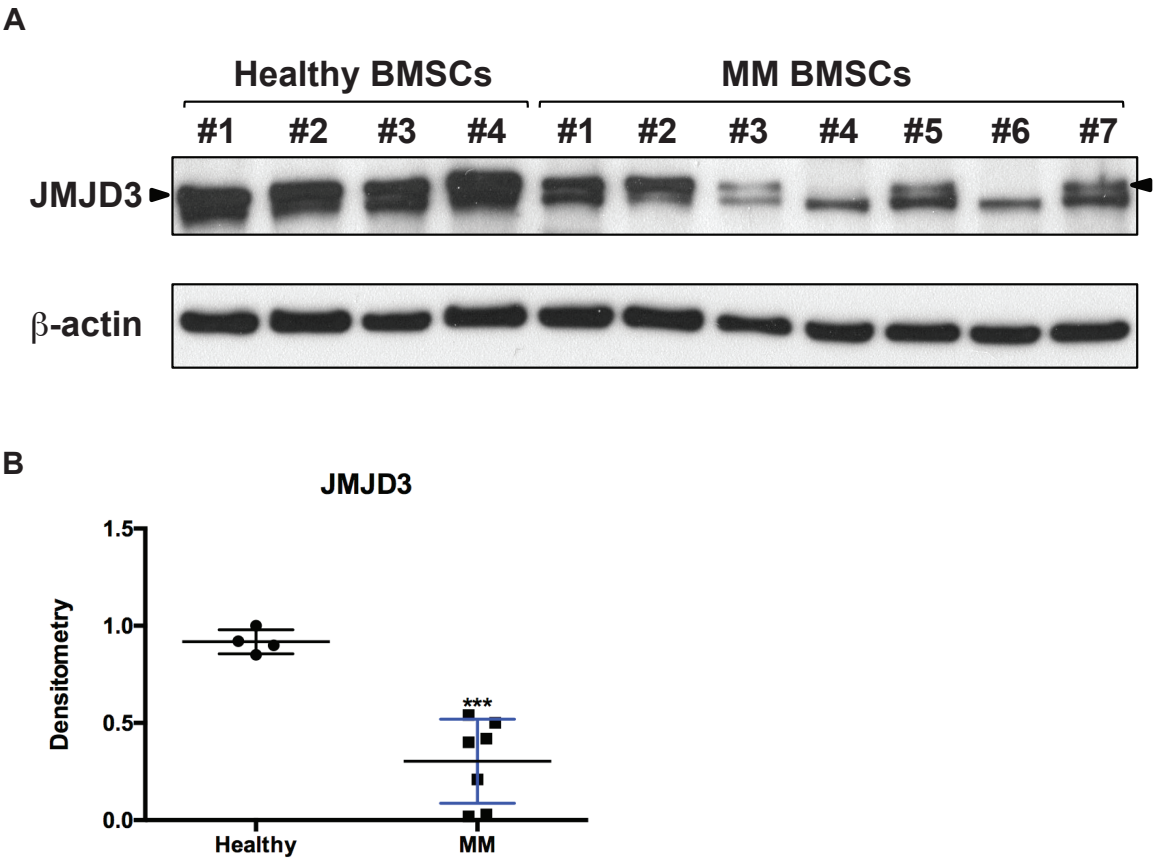

Figure 3-6: JMJD3 Protein Levels were Decreased in BMSCs Isolated from MM Patients.

(A) Human BMSCs were isolated from bone marrow of healthy donors and myeloma patients, and cultured until passage 3. JMJD3 protein levels in human BMSCs were measured using Western blot with β-actin as the internal control. **(B)** Densitometry analysis of JMJD3 protein levels in BMSCs isolated from healthy donors and MM patients was performed. Error bars in each column graph represent SD of three biological replicates. * $p < 0.05$; ** $p < 0.01$; ***$p < 0.001$ compared with the black bar in individual group. The numbers shown in the Western blot indicate normalized densitometry values.

3.2.3 JMJD3 contributes to normal osteoblast differentiation

We then assessed if JMJD3 regulated Runx2 and Osterix expression in MC4 cells. By delivering two different sets of ON-TARGETplus siRNAs that targeted mouse JMJD3 ORF regions, JMJD3 was knocked down by approximately 50% in MC4 cells (Figure 3-7A). The JMJD3 knockdown efficiency was optimized by adjusting the concentration of siRNAs used in transfection to mimic the extent of JMJD3 downregulation in MC4 cells treated with TNF-α or co-cultured with 5TGM1 cells. We used ONTARGETplus siRNAs because of their few off-target effects. Knockdown of JMJD3 in MC4 cells decreased the mRNA and protein levels of Runx2 and Osterix compared to MC4 cells transfected with scrambled siRNA (Figure 3-7B). Further supporting the role of JMJD3 in osteoblast differentiation, we cloned the full-length mouse JMJD3 gene into the iCumate-pLenti-Cloning-SV40-GFP lentiviral vector. JMJD3 expression was driven by a hybrid CMV promoter. MC4 cells stably infected with the JMJD3-overexpressing vector (MC4/JMJD3 cells) had a 30% increase in JMJD3 expression compared to cells infected with an empty vector (MC4/EV cells) (Figure 3-8A). Consistent with JMJD3 knockdown data, ectopic overexpression of JMJD3 in MC4/JMJD3 cells increased Runx2 and Osterix mRNA and protein levels (Figure 3-8B). To determine if JMJD3 overexpression in osteoblast precursors ultimately affects mineralization activity of mature osteoblasts, we cultured both MC4/EV and MC4/JMJD3 cells in osteogenic medium for 14 and 21 days. Mineralization activity was semi-quantitatively measured by Alizarin Red S, which forms a bright red stain after chelating calcium. As shown in Figure 3-9C, Alizarin Red S staining

showed enhanced mineralization of MC4/JMJD3 cells compared to MC4/EV cells after they were cultured in osteogenic medium for 14 and 21 days.

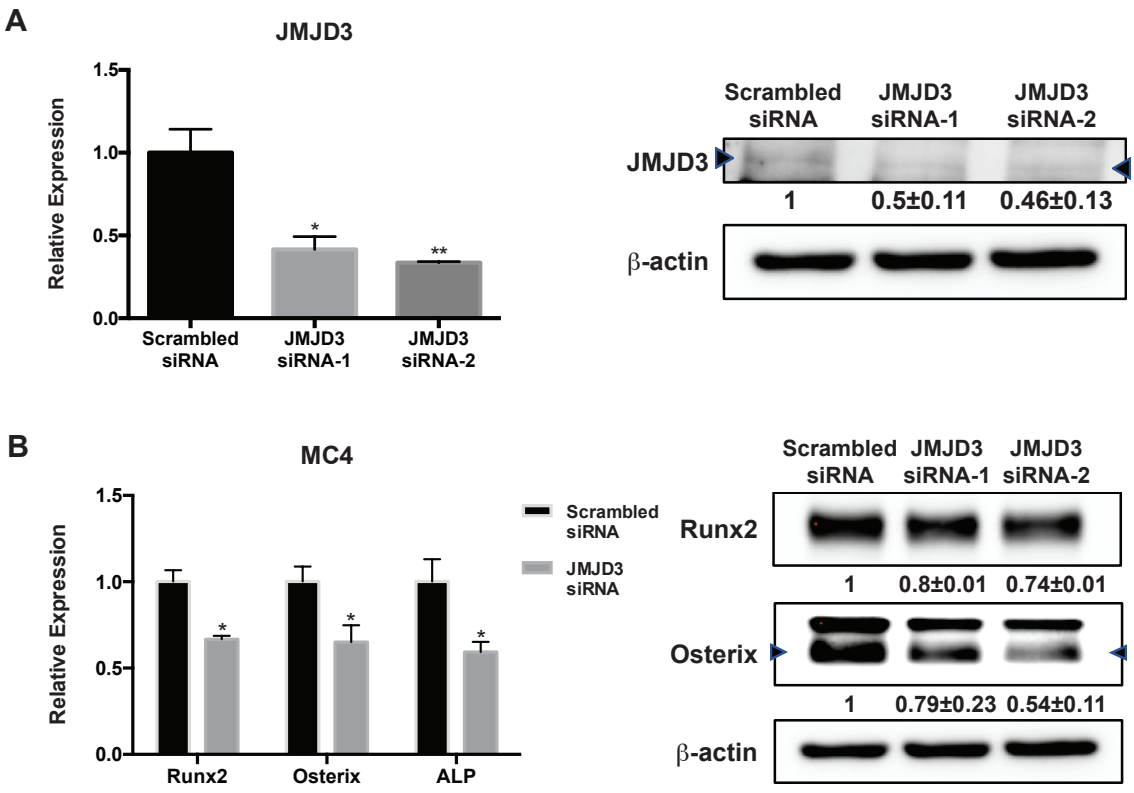

Figure 3-7: Knockdown of JMJD3 in MC4 Cells Decrease the Expression of Runx2, Osterix and ALP.

MC4 cells were transfected with scrambled siRNA or two different sets of JMJD3 siRNA. The mRNA and protein levels of JMJD3 **(A)**, Runx2, Osterix and ALP **(B)** were measured 48 hours later by qPCR and Western blot, respectively; Error bars in each column graph represent SD of three biological replicates. * $p < 0.05$; ** $p < 0.01$; ***$p < 0.001$ compared with the black bar in individual group. The numbers shown in the Western blot indicate normalized densitometry values.

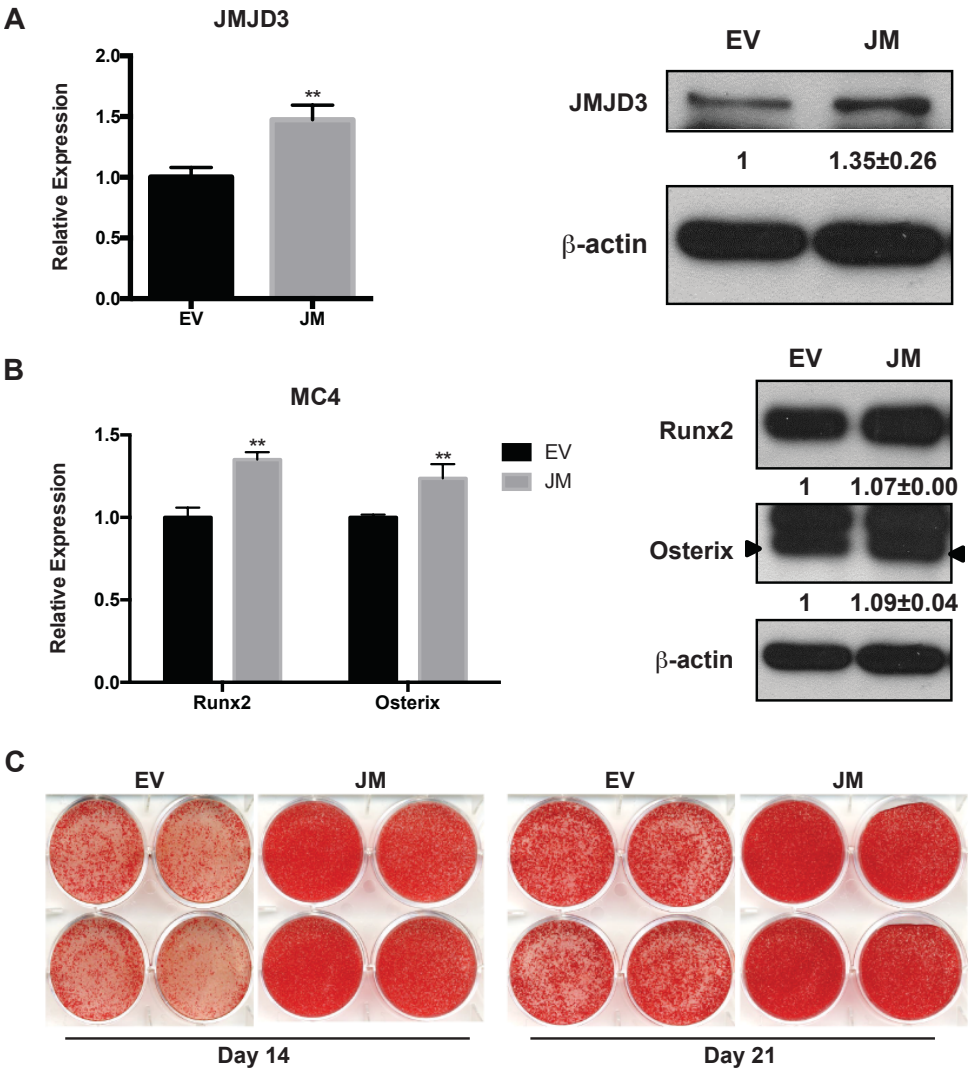

Figure 3-8: Ectopic Overexpression of JMJD3 in MC4 Cells Contributes to Osteoblast Differentiation and Mineralization.

MC4 cells were stably infected with an empty vector (EV) or JMJD3-overexpressing lentivirus (JM). The mRNA and protein levels of JMJD3 **(A)**, Runx2 and Osterix **(B)** were measured by qPCR and Western blot, respectively. **(C)** MC4 cells stably infected with EV or JM were cultured in osteogenic medium for 14 and 21 days. Alizarin Red S staining was performed to assess mineralization activity. Error bars in each column graph represent SD of three biological replicates. * $p < 0.05$; ** $p < 0.01$; ***$p < 0.001$ compared with the black bar in individual group. The numbers shown in the Western blot indicate normalized densitometry values.

3.3 Discussion

BMSCs from myeloma patients differ in many aspects compared with those from healthy donors, including spontaneous or myeloma-induced cytokine production[56,57], support of MM cell-mediated drug resistance[58,59], enhancement of MM proliferation[60], and impaired osteoblast differentiation potential[52-55]. Dysregulated gene and microRNA profiles in BMSCs from MM patients have been demonstrated and provide valuable insight into how they possibly contribute to distinct phenotypes of BMSCs in MM. However, how healthy BMSCs gradually become malfunctioning BMSCs in MM patients and how these defects are maintained in the absence of MM cells are still unclear.

We found co-occupancy of H3K4me3 and H3K27me3 marks, known as bivalent domains, at the Runx2 and Osterix TSSs in BMSCs, and that TNF-α and MM cells resolved these bivalent domains into transcriptionally silent domains. This observation is consistent with previous studies showing that histone methylation is constantly subject to the regulation of methyltransferases and demethylases, and that the equilibrium between H3K4me3 and H3K27me3 levels on bivalent domains is kept delicately balanced unless it's severely disturbed. Bivalent domains developmentally resolve into either transcriptionally active domains featured by predominance of H3K4me3 marks over H3K27me3 marks, or transcriptionally silent domains featured by predominance of H3K27me3 marks over H3K4me3 marks[96]. Each epigenetic state is stably maintained in a noise-resistant manner by self-enforcement, resulting from the ability of methylated histones to propagate the same type of methylation as well as remove the competing type of methylation on neighboring histones. In the scenario of transcriptionally silent

domains, H3K27me3 marks help recruit more PRC2 complexes that mediate H3K27 tri-methylation by binding its component EED[156]. Moreover, they destabilize the interaction between H3 and H3K4 methyltransferase complexes[105]. This demonstrates a positive feedback loop that reinforces its epigenetic memory in the absence of the initial developmental cue. Therefore, our results provide a mechanism by which suppression of osteoblast differentiation persists in MM patients after complete remission. Of note, we were unable to show that TNF-α increased H3K27me3 levels on the Runx2 promoter, which may contradict with the findings of two other studies that reported that silencing JMJD3 via knockdown or knockout techniques accumulates H3K27me3 marks on the Runx2 promoter[165,166]. One possible explanation is that TNF-α signaling in addition to decreasing JMJD3 expression may also affect other aspects of JMJD3, such as PTMs of JMJD3 following activation of a variety of kinases by TNF-α and its recruitment by accessary proteins to the Runx2 promoter.

We found persistently decreased expression of JMJD3 in BMSCs from myeloma patients compared to BMSCs from healthy donors, even after the BMSCs were cultured in the absence of myeloma cells for more than one month. These data suggest a potential role for loss of JMJD3 in the inhibition of osteoblast differentiation in MM. JMJD3 has been found to play essential roles in cell differentiation[167-169], inflammation[163,170], wound healing[171,172] and tumorigenesis[173-175]. Importantly, JMJD3 plays an important role in bone formation since it not only contributes to intramembranous and endochondral ossification, but also helps maintain bone homeostasis. Silencing JMJD3 suppresses osteoblast differentiation *in vitro* and *in*

vivo[165,166]. However, the role of JMJD3 in pathological bone disease has not been investigated. Our results suggest that loss of JMJD3 contributed to the pathogenesis and maintenance of MMBD. However, our study was limited to clarifying the demethylase-dependent function of JMJD3 on Runx2 and Osterix expression in BMSCs. The other genes affected by JMJD3 in BMSCs and the demethylase-independent functions of JMJD3 were not investigated and are beyond the scope of this study. We cannot exclude that decreased production of other factors regulated by JMJD3 may also participate in MMBD. The endogenous levels of osteogenic cytokine BMP2/4 in BMSCs have been reported to decrease in cells with JMJD3 knockdown[176]. Bcl-2, an anti-apoptotic protein, is also downregulated in JMJD3-knockdown MC3T3-E1 cells, inducing intrinsic mitochondrial apoptosis of osteoblasts[177]. In addition, JMJD3 interacts with other proteins independent of its demethylase activity to regulate their activity. Chen et al. reported that JMJD3 recruits the transcription elongation factors SPT6/16 to support productive transcriptional elongation[110]. Thus, characterizing if these other known effects of JMJD3 contribute to MMBD are fruitful areas for further investigation.

CHAPTER 4

TNF-α MEDIATED REGULATION OF JMJD3 GENE EXPRESSION

4.1 Introduction

Adaptation to the surrounding environment requires the ability of cells to convert ephemeral stimuli into persistent phenotypic changes. One excellent example is "ischemic preconditioning" of cardiomyocytes in patients who are suffering from coronary heart diseases. Recurrent ischemic episodes/angina switches cardiomyocytes to a long-lasting low metabolic status and protects patients against serious complications if myocardial infarction follows[178]. One underlying mechanism responsible for persistent phenotypic changes involves the PTMs on histone tails. The density and variety of PTMs on histone tails function as a platform that incorporates multiple on and off signals received by cells and convert them into a few directed outputs: increased or decreased gene expression. This feature of histone modifications is comparable to a multiple-inputs-single-output system[125]. Characterizing the signaling pathways that relay extracellular stimuli to histone PTMs in nucleus is imperative to understand how cells maintain their phenotypes after the initial stimuli are long gone, and may provide a way to reverse the unfavorable traits cells acquire in a pathological setting.

Emerging evidence has shown that varying levels of metabolites are able to reshape the chromatin landscape by directly regulating the enzymatic activity of histone modifiers. For example, accumulating β-hydroxybutarate during starvation inhibits HDAC activity and increases global histone acetylation[179]. α-ketoglutarate, an intermediate metabolite involved in Krebs Cycle and protein transamination, enhances the histone demethylating activity of Jumonji proteins[180,181]. Further, several signaling

cascades have been reported to catalyze PTMs of histone modifiers, modulate their expression levels or recruit them to specific loci by activated transcription factors. A well-studied signaling pathway capable of modifying histone tails is PI3K-AKT. Activation of PI3K-AKT in response to growth factors, hormones and extracellular matrix phosphorylates the histone modifiers that contain the sequence within AKT consensus motifs, including the H3K27 methyltransferase EZH2[182], the H2AK119 ubiquitin ligase BMI1[183], the histone acetyltransferase p300[184], the H3K9 demethylase KDM4B and the H3K4 methyltransferase SET1A (identified in large proteomic studies). Phosphorylation of these histone modifiers significantly changes their enzymatic activity or protein stability. Other signaling pathways that actively regulate histone modifications include MAPKs[185,186], NF-κB[187], PKA[188] and CDK1/2[189-193]. During osteoblast differentiation, sustained CDK1 activation in human BMSCs phosphorylates EZH2 at Thr 487, leading to compromised EZH2 methyltransferase activity, decreased global H3K27me3 levels and an accessible chromatin landscape on osteoblast-specific genes[193].

The H3K27me2/3 demethylase JMJD3 is presumably regulated by PTMs, upstream transcription factors and gene-specific recruitment, similar as other histone modifiers. In support of this notion, human JMJD3 possibly has 20 phosphorylation sites, 2 ubiquitination sites, 2 acetylation sites and 1 sumoylation site over the entire 1643 amino acid sequence based on the bioinformatics prediction of iPTMnet (http://research.bioinformatics.udel.edu/iptmnet/). Consistent with iPTMnet, the database PhosphoSitePlus (https://www.phosphosite.org/) shows 22 phosphorylation sites on human JMJD3 based on low- and high- throughput mass spectrometry (MS)

data collected over 16 years. However, the biological effects of individual PTM sites on JMJD3 function haven't been investigated experimentally and should be a promising direction for future research. Besides PTMs, the gene expression of JMJD3 is under the regulation of multiple signaling pathways. Yang et al. have reported that JMJD3 is markedly induced in the pre-osteoblast MC3T3-E1 cells treated with BMP-2 and that silencing of the downstream mediators Smad1/5 by siRNA inhibits JMJD3 induction[165]. In an independent study by Fei at al., ChIP analyses using anti-SMAD1/5 and anti-SMAD4 antibodies have shown that SMAD1/4/5 occupy the mouse JMJD3 promoter in undifferentiated R1 ES cells[194]. These studies collectively suggest the involvement of BMP2-SMADs signaling in activating JMJD3 gene transcription. Interestingly, SMADs directly interact with JMJD3 and recruit JMJD3 to their target genes[195,196]. Other recognized signaling pathways capable of regulating JMJD3 expression include NF-κB[163,197], STATs[170], and vitamin D[173,198]. In last chapter, we found decreased JMJD3 expression in BMSCs treated with TNF-α or co-cultured with myeloma cells for 2 days. In line with the *in vitro* findings, BMSCs isolated from MM patients expressed significantly lower levels of JMJD3 compared to BMSCs isolated from age-matched healthy donors. The molecular mechanism(s) responsible for the downregulation of JMJD3 in stromal cells in MM, however, remains to be determined.

We utilized MC4 cells treated with TNF-α as our *in vitro* model to pinpoint the signaling pathway(s) that inhibits JMJD3 expression. The activation of TNF-α signaling starts from binding of homotrimeric TNF-α to its cognate receptors: TNF receptor type 1 (TNF-R1) and TNF receptor type 2 (TNF-R2). This interaction is followed by

reorganization of pre-assembled TNF receptors, dissociation of silencer of death domain (SODD) to expose the death domain (DD) of TNF receptors, and subsequent recruitment of death domain-containing adaptor protein TRADD. Other adaptor proteins, kinases, ubiquitin ligases and proteases then join to mediate the pleiotropic biological effects of TNF-α signaling. The stereotyped mediators that TNF-α activates include NF-κB, ERK, JNK, p38 and caspases[40]. PI3K/AKT[199] and STATs[200] have also been reported to be activated by TNF-α in certain cell types. Gilbert et al. reported that pretreatment of BMSCs and MC3T3-E1 cells with three different caspase inhibitors fails to prevent the inhibitory effects of TNF-α on osteoblast differentiation, suggesting the unimportant role of TNF-α-induced apoptosis in regulating osteoblast differentiation[201]. This finding encouraged us to focus on the pathways other than apoptosis. Despite of the extensive research for more than 40 years, the signaling map of TNF-α is far from complete. The possible existence of unidentified mediators of TNF-α signaling might be the caveat of our study.

As discussed in the Chapter 1.3, we showed that Gfi1 expression in BMSCs is induced by MM cells to mediate long-term suppression of osteoblast differentiation[64]. Gfi1 recruits the histone modifiers HDAC1 and EZH2 to the Runx2 promoter, which cause H3K9ac deacetylation and H3K27 tri-methylation, respectively. These epigenetic changes inhibit Runx2 productive transcription and persist after removal of myeloma cells. Ectopic overexpression of Gfi1 in stromal cells is sufficient to maintain Runx2 suppression in osteogenic conditions[78]. Considering our recent finding that decreased JMJD3 expression in BMSCs similarly contributes to the repressive remodeling of

epigenetic landscape on the Runx2 promoter, it's intriguing to investigate the possible interaction between Gfi1 and JMJD3. Our preliminary studies identified multiple Gfi1 binding sites existing on the mouse and human JMJD3 promoter based on the bioinformatics prediction of JASPAR core database (http://jaspar.genereg.net/). It's currently unknowing if Gfi1 could inhibit JMJD3 transcription by bringing repressive histone marks to the JMJD3 promoter as it does to the Runx2 promoter. If so, this may explain the sustained suppression of JMJD3 expression in BMSCs isolated from MM patients compared to BMSCs from healthy donors, even after MM cells were removed more than one month before.

4.2 Results

4.2.1 NF-κB pathway activation is responsible for the downregulation of JMJD3 induced by prolonged TNF-α Treatment

TNF-α activates several signaling pathways, including NF-κB, JNK, p38, ERK1/2 and apoptosis. We investigated the detailed molecular mechanism(s) that regulated JMJD3 expression to identify targetable proteins to mitigate the effects of decreased JMJD3 in MMBD, since no specific JMJD3 agonist has been developed. MC4 cells were treated with 10 ng/ml TNF-α for 0.5, 1, 2, 6, 24 and 30 hours. qPCR data showed that JMJD3 gene expression was initially induced in MC4 cells treated with TNF-α but became persistently lower after 6 hours compared to MC4 cells treated with vehicle (Figure 4-1). This finding suggests that prolonged TNF-α treatment, which models the chronic elevation of TNF-α levels in bone marrow microenvironment in MM, is needed to decrease JMJD3 gene expression. To determine the signaling pathway(s) responsible for the downregulation of JMJD3 by TNF-α, MC4 cells were pretreated for 2 hours with 70 μM NF-κB inhibitor quinazoline (QNZ), 10 μM JNK inhibitor SP600125, 10 μM p38 inhibitor SB203580 or 20 μM MEK1 inhibitor PD98059, followed by TNF-α treatment for 24 hours. This experimental regimen was utilized because TNF-α consistently decreased JMJD3 expression in MC4 cells after 24-hour treatment and the cytotoxicity of each inhibitor was minimized with shorter exposure time. The optimal concentration of each inhibitor needed to block individual signaling pathway in MC4 cells was also determined

experimentally (Figure 4-2). qPCR data showed that none of the MAPK inhibitors reversed the inhibition of JMJD3 expression in MC4 cells treated with TNF-α (Figure 4-3A). In contrast, the NF-κB inhibitor QNZ partially rescued the inhibition of JMJD3 expression (Figure 4-3B). QNZ is a potent inhibitor of NF-κB transcriptional activation permeable to cells. QNZ was selected over BAY 11-7082 and Bortezomib in our study due to its minimal cytotoxicity and high specificity (data not shown).

Chauhan et al. has reported that adhesion of the MM cell line IM-9 with the BMSC line LP101 induces IL-6 expression in LP101 cells. A single base pair deletion of the NF-κB binding site on the IL-6 promoter blocks MM-mediated IL-6 induction. This finding indicates the activation of NF-κB signaling in stromal cells directly co-cultured with myeloma cells in their system, although phosphorylation and nuclear translocation of p65, the hallmark of NF-κB activation, was not shown. We investigated if the myeloma cell line 5TGM1 could activate NF-κB signaling in MC4 cells the same way as TNF-α treatment to inhibit JMJD3 gene expression. MC4 cells were treated with 10 ng/ml TNF-α, the conditioned medium from 5TGM1 cells, or directly co-cultured with 5TGM1 cells for 15 and 30 minutes. IκB degradation was measured by Western blot as the readout of NF-κB activation. Western blot showed that TNF-α rapidly induced IκB degradation in MC4 cells. Conversely, neither the conditioned medium from 5TGM1 cells nor the direct contact with 5TGM1 cells degraded IκB in MC4 cells at 15 and 30 minutes, suggesting the lack of NF-κB activation in both conditions (Figure 4-3C). These results imply either a completely different mechanism by which 5TGM1 cells inhibit JMJD3 gene expression in MC4 cells through direct cell-cell interaction or inadequate levels of TNF-α expressed by

MM cells to show similar results. However, investigating a novel mechanism responsible for these results is beyond the scope of my dissertation.

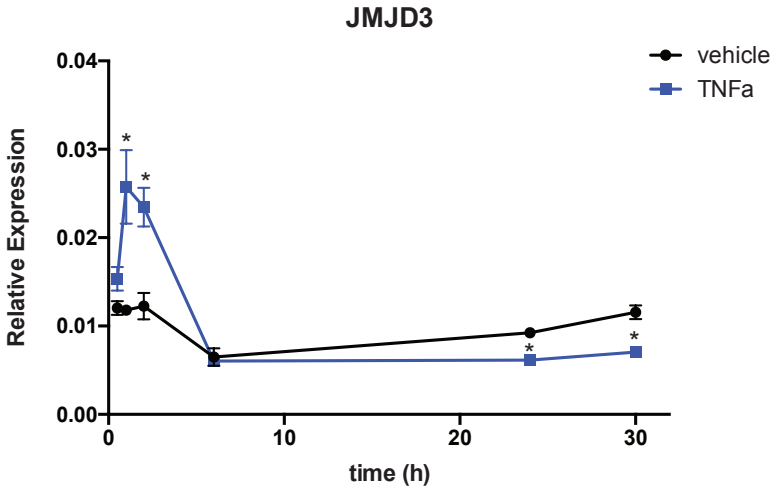

Figure 4-1: TNF-α Regulates JMJD3 Gene Expression in a Time-dependent Manner.

MC4 cells were treated with 10 ng/ml TNF-α for 0.5, 1, 2, 6, 24 and 30 hours. JMJD3 mRNA level was measured using qPCR with the geometric mean of the CT values of β-actin, GAPDH and HMBS as the internal control. Error bars in each column graph represent SD of three biological replicates. * $p < 0.05$; ** $p < 0.01$; ***$p < 0.001$ compared with the black bar in individual group.

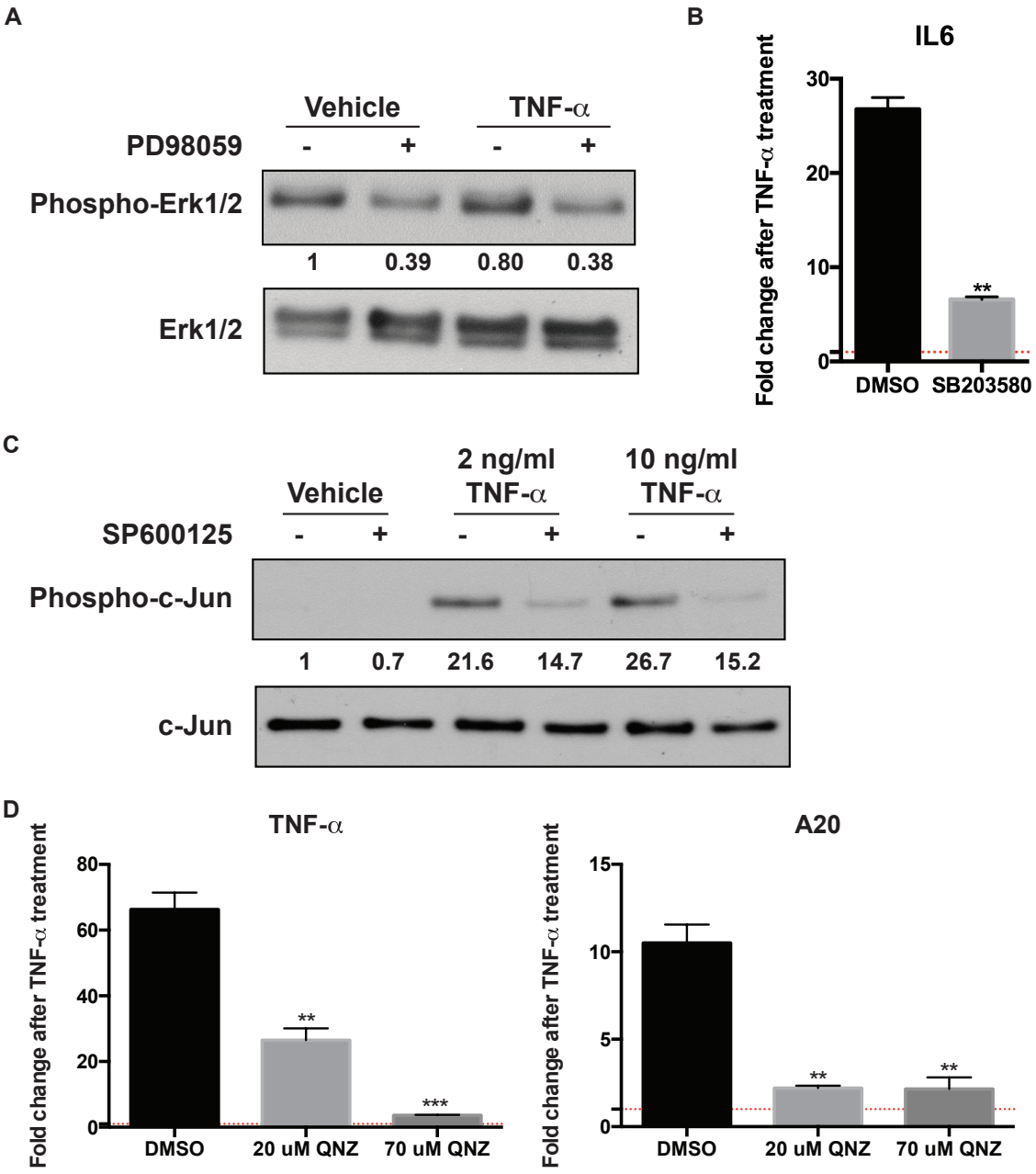

Figure 4-2: Determining the Optimal Concentration of Small Molecule Inhibitors to Block the Signaling Pathways Activated by TNF-α.

(A) MC4 cells were pretreated with DMSO or 20 μM PD98059 for 2 hours, followed by 10 ng/ml TNF-α treatment for 15 minutes. Phospho-Erk1/2 protein level was measured

by western bot with total Erk1/2 as the internal control; **(B)** p38 activation has been reported to mediate IL-6 induction by TNF-α treatment. MC4 cells were pretreated with DMSO or 10 μM SB203580 for 2 hours, followed by 10 ng/ml TNF-a treatment for 6 hours. IL-6 mRNA level was measured using qPCR with the geometric mean of the CT values of β-actin, GAPDH and HMBS as the internal control; **(C)** MC4 cells were pretreated with DMSO or 10 μM SP600125 for 2 hours, followed by 2 or 10 ng/ml TNF-α treatment for 15 minutes. Phospho-c-Jun protein level was measured by western bot with total c-Jun as the internal control; **(D)** MC4 cells were pretreated with DMSO, 20 or 70 μM QNZ for 2 hours, followed by 10 ng/ml TNF-α treatment for 2 hours. The mRNA levels of TNF-α and A20, which have been shown to be induced by TNF-α treatment, were measured using qPCR with the geometric mean of the CT values of β-actin, GAPDH and HMBS as the internal control; The red dotted line in each column graph represents the basal level of the measured gene before TNF-α treatment. Error bars in each column graph represent SD of three biological replicates. * $p < 0.05$; ** $p < 0.01$; ***$p < 0.001$ compared with the black bar in individual group. The numbers shown in the Western blot indicate normalized densitometry values.

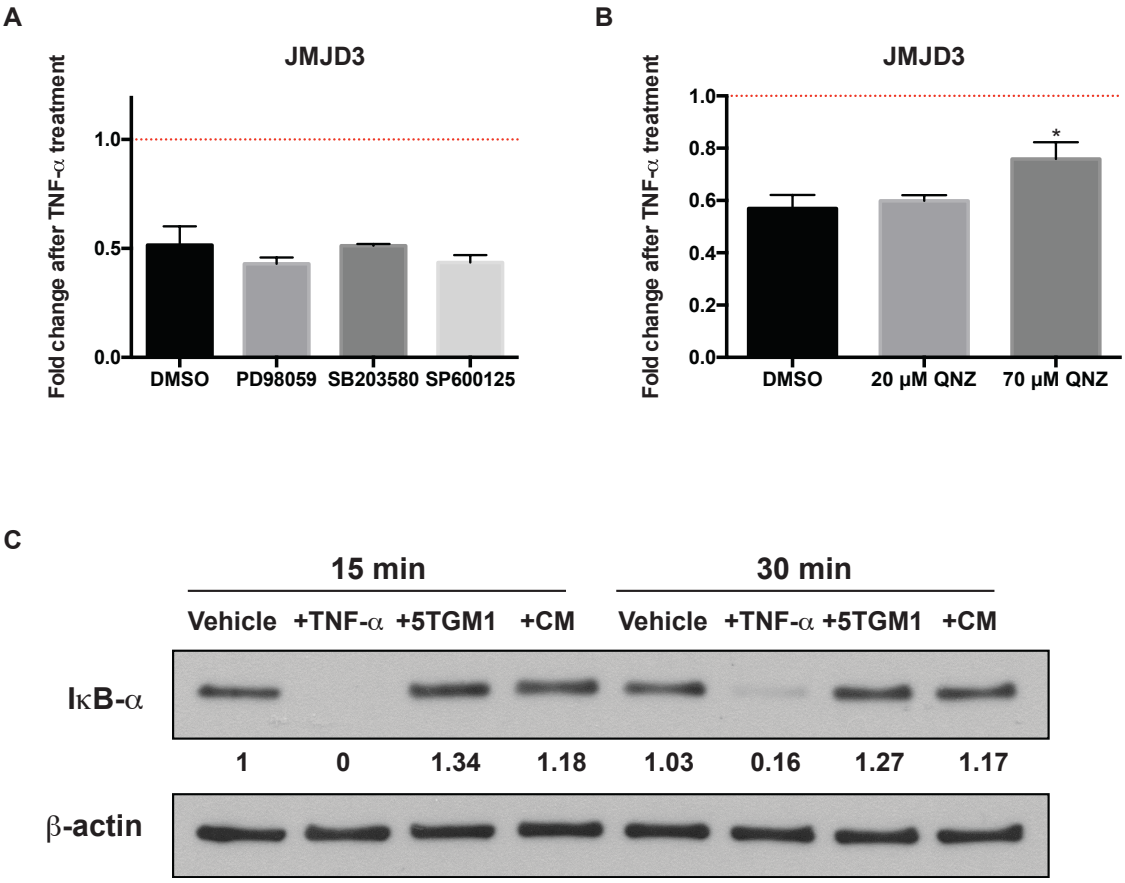

Figure 4-3: The Activation of NF-κB Signaling by TNF-α Mediates the Inhibition of JMJD3 Gene Expression.

MC4 cells were pretreated with equal volume of DMSO, 20 μM MEK1 inhibitor PD98059, 10 μM p38 inhibitor SB203580, 10 μM JNK inhibitor SP600125 **(A)**, or 20 and 70 μM NF-κB inhibitor QNZ **(B)** for 2 hours. MC4 cells were then treated with 10 ng/ml TNF-α for 24 hours. JMJD3 mRNA level was measured using qPCR with the geometric mean of the CT values of β-actin, GAPDH and HMBS as the internal control; **(C)** The conditioned medium (CM) was collected by culturing 10^6/ml 5TGM1 cells for 2 days. MC4 cells were treated with 10 ng/ml TNF-α, CM or co-cultured with 5TGM1 cells for 15 and 30 minutes. IκB-α protein level was measured by western bot with β-actin as the internal control. Error bars in each column graph represent SD of three biological replicates. * $p < 0.05$; ** $p < 0.01$; ***$p < 0.001$ compared with the black bar in individual group. The numbers shown in the Western blot indicate normalized densitometry values.

4.2.2 Induction of Gfi1 by TNF-α and MM cells is not responsible for the downregulation of JMJD3

We reported that Gfi1 induced by MM cells and TNF-α treatment represses Runx2 expression and osteoblast differentiation in BMSCs from MM patients. As a transcriptional repressor, Gfi1 binds to its cognate consensus DNA sequence AA(T/G)C and recruits histone modifiers, including LSD-1/CoRest, HDAC1/2/3, G9a and EZH2, to reversibly and irreversibly impair target gene transcription. The inverse correlation of Gfi1 and JMJD3 expression levels and the shared functionality in regulating osteoblast differentiation encouraged us to investigate their possible interactions. We found that multiple Gfi1 binding sites are present on the human (Table 4-1A) and mouse (Table 4-1B) JMJD3 promoters based on the bioinformatics analysis using the JASPAR core database (http://jaspar.genereg.net/). It's reasonable to infer that targeting of Gfi1 to the JMJD3 promoter should accumulate transcriptionally repressive histone marks and block JMJD3 gene transcription. To validate if JMJD3 expression was regulated by Gfi1 in BMSCs, we transiently overexpressed flag-tagged Gfi1 in MC4 cells (Figure 4-4A). MC4 cells transfected with a Gfi1-overexpressing plasmid had a similar expression level of JMJD3 compared to MC4 cells transfected with an empty vector (Figure 4-4B). This finding argues against the transcriptional regulation of JMJD3 by Gfi1 in MC4 cells. Further supporting this, similar findings were also obtained in 293FT cells (Figure 4-5). These results collectively demonstrate that MM cells employ at least two independent

mechanisms to induce long-term suppression of osteoblast differentiation, persistent upregulation of Gfi1 and downregulation of JMJD3.

A. Predicted Gfi1 binding sites on the human JMJD3 promoter

Predicted Site Sequence	Strand	Start	End	Relative Score
CCAATCTCCA	-1	-2000	-1991	0.865
CAAATCTGCC	-1	-1930	-1921	0.873
TTAATCCCTC	-1	-1381	-1372	0.812
TAAAGCTCTG	1	-1374	-1365	0.827
CTAATCTCTA	-1	-877	-868	0.823
CCAATCTAAT	-1	-872	-863	0.827
TTAATCATAG	-1	-828	-819	0.837

B. Predicted Gfi1 binding sites on the mouse JMJD3 promoter

Predicted Site Sequence	Strand	Start	End	Relative Score
CAAATCCCCA	-1	-1877	-1868	0.865
TAAATCATTT	-1	-1736	-1727	0.866
AGAATCTGTG	1	-1483	-1474	0.845
GAAATAACAC	1	-935	-926	0.807
TAAGTCTCTG	1	-856	-847	0.806
GAAAACACTG	1	-768	-759	0.842
CCAGTCACAG	1	-512	-503	0.826
CGAATCTCCC	1	-116	-107	0.857

Table 4-1: Prediction of Gfi1 Binding Sites on the JMJD3 Promoter Using JASPAR Core Database.

2000 bp DNA sequences upstream of the TSSs of both the mouse and human JMJD3 genes were obtained using Ensembl Genomes (http://ensemblgenomes.org/) and regarded as their promoter regions. These sequences were subsequently analyzed using JASPAR core database to predict Gfi1 binding sites based on Gfi1 DNA-binding matrix profile. In the column “Strand”, “1” indicates leading DNA strand and “-1” indicates complementary DNA strand. The column “Start” and “End” marks the position of the potential Gfi1 binding sites relative to the first transcribed nucleotide of JMJD3.

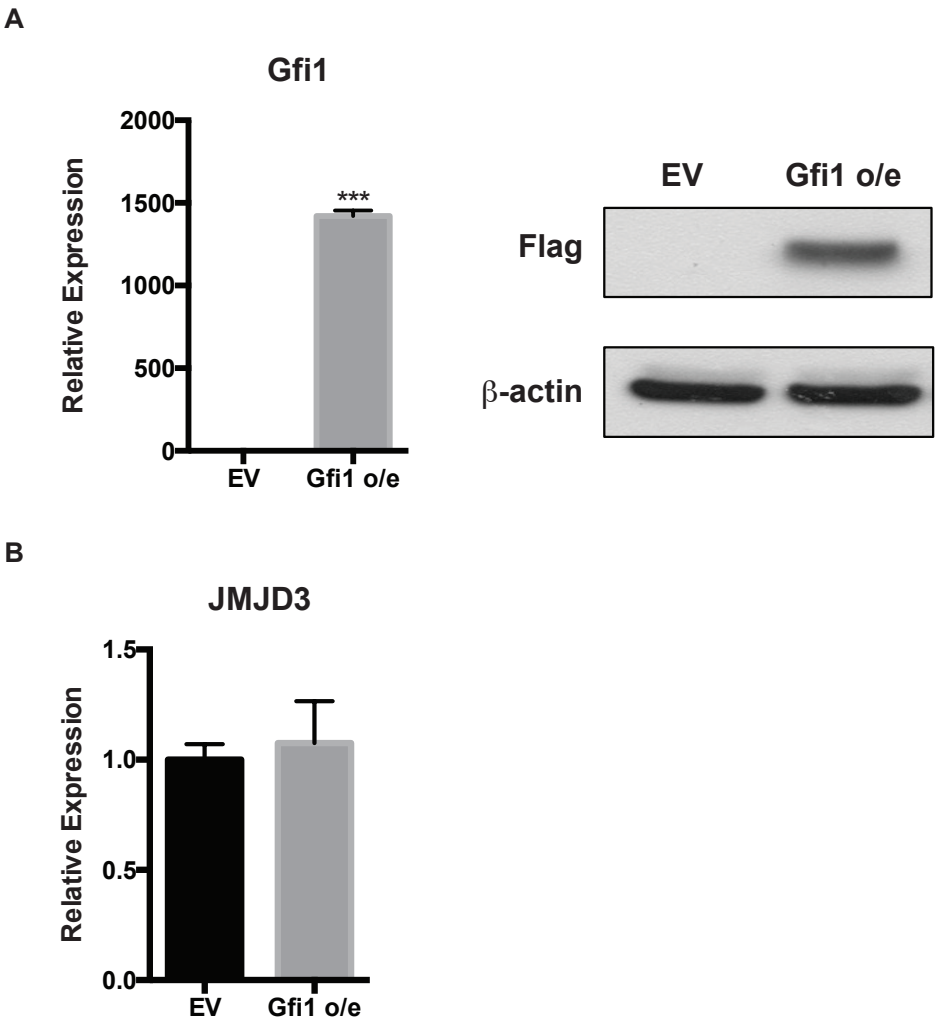

Figure 4-4: Gfi1 does not Regulate JMJD3 Gene Expression in MC4 cells.

MC4 cells were transiently transfected with empty pcDNA3.1 vector (EV) or flag-tagged Gfi1-overexpressing pcDNA3.1 (Gfi1 o/e) for 2 days. (A) Gfi1 mRNA level was measured using qPCR with the geometric mean of the CT values of β-actin, GAPDH and HMBS as the internal control. Gfi1 protein levels were measured by western with β-actin as the internal control; (B) JMJD3 mRNA level was measured using qPCR with the geometric mean of the CT values of β-actin, GAPDH and HMBS as the internal control. Error bars in each column graph represent SD of three biological replicates. * $p < 0.05$; ** $p < 0.01$; ***$p < 0.001$ compared with the black bar in individual group.

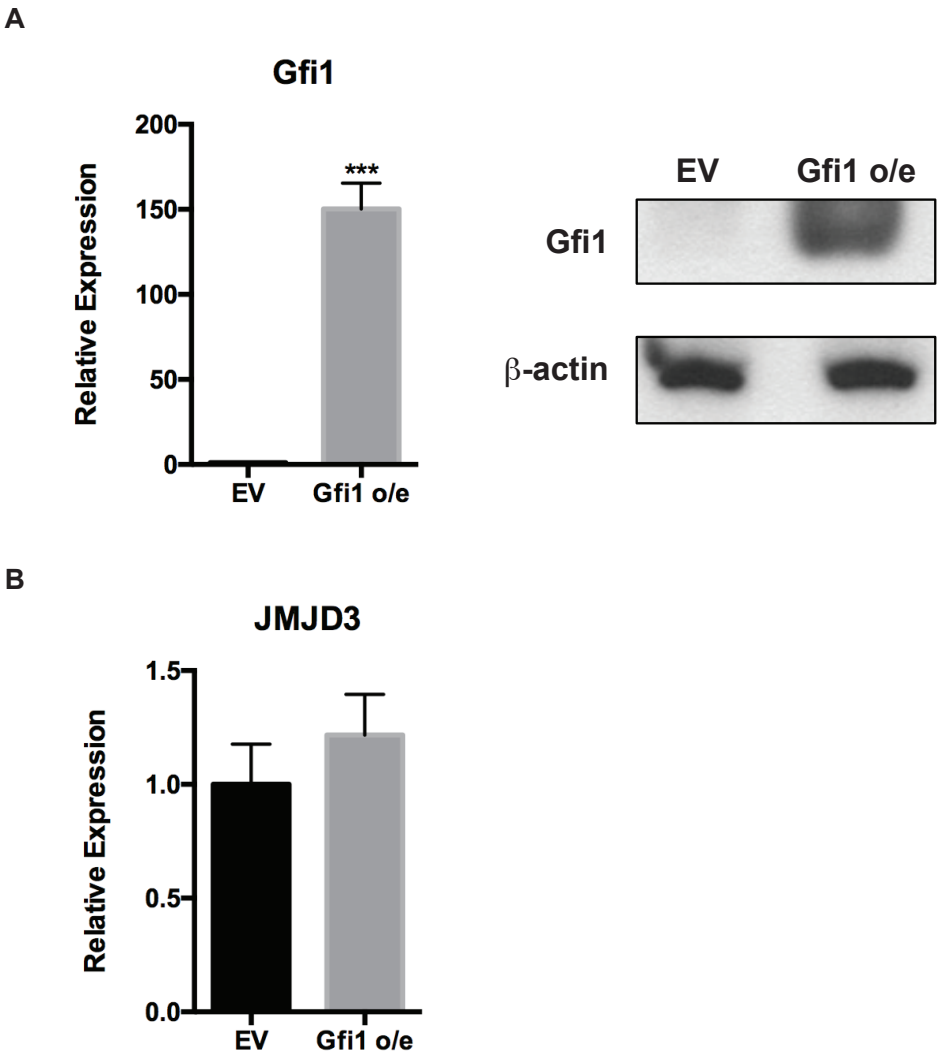

Figure 4-5: Gfi1 does not Regulate JMJD3 Gene Expression in 293FT cells.

293FT cells were transiently transfected with empty pcDNA3.1 vector (EV) or flag-tagged Gfi1-overexpressing pcDNA3.1 (Gfi1 o/e) for 2 days. (A) Gfi1 mRNA level was measured using qPCR with the geometric mean of the CT values of β-actin, GAPDH and HMBS as the internal control. Gfi1 protein levels were measured by western with β-actin as the internal control; (B) JMJD3 mRNA level was measured using qPCR with the geometric mean of the CT values of β-actin, GAPDH and HMBS as the internal control. Error bars in each column graph represent SD of three biological replicates. * $p < 0.05$; ** $p < 0.01$; ***$p < 0.001$ compared with the black bar in individual group.

4.3 Discussion

We have shown that suppressed JMJD3 expression in BMSCs impaired osteoblast differentiation by resolving the bivalent domains on the Runx2 and Osterix promoters to transcriptionally silent domains. This molecular mechanism, together with elevated Gfi1 expression in BMSCs, contributes to the protracted lytic bone lesions in MM patients. One would assume that activating JMJD3 enzymatic activity or restoring its expression level in BMSCs could mitigate MMBD. However, no specific JMJD3 agonist is currently available for both clinical and research use. Further, it is unlikely one will be developed in the near future due to the conserved amino acid sequences shared by a group of 27 proteins, 15 of which possess demethylase activity[202].

By determining the upstream signaling that regulates JMJD3 transcription, we suggest alternative ways to target JMJD3 and possibly reverse MMBD in patients. One solution is to use a JMJD3 physiological agonist—the H3K27 methyltransferase EZH2 inhibitor—to counteract the accumulation of repressive H3K27me3 marks on genes orchestrating osteoblast differentiation. In agreement with the feasibility of this notion, Adamik et al. reported that blocking EZH2 enzymatic activity with the small molecule inhibitor GSK126 reverses MM-induced suppression of osteoblast differentiation[78]. In addition, myeloma cells isolated from MM patients and MM cell lines express higher levels of EZH2 compared to their control counterparts[203,204]. Inhibition of EZH2 using small molecules arrests tumor growth and sensitizes tumor cells to routine MM chemotherapy[204,205]. The other solution involves targeting the NF-κB signaling pathway

that we have shown regulated JMJD3 transcription. Inhibiting NF-κB activation in MM patients could potentially mitigate MMBD and offers several advantages. First, NF-κB serves as the signaling hub activated by a variety of inflammatory cytokines elevated in the bone marrow microenvironment of MM patients, including TNF-α, IL-1β[21,206], B-cell activating factor (BAFF)[207,208], a proliferation-inducing ligand (APRIL)[207] and lymphotoxin[209]. Antagonizing NF-κB should be more effective than targeting an individual cytokine. Second, JMJD3 has been reported to exert its biological functions without demethylating associated proteins. For example, the promoting effects of JMJD3 on target gene expression not only depends on its activity to remodel surrounding epigenetic landscape, but also recruits the transcription elongation factors SPT6/16 to ensure productive transcription[110]. Therefore, restoring JMJD3 expression in BMSCs with NF-κB inhibitors alleviates MM-induced suppression of osteoblast differentiation both dependent and independent of its demethylase activity.

It's worth noting that previous studies have shown transient upregulation of JMJD3 transcription by activating NF-κB in macrophages[163] and vascular endothelial cells[210]. They are consistent with our results in MC4 cells exposed to TNF-α treatment within 6 hours. Interestingly, after 6 hours JMJD3 expression decreased and remained suppressed thereafter. This result demonstrates the time-dependent regulation of JMJD3 by NF-κB signaling and supports the contribution of chronic inflammation to bone lesions in MM patients. The detailed mechanisms of how NF-κB activation inhibits JMJD3 expression still remains to be determined in future studies. Two studies may shed light on this research question. Levy et al. have reported that mono-methylation

of activated p65 by SETD6 in nucleus creates a docking site for the H3K9 methyltransferase G9a-like protein (GLP) and subsequently represses NF-κB target gene expression by inducing H3K9 methylation, which is the epigenetic mark of heterochromatin[187]. This study could explain both the temporal changes of JMJD3 expression following NF-κB activation and the sustained suppression of JMJD3 expression in BMSCs isolated from MM patients. Another study by Yamazaki et al. found that activated p65 complexes with SMAD1/4 and interferes with their DNA binding activity[211]. As discussed in Chapter 4.1, SMAD1/4 transcriptionally activate JMJD3. Therefore, disruption of SMADs by NF-κB activation should inhibit JMJD3 gene expression.

CHAPTER 5

JMJD3 OVEREXPRESSION IN MC4 CELLS PARTIALLY OVERCOMES THE SUPPRESSION OF OSTEOBLAST DIFFERENTIATION BY TNF-α

5.1 Introduction

Multiple molecular mechanisms have been reported to be responsible for TNF-α-induced suppression of osteoblast differentiation. Gilbert et al has shown that TNF-α inhibits the expression of insulin-like growth factor I (IGF-1), a growth factor that stimulates osteoblast differentiation via activating mammalian target of rapamycin (mTOR) pathway[212]. They have also found that TNF-α shortens the half-life of Runx2 mRNA from 1.8 h to 0.9 h[213]. Consistent with the inhibitory effects of TNF-α on Runx2 expression, Kaneki et al has reported that TNF-α induces the expression of Runx2 E3 ubiquitin ligases, Smurf1 and Smurf2, in osteoblast precursor cell lines, resulting in proteasome-mediated degradation of endogenous Runx2 protein. Treating cells with the proteasomal inhibitor MG132 or transfecting cells with Smurf1/2 siRNAs blocks Runx2 degradation[214]. Lu et al has reported that TNF-a markedly increases the gene expression of paired related homeobox protein (Prx1) that accumulates on the promoter regions of Runx2 and Osterix, and impairs their transcription[215]. In addition to inducing negative regulators of osteoblast differentiation, TNF-α disrupts the osteogenic BMP-2 signaling by preventing phosphorylation of SMADs[216], interfering with the DNA binding of SMADs[217], and increasing the transcriptional repressor Msx2[218]. Other mechanisms have been thoroughly discussed in the review by Osta et al.

We have shown that prolonged TNF-α treatment decreased JMJD3 gene expression in BMSCs. Further, JMJD3 knockdown using siRNA alone was sufficient to inhibit osteoblast differentiation. Our findings collectively suggest a novel mechanism by

which TNF-α negatively regulates osteoblast differentiation. However, little is known about how much JMJD3 downregulation in BMSCs contributes to the suppression of osteoblast differentiation in the inflammatory microenvironment of patients with MMBD. Currently over ten molecular mechanisms have been recognized to be involved in TNF-α-induced suppression of osteoblast differentiation[219]. All the studies, including ours, could just reveal a tip of "iceberg". More mechanisms are expected to be uncovered in future studies. Therefore, determining the relative contribution of JMJD3 dysregulation is crucial to understanding its importance compared to other mechanisms and justifying possible epigenetic therapies in the management of MMBD.

To accurately assess the role of JMJD3 downregulation in TNF-α-induced suppression of osteoblast differentiation, we ectopically overexpressed wild-type mouse JMJD3 in MC4 cells using lentiviruses and selected the colony that approximately maintains the baseline JMJD3 level after TNF-α treatment. Using a colony with dramatic increase in JMJD3 expression instead will exaggerate the importance of decreased JMJD3 expression in TNF-α-induced suppression of osteoblastogenesis. The gene expression of osteoblast marker genes and the ALP activity was subsequently compared between MC4 cells with or without JMJD3 overexpression in presence of TNF-α. Also, we purposely avoided using NF-κB inhibitors in these experiments since NF-κB activation should have unidentified effects on osteoblast differentiation independent of JMJD3. Using NF-κB inhibitors to determine the relative contribution of JMJD3 downregulation to TNF-α-induced suppression of osteoblast differentiation will inevitably introduce confounding factors.

5.2 Results

To determine the relative contribution of JMJD3 downregulation to TNF-α-induced suppression of osteoblast differentiation, we used MC4/JMJD3 cells that stably overexpressed mouse wild-type JMJD3 and their control counterpart MC4/EV cells that harbored an empty vector. Both PCR and Western blot showed that MC4/JMJD3 cells maintained increased JMJD3 expression level following a 2-day treatment of 10 ng/ml TNF-α compared with MC4/EV cells (Figure 5-1A and B). Importantly, the mRNA and protein levels of Runx2 and Osterix were less inhibited by TNF-α in MC4/JMJD3 cells compared to MC4/EV cells (Figure 5-1A and B). TNF-α has been reported by others to inhibit ALP activity during induction of osteoblast differentiation. To determine if JMJD3 overexpression in MC4 cells could rescue the impaired ALP activity in presence of TNF-α, we cultured MC4/EV or MC4/JMJD3 cells in osteogenic medium with or without 5 ng/ml TNF-α for 7 days. 5 ng/ml instead of 10 ng/ml TNF-α was used to minimize the cytotoxic effects of TNF-α on MC4 cells. In agreement with the expression data, ALP staining showed that the violet intensity that positively correlates with ALP activity was less inhibited by TNF-α in MC4/JMJD3 cells compared to MC4/EV cells (Figure 5-2). These data suggest that JMJD3 downregulation in stromal cells is partially responsible for the suppression of osteoblast differentiation induced by TNF-α.

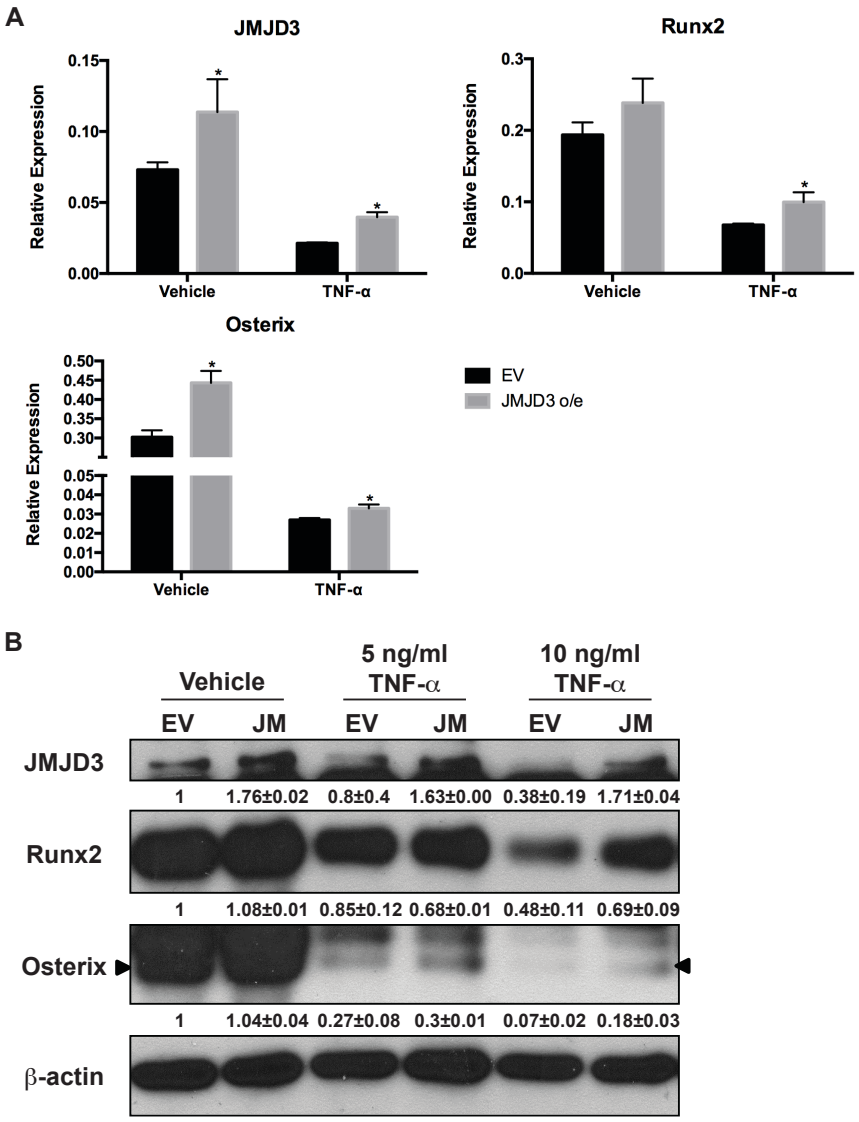

Figure 5-1: JMJD3 Overexpression in MC4 Cells Partially Rescued the Inhibition of Runx2 and Osterix by TNF-α.

MC4 cells stably infected with EV or JM were cultured in osteogenic medium with or without TNF-α for 2 days. The concentration of TNF-α used in each experiment is indicated in each graph. **(A)** The mRNA levels of JMJD3, Runx2 and Osterix were measured using qPCR with the geometric mean of the CT values of β-actin, GAPDH and HMBS as the internal control; **(B)** The protein levels of JMJD3, Runx2 and Osterix were measured by western with β-actin as the internal control; Error bars in each column graph represent SD of three biological replicates. * $p < 0.05$; ** $p < 0.01$; ***$p < 0.001$ compared with the black bar in individual group. The numbers shown in the Western blot indicate normalized densitometry values.

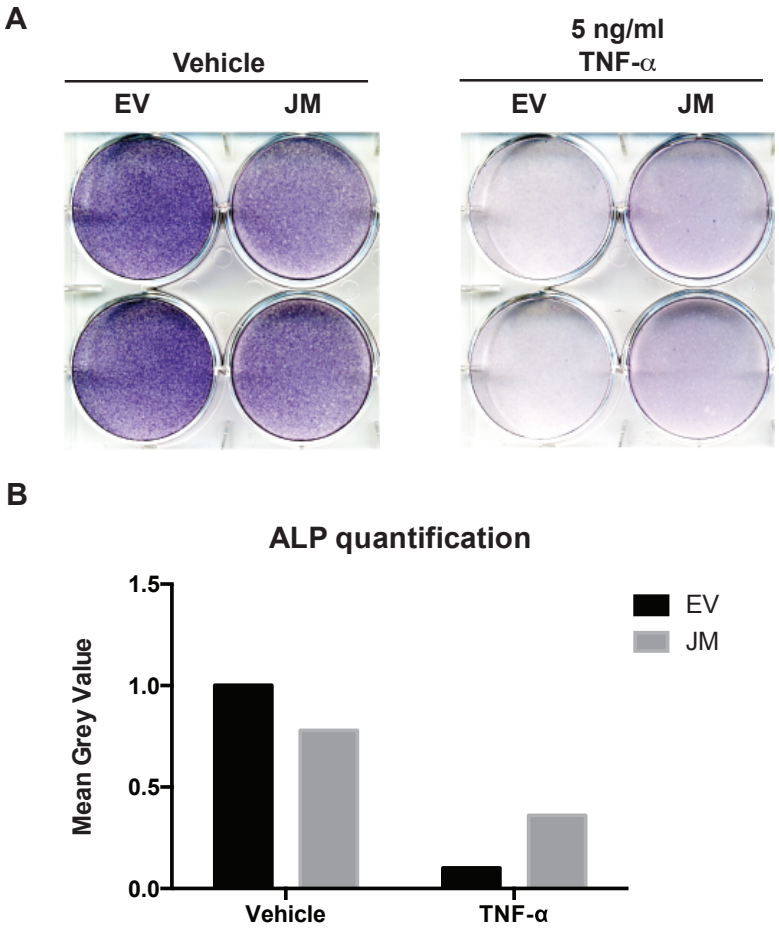

Figure 5-2: JMJD3 Overexpression in MC4 Cells Partially Rescued the Suppression of Osteoblast Differentiation by TNF-α.

MC4 cells stably infected with EV or JM were cultured in osteogenic medium with or without 5 ng/ml TNF-α for 7 days. **(A)** ALP staining was performed to assess ALP activity; **(B)** ImageJ software was used to quantify the intensity of ALP staining.

5.3 Discussion

We treated MC4 cells with TNF-α or co-cultured them with 5TGM1 cells as the major *in vitro* model to study the persistently impaired osteoblast differentiation in MMBD. We have shown that JMJD3 expression in MC4 cells was decreased in response to prolonged TNF-α treatment or direct contacts with myeloma cells. The decreased expression of JMJD3 contributed to the resolution of the bivalent domains at the Runx2 and Osterix TSSs to transcriptionally silent domains. Silencing JMJD3 in MC4 cells sufficed to inhibit normal osteoblast differentiation. Based on the findings above, it's reasonable to conclude that JMJD3 dysregulation and resulting epigenetic changes are involved in the suppression of osteoblast differentiation mediated by TNF-α or MM cells. Our recent finding showing the partial rescue of osteoblast differentiation by overexpressing JMJD3 in MC4 cells further supports this notion. Consistent with the *in vitro* findings, BMSCs isolated from MM patients (MM-BMSCs) expressed significantly lower levels of JMJD3 compared to BMSCs isolated from age-matched healthy donors. Of note, loss of JMJD3 expression persisted in MM-BMSCs even after they were continuously cultured without CD138+ MM cells for more than one month. The lasting nature of JMJD3 dysregulation and the accumulation of dynamically stable H3K27 marks on the Runx2 and Osterix TSSs in BMSCs at least partially explains the protracted bone lesions in MM patients having acquired complete remission. In summary, our study provides the initial insight into how the suppression of osteoblast differentiation is

maintained in MM patients. Developing strategies to target JMJD3 or its upstream regulators could potentially mitigate MMBD and associated comorbidities.

CHAPTER 6

CONCLUDING REMARKS ON FUTURE RESEARCH DIRECTIONS AND POTENTIAL CLINICAL TRANSLATION OF JMJD3 IN MMBD

6.1 Future Research Direction of JMJD3 in MMBD

We report a novel mechanism that contributes to the persistence of lytic bone lesions in MM patients even after they achieve complete remission. We have found that BMSCs from MM patients express significantly lower levels of the H3K27 demethylase JMJD3 than BMSCs from healthy donors. Decreased JMJD3 expression inhibits the gene expression of Runx2 and Osterix, the master transcription factors of osteoblast differentiation, by resolving the bivalent domains on their promoters to transcriptionally silent domains. Our results further demonstrate that the NF-κB-JMJD3-Runx2/Osterix axis is a major contributor to the prolonged suppression of osteoblast differentiation in MM and provides a potential new therapeutic target for treating MMBD. Studying the role of JMJD3 in MMBD, however, only opens more questions that need to be properly addressed in future research. Currently we have three directions worthy of pursuing. Investigating the fundamental functions of JMJD3 will help us better understand the pathophysiology of MMBD. Moreover, this knowledge should also be useful in understanding other diseases since JMJD3 is actively involved in malignancy, senescence, inflammation, trauma and fetal development.

Human JMJD3 protein has 22 phosphorylation sites throughout the entire protein length based on low- and high- throughput MS data collected over 16 years. This information has not been pursued to date by researchers. Nearly all existing studies related to JMJD3 solely focus on examining its expression change in different cellular states. Our study is no exception so far. However, the biological effects of

phosphorylation of these sites is poorly understood. It's possible that TNF-α or direct contacts with myeloma cells could affect JMJD3 enzymatic activity by phosphorylating key amino acids. Group-based Prediction System 3.0 (GPS 3.0) which is used to predict proteins' cognate kinases reveals that JMJD3 can be phosphorylated by JNK, p38, ERK and IKK with high confidence (data not shown). Combining JMJD3 immunoprecipitation and Western blot using anti-phospho-(Ser/Thr) antibodies would allow us to compare the levels of phosphorylated JMJD3 in BMSCs exposed to TNF-α or myeloma cells with the levels of phosphorylated JMJD3 in control cells. To correlate the phosphorylation status of JMJD3 with its enzymatic activity, *In vitro* histone demethylase assay[220] could be performed by incubating purified JMJD3 protein with H3K27me3 H3 substrates in a reaction supplemented with Fe (II) and α-ketoglutarate. Following the reaction, the JMJD3 demethylase activity could be detected by immunoblotting the histone substrates using anti-H3K27me3 antibodies. Furthermore, transfection of truncated and mutated JMJD3 into stromal cells will help localize the phosphorylated site(s) induced by TNF-α treatment and direct contacts with myeloma cells.

The second potential future research direction is to investigate the detailed molecular mechanism(s) by which NF-κB activation inhibits JMJD3 gene expression. We found that TNF-α initially induces JMJD3 expression within 6-hours of exposure and suppresses its expression thereafter via NF-κB signaling. The time-dependent regulation of JMJD3 reveals different effects of short- and long-term inflammation on epigenetics in cells. One hypothesis is that persistent NF-κB activation inhibits the transcription of its target genes by remodeling the histone methylations on their promoters. Levy et al.

have reported that mono-methylation of activated p65 by SETD6 in nucleus recruits the H3K9 methyltransferase GLP and subsequently introduces transcriptionally repressive mark H3K9me to their target genes[187]. Based on this evidence, activated p65 in stromal cells may recruit GLP to the JMJD3 promoter and shut down its gene expression. To test this hypothesis, the methylated p65 levels in the nucleus could be examined by Western blot in stromal cells with or without SETD6 knockdown. ChIP could be performed to compare the occupying levels of H3K9me, GLP, p65 and RNA polymerase II (Pol II) Ser 2 on the JMJD3 gene in stromal cells treated with vehicle or TNF-α. Increased H3K9me and GLP on the JMJD3 promoter, and decreased Pol II Ser 2 on the JMJD3 gene body in stromal cells previously exposed to TNF-α should support this hypothesis. Another hypothesis for the effects of TNF-α on JMJD3 is that activated p65 interferes the DNA binding of SMADs to the JMJD3 promoter by sequestering SMADs into a complex[217]. Independent studies have reported that SMADs activate JMJD3 gene expression by binding to its promoter. Therefore, disruption of this process presumably downregulates JMJD3 expression. To test this hypothesis, one could examine the direct binding of activated p65 with SMAD1/4 by immunoprecipitation and the occupancy of SMAD1/4 on the JMJD3 promoter by ChIP in BMSCs treated with or without TNF-α. Decreased SMADs occupancy on the JMJD3 promoter after TNF-α treatment would support this hypothesis.

Lastly, loss of JMJD3 expression in stromal cells may “lock” them into a precursor state. Zhao et al. reported that knockdown of JMJD3 in MEFs significantly promotes their reprogramming into inducible pluripotent stem cells (iPSCs), as evidenced by

increased number of positive colonies. Conversely, ectopic overexpression of JMJD3 in MEFs markedly inhibits reprogramming efficiency[221]. These findings suggest that JMJD3 can be generally considered as a promoter of cell differentiation. In line with this argument, loss of JMJD3 expression in BMSCs should result in these cells expressing an immature phenotype. Supporting our hypothesis, our preliminary data showed that the marker genes of mouse BMSCs, namely Nestin[222], Prx1[223], Sca1[224] and PDGFRα[224], were induced in MC4 cells after TNF-α treatment for 2 days (Figure 6). In addition, Xu et al. have reported that CD166, a human BMSC marker gene, is highly expressed in MM cell lines and stromal cells isolated from MM patients[225]. To establish the causal relationship, one could examine if knockdown of JMJD3 alone is sufficient to induce the expression of BMSC marker genes. Also, isolation of BMSCs from age-matched healthy donors and MM patients would allow comparison of the abundancy of human BMSC surface markers by flow cytometry.

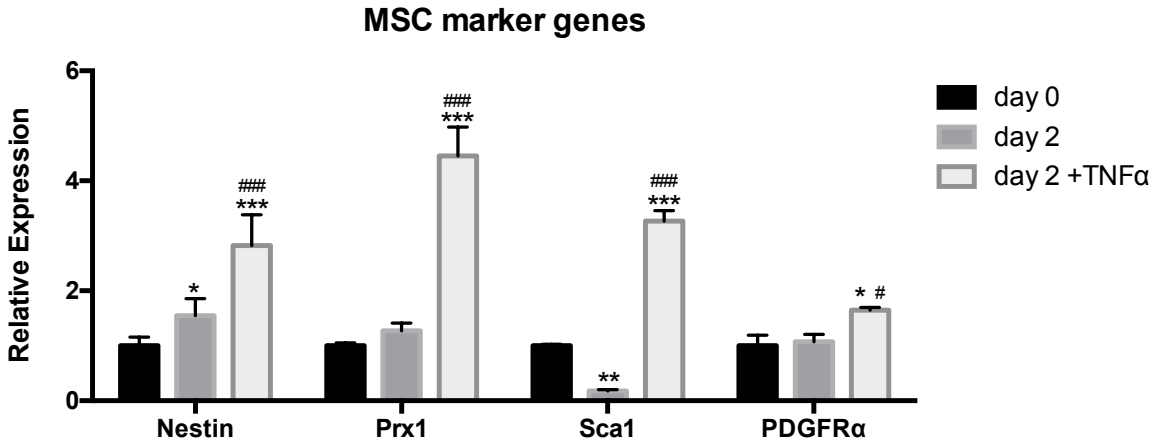

Figure 6: TNF-α Increases the Expression of Mouse BMSC Marker Genes.

MC4 cells were treated with or without 10 ng/ml TNF-α for 2 days. The mRNA levels of Nestin, Prx1, Sca1 and PDGFRα were measured using qPCR with the geometric mean of the CT values of β-actin, GAPDH and HMBS as the internal control. Error bars in each column graph represent SD of three biological replicates. * $p < 0.05$; ** $p < 0.01$; ***$p < 0.001$ compared with the black bar in individual group. # $p < 0.05$; ## $p < 0.01$; ### $p < 0.001$ compared with the grey bar in individual group.

6.2 Potential Epigenetic Therapies in the Management of MMBD

The epigenome in cells possesses a certain degree of plasticity to incorporate new information from the surrounding environment. This feature makes epigenetic therapy a legitimate approach to reverse an established pathological status. To date, five compounds selectively targeting the enzymes involved in epigenetic regulation have been approved by the US Food and Drug Administration (FDA) to treat hematological malignancies. These compounds include two DNMT inhibitors (Azacitidine and Decitabine) and three HDAC inhibitors (Vorinostat, Romidepsin and Belinostat)[226]. Azacitidine[227] and Decitabine[228] are both cytidine analogs that covalently sequester DNMTs, trigger DNMT degradation and cause reduction in DNA methylation. In a randomized controlled clinical trial determining the efficacy of Azacitidine in treating myelodysplastic syndrome (MDS), 16% of patients receiving subcutaneous Azacitidine partially or completely restored their blood cell counts and bone marrow morphology to normal compared to none of patients only receiving supportive care[229]. The improved clinical outcome through solely modulating epigenetics demonstrates a novel therapeutic strategy to treat diseases. Further supporting this notion, intravaneous administration of Belinostat increases the overall response rate (ORR) of patients diagnosed with peripheral T-cell lymphomas[230].

Besides these officially approved epigenetic agents, several inhibitors of histone modifiers are currently undergoing preclinical and clinical trials. These small molecule inhibitors specifically target G9a, EZH2, DOT1L or LSD1, and show anti-tumor activity as

a single agent or in combination with other standard chemotherapies. These compounds are also being actively tested in the medical conditions other than malignancy, in which epigenetic alterations have been reported to play a pivotal role in disease pathogenesis and progression. The success of epigenetic therapy relies on not only the continuous development of specific, well-tolerated compounds that target key epigenetic enzymes, but also the growing knowledge of how epigenetics is involved in each disease. In this dissertation, we have shown that the downregulation of JMJD3 in BMSCs suppresses osteoblast differentiation by resolving the bivalent domains on the Runx2 and Osterix promoters to transcriptionally silent domains in MMBD. Ectopic JMJD3 overexpression in BMSCs partially overcomes the inhibitory effects of MM on osteoblast differentiation. Our findings provide the first theoretical basis that targeting JMJD3 could potentially benefit the healing process of lytic bone lesions in MMBD patients. Also, we and our colleagues have collectively reported that Gfi1 mediates MM-induced long-term suppression of osteoblast differentiation by recruiting co-repressors EZH2 and HDACs to the Runx2 promoter. These findings suggest that administration of EZH2 or HDAC inhibitors in MMBD patients might be promising to control this dire complication. Considering the availability of FDA-approved HDAC inhibitors and the EZH2 inhibitor Tazemetostat[231] currently undergoing phase II clinical trials, determining the efficacy of these compounds in treating MMBD will significantly shorten the lengthy process of drug development.

There exist many challenges for epigenetic therapies, the major one being “off-target” effects. This issue is inherent in the compounds developed to target epigenetic

enzymes due to the conserved amino acid sequences shared by these enzymes with different substrate specificity. One elegant example is the carefully designed H3K27 demethylase inhibitor GSK-J1 based on crystal structures. GSK-J1 works by masking the binding sites of JMJD3 for both α-ketoglutarate and Pro 30 (P30) of H3 tails. The original study showed that the half-maximum inhibitory concentration (IC50) of GSK-J1 was 60 nM in the JMJD3 AlphaScreen assay. Further, GSK-J1 didn't significantly inhibit 100 protein kinases at a concentration of 30 μM and had negligible off-target activity against other chromatin-modifying enzymes[232]. However, the specificity of GSK-J1 was subsequently questioned by another study showing that GSK-J1 inhibited the activity of the H3K4 demethylase KDM5B and the H3K9/36 demethylase KDM4C with a similar extent to JMJD3/UTX in cells[233]. To make things more complicated, histone modifiers are not limited to modifying only histones, they can also modify non-histone proteins[234-236]. Deregulated modifications of non-histone proteins unavoidably invite unwanted side effects. Lastly, maintaining epigenetic homeostasis is important in normal cell function. Epigenetic therapies in the management of MMBD can equally affect cells other than BMSCs in bone marrow microenvironment. The effects of epigenetic therapies on each cell subpopulation must be thoroughly examined and the benefits/risks be assessed before they can be considered for testing in patients.

Our findings showing the inhibition of JMJD3 gene expression by NF-κB activation provide an alternative strategy to overcome the challenges met in epigenetic therapies. Instead of targeting the key enzyme itself, targeting its upstream regulators gives a higher chance of developing a specific, well-tolerated, FDA-approved compound

simply because there are more targets to work on. In the management of MMBD, NF-κB activation can be inhibited using small molecules to restore JMJD3 expression in BMSCs. While no selective JMJD3-activating compound has been developed, over 20 inhibitors are readily available to block NF-κB activation through different mechanisms, including inhibition of IKK complex, IκB degradation, NF-κB nuclear translocation, p65 acetylation, NF-κB DNA binding, and NF-κB transactivation. In addition, 19 FDA-approved drugs have been reported to show inhibitory effects on NF-κB with IC50 ranging from 0.02 to 40 μM[237].

As new compounds that target epigenetics become available and our understanding of MMBD increases, epigenetic therapies are promising agents to be applied to the management of MM patients and could show efficacy in healing protracted lytic bone lesions. Epigenetic therapies could correct the dysregulated histone methylations in BMSCs from MM patients without the need of depleting the BMSC population. Following treatment, the BMSCs restore their capacity of osteoblastogenesis and cease secreting cytokines to support MM growth. As a result, epigenetic therapies might also decrease tumor burden and improve 5-year survival rates for MM patients.

APPENDIX

Gene	Forward sequence (5'-3')	Reverse sequence (5'-3')
mbeta-actin	CTCTGGCTCCTAGCACCATGAAGA	GTAAAACGCAGCTCAGTAACAGTCCG
mJMJD3	CTGCACCTTGAGCACAAACG	CTAAGGCCCTCCTCTCCTGA
mUTX	TTAGTAAGTGAAATCAACATGCTCC	TCAAGATGAGGCGGATGGTA
mEZH2	TCCATGCAACACCCAACACAT	CTCCCTCCAGATGCTGGTAAC
mEED	GGGCGATTTGATTACAGCCAG	TGCCCAATGCAAGCATCTTT
mSuz12	AGAGCAAGAATCTCATAGCTTGTC	GCAGGACTTCCAGGGTAACA
mRunx2	AGGGACTATGGCGTCAAACA	AGAAGCTTTGCTGACACGGT
mOsterix	AGAGGTTCACTCGCTCTGACGA	TTGCTCAAGTGGTCGCTTCTG
mGfi1	GGCTCCTACAAATGCATCAAATG	TGCCACAGATCTTACAGTCAAAG
mTNF-α	TAGCCCACGTCGTAGCAAAC	ACAAGGTACAACCCATCGGC
mA20	CTCAGAGAGGCGCCAAAAGA	TTTGAGGAGCCAAGTCCCAC
mIL-6	CAAAGCCAGAGTCCTTCAGA	GCCACTCCTTCTGTGACTCC

ChIP primers	Forward sequence (5'-3')	Reverse sequence (5'-3')
Runx2 p -670	AAGGCAAACAGAAGGAAGCA	TGCTGCTTTGCAGTAATTCG
Runx2 p -336	GGCTCCTTCAGCATTTGTGT	TCCCTTTCTCCCTCTGACAA
Runx2 p 51	CTTCATTCGCCTCACAAACA	TAAACGCCAGAGCCTTCTTG
Runx2 p 33130	AGGTAGCCCAGCAAAAACCT	CCCCTCTGTGAGCCAAAATA
Osterix p -428	GCCACCCATTGCCAGTAATCT	ACCTGGGTAGGCTAGGGTTG
Osterix p -306	TGGGGTATGTAGGACTCCCG	CTTCCTTGGGGGTGCTATGG
Osterix p -96	ATCCGGAGTCTTCTCCGCT	TGTCTGTAGGGATCCACCCTC
Osterix p144	GGCGTCCTCTCTGCTTGAG	GGTGGGGTAGGCATGGATTAG

REFERENCES

1 Silbermann, R. & Roodman, G. D. Myeloma bone disease: pathophysiology and management. *Journal of bone oncology* **2**, 59-69 (2013).

2 Melton, L. J., Kyle, R. A., Achenbach, S. J., Oberg, A. L. & Rajkumar, S. V. Fracture Risk With Multiple Myeloma: A Population‐Based Study. *Journal of Bone and Mineral Research* **20**, 487-493 (2005).

3 Saad, F. *et al.* Pathologic fractures correlate with reduced survival in patients with malignant bone disease. *Cancer* **110**, 1860-1867 (2007).

4 Hill, P. A. Bone remodelling. *British journal of orthodontics* **25**, 101-107, doi:10.1093/ortho/25.2.101 (1998).

5 Clarke, B. Normal Bone Anatomy and Physiology. *Clinical Journal of the American Society of Nephrology : CJASN* **3**, S131-139, doi:10.2215/cjn.04151206 (2008).

6 Hadjidakis, D. J. & Androulakis, I. I. Bone remodeling. *Annals of the New York Academy of Sciences* **1092**, 385-396 (2006).

7 Tamma, R. & Zallone, A. Osteoblast and osteoclast crosstalks: from OAF to Ephrin. *Inflammation & Allergy-Drug Targets (Formerly Current Drug Targets-Inflammation & Allergy)* **11**, 196-200 (2012).

8 Zhao, C. *et al.* Bidirectional ephrinB2-EphB4 signaling controls bone homeostasis. *Cell metabolism* **4**, 111-121 (2006).

9 Martin, T. *et al.* in *Osteoimmunology* 51-60 (Springer, 2009).

10 Hsu, H. *et al.* Tumor necrosis factor receptor family member RANK mediates osteoclast differentiation and activation induced by osteoprotegerin ligand. *Proceedings of the National Academy of Sciences* **96**, 3540-3545 (1999).

11 Nakagawa, N. *et al.* RANK is the essential signaling receptor for osteoclast differentiation factor in osteoclastogenesis. *Biochemical and biophysical research communications* **253**, 395-400 (1998).

12 Hanley, D., Adachi, J., Bell, A. & Brown, V. Denosumab: mechanism of action and clinical outcomes. *International journal of clinical practice* **66**, 1139-1146 (2012).

13 Kobayashi, Y., Udagawa, N. & Takahashi, N. Action of RANKL and OPG for osteoclastogenesis. *Critical Reviews™ in Eukaryotic Gene Expression* **19** (2009).

14 Hofbauer, L. C., Dunstan, C. R., Spelsberg, T. C., Riggs, B. L. & Khosla, S. Osteoprotegerin production by human osteoblast lineage cells is stimulated by vitamin D, bone morphogenetic protein-2, and cytokines. *Biochemical and biophysical research communications* **250**, 776-781 (1998).

15 Huang, J. C. *et al.* PTH differentially regulates expression of RANKL and OPG. *Journal of Bone and Mineral Research* **19**, 235-244 (2004).

16 LIU, X. H., Kirschenbaum, A., Yao, S. & Levine, A. C. Interactive Effect of Interleukin‐6 and Prostaglandin E2 on Osteoclastogenesis via the OPG/RANKL/RANK System. *Annals of the New York Academy of Sciences* **1068**, 225-233 (2006).

17 Ishimi, Y. *et al.* IL-6 is produced by osteoblasts and induces bone resorption. *The Journal of Immunology* **145**, 3297-3303 (1990).

18 Vallet, S. *et al.* Activin A promotes multiple myeloma-induced osteolysis and is a promising target for myeloma bone disease. *Proceedings of the National Academy of Sciences* **107**, 5124-5129 (2010).
19 Li, F. *et al.* Annexin II stimulates RANKL expression through MAPK. *Journal of Bone and Mineral Research* **20**, 1161-1167 (2005).
20 Lam, J. *et al.* TNF-α induces osteoclastogenesis by direct stimulation of macrophages exposed to permissive levels of RANK ligand. *Journal of Clinical Investigation* **106**, 1481 (2000).
21 Yamamoto, I. *et al.* Production of interleukin 1β, a potent bone resorbing cytokine, by cultured human myeloma cells. *Cancer research* **49**, 4242-4246 (1989).
22 Abe, M. *et al.* Role for macrophage inflammatory protein (MIP)-1α and MIP-1β in the development of osteolytic lesions in multiple myeloma. *Blood* **100**, 2195-2202 (2002).
23 Choi, S. J. *et al.* Antisense inhibition of macrophage inflammatory protein 1-α blocks bone destruction in a model of myeloma bone disease. *Journal of Clinical Investigation* **108**, 1833 (2001).
24 Oyajobi, B. O. *et al.* Dual effects of macrophage inflammatory protein-1α on osteolysis and tumor burden in the murine 5TGM1 model of myeloma bone disease. *Blood* **102**, 311-319 (2003).
25 Han, J.-H. *et al.* Macrophage inflammatory protein-1α is an osteoclastogenic factor in myeloma that is independent of receptor activator of nuclear factor κB ligand. *Blood* **97**, 3349-3353 (2001).
26 Magrangeas, F. *et al.* Gene expression profiling of multiple myeloma reveals molecular portraits in relation to the pathogenesis of the disease. *Blood* **101**, 4998-5006 (2003).
27 Kim, J. H. *et al.* The mechanism of osteoclast differentiation induced by IL-1. *Journal of immunology (Baltimore, Md. : 1950)* **183**, 1862-1870, doi:10.4049/jimmunol.0803007 (2009).
28 Westendorf, J. J., Kahler, R. A. & Schroeder, T. M. Wnt signaling in osteoblasts and bone diseases. *Gene* **341**, 19-39 (2004).
29 Day, T. F., Guo, X., Garrett-Beal, L. & Yang, Y. Wnt/β-catenin signaling in mesenchymal progenitors controls osteoblast and chondrocyte differentiation during vertebrate skeletogenesis. *Developmental cell* **8**, 739-750 (2005).
30 Krishnan, V., Bryant, H. U. & MacDougald, O. A. Regulation of bone mass by Wnt signaling. *Journal of Clinical Investigation* **116**, 1202 (2006).
31 Kobayashi, Y., Maeda, K. & Takahashi, N. Roles of Wnt signaling in bone formation and resorption. *Japanese Dental Science Review* **44**, 76-82 (2008).
32 Gong, Y. *et al.* LDL receptor-related protein 5 (LRP5) affects bone accrual and eye development. *Cell* **107**, 513-523 (2001).
33 Tian, E. *et al.* The role of the Wnt-signaling antagonist DKK1 in the development of osteolytic lesions in multiple myeloma. *New England Journal of Medicine* **349**, 2483-2494 (2003).

34 Yaccoby, S. *et al.* Antibody-based inhibition of DKK1 suppresses tumor-induced bone resorption and multiple myeloma growth in vivo. *Blood* **109**, 2106-2111 (2007).
35 Winkler, D. G. *et al.* Osteocyte control of bone formation via sclerostin, a novel BMP antagonist. *The EMBO journal* **22**, 6267-6276 (2003).
36 Poole, K. E. *et al.* Sclerostin is a delayed secreted product of osteocytes that inhibits bone formation. *The FASEB journal* **19**, 1842-1844 (2005).
37 Colucci, S. *et al.* Myeloma cells suppress osteoblasts through sclerostin secretion. *Blood cancer journal* **1**, e27 (2011).
38 Bellido, T. & Roodman, G. D. D. (Am Soc Hematology, 2013).
39 McDonald, M. M. *et al.* Inhibiting the osteocyte-specific protein sclerostin increases bone mass and fracture resistance in multiple myeloma. *Blood* **129**, 3452-3464 (2017).
40 Wajant, H., Pfizenmaier, K. & Scheurich, P. Tumor necrosis factor signaling. *Cell Death & Differentiation* **10**, 45-65 (2003).
41 Mukai, T. *et al.* TNF-α inhibits BMP-induced osteoblast differentiation through activating SAPK/JNK signaling. *Biochemical and biophysical research communications* **356**, 1004-1010 (2007).
42 Li, W. *et al.* NEMO-binding domain peptide promotes osteoblast differentiation impaired by tumor necrosis factor alpha. *Biochemical and biophysical research communications* **391**, 1228-1233 (2010).
43 McCloskey, E. *et al.* A randomized trial of the effect of clodronate on skeletal morbidity in multiple myeloma. *British journal of haematology* **100**, 317-325 (1998).
44 Morgan, G. J. *et al.* First-line treatment with zoledronic acid as compared with clodronic acid in multiple myeloma (MRC Myeloma IX): a randomised controlled trial. *The Lancet* **376**, 1989-1999 (2010).
45 Kyle, R. A. *et al.* American Society of Clinical Oncology 2007 clinical practice guideline update on the role of bisphosphonates in multiple myeloma. *Journal of Clinical Oncology* **25**, 2464-2472 (2007).
46 Rogers, M. From molds and macrophages to mevalonate: a decade of progress in understanding the molecular mode of action of bisphosphonates. *Calcified tissue international* **75**, 451-461 (2004).
47 Shipman, C. M., Rogers, M. J., Apperley, J. F., Russell, R. G. G. & Croucher, P. I. Bisphosphonates induce apoptosis in human myeloma cell lines: a novel anti-tumour activity. *British journal of haematology* **98**, 665-672 (1997).
48 Dimopoulos, M. A. *et al.* Osteonecrosis of the jaw in patients with multiple myeloma treated with bisphosphonates: evidence of increased risk after treatment with zoledronic acid. *haematologica* **91**, 968-971 (2006).
49 Hageman, K., Patel, K. C., Mace, K. & Cooper, M. R. The role of denosumab for prevention of skeletal-related complications in multiple myeloma. *Annals of Pharmacotherapy* **47**, 1069-1074 (2013).

50 Aghaloo, T. L., Felsenfeld, A. L. & Tetradis, S. Osteonecrosis of the jaw in a patient on Denosumab. *Journal of oral and maxillofacial surgery: official journal of the American Association of Oral and Maxillofacial Surgeons* **68**, 959 (2010).
51 Watts, N. *et al.* Infections in postmenopausal women with osteoporosis treated with denosumab or placebo: coincidence or causal association? *Osteoporosis International* **23**, 327-337 (2012).
52 Corre, J. *et al.* Bone marrow mesenchymal stem cells are abnormal in multiple myeloma. *Leukemia* **21**, 1079-1088 (2007).
53 André, T. *et al.* Evidences of early senescence in multiple myeloma bone marrow mesenchymal stromal cells. *PloS one* **8**, e59756 (2013).
54 Xu, S. *et al.* Upregulation of miR-135b is involved in the impaired osteogenic differentiation of mesenchymal stem cells derived from multiple myeloma patients. *PloS one* **8**, e79752 (2013).
55 Reagan, M. R. *et al.* Investigating osteogenic differentiation in multiple myeloma using a novel 3D bone marrow niche model. *Blood* **124**, 3250-3259 (2014).
56 Arnulf, B. *et al.* Phenotypic and functional characterization of bone marrow mesenchymal stem cells derived from patients with multiple myeloma. *Leukemia* **21**, 158-163 (2007).
57 Zdzisińska, B., Bojarska-Junak, A., Dmoszyńska, A. & Kandefer-Szerszeń, M. Abnormal cytokine production by bone marrow stromal cells of multiple myeloma patients in response to RPMI8226 myeloma cells. *Archivum immunologiae et therapiae experimentalis* **56**, 207 (2008).
58 Hao, M. *et al.* Bone marrow stromal cells protect myeloma cells from bortezomib induced apoptosis by suppressing microRNA-15a expression. *Leukemia & lymphoma* **52**, 1787-1794 (2011).
59 Markovina, S. *et al.* Bone marrow stromal cells from multiple myeloma patients uniquely induce bortezomib resistant NF-κB activity in myeloma cells. *Molecular cancer* **9**, 176 (2010).
60 Garderet, L. *et al.* Mesenchymal stem cell abnormalities in patients with multiple myeloma. *Leukemia & lymphoma* **48**, 2032-2041 (2007).
61 Li, B. *et al.* Elevated tumor necrosis factor-α suppresses TAZ expression and impairs osteogenic potential of Flk-1+ mesenchymal stem cells in patients with multiple myeloma. *Stem cells and development* **16**, 921-930 (2007).
62 Li, B. *et al.* The effect of TNF-alpha on TAZ expression and osteogenic potential of mesenchymal stem cells from myeloma patients. *Zhonghua zhong liu za zhi [Chinese journal of oncology]* **31**, 5-9 (2009).
63 Garayoa, M. *et al.* Mesenchymal stem cells from multiple myeloma patients display distinct genomic profile as compared with those from normal donors. *Leukemia* **23**, 1515-1527 (2009).
64 D'Souza, S. *et al.* Gfi1 expressed in bone marrow stromal cells is a novel osteoblast suppressor in patients with multiple myeloma bone disease. *Blood* **118**, 6871-6880 (2011).
65 Van der Meer, L., Jansen, J. & Van Der Reijden, B. Gfi1 and Gfi1b: key regulators of hematopoiesis. *Leukemia* **24**, 1834-1843 (2010).

66 Phelan, J. D., Shroyer, N. F., Cook, T., Gebelein, B. & Grimes, H. L. Gfi1—Cells & Circuits: Unraveling transcriptional networks of development and disease. *Current opinion in hematology* **17**, 300 (2010).
67 Duan, Z., Zarebski, A., Montoya-Durango, D., Grimes, H. L. & Horwitz, M. Gfi1 coordinates epigenetic repression of p21Cip/WAF1 by recruitment of histone lysine methyltransferase G9a and histone deacetylase 1. *Molecular and cellular biology* **25**, 10338-10351 (2005).
68 Chen, T. & Dent, S. Y. Chromatin modifiers and remodellers: regulators of cellular differentiation. *Nature Reviews Genetics* **15**, 93-106 (2014).
69 Wu, H. *et al.* Histone methyltransferase G9a contributes to H3K27 methylation in vivo. *Cell research* **21**, 365 (2011).
70 Montoya-Durango, D. E. *et al.* Ajuba functions as a histone deacetylase-dependent co-repressor for autoregulation of the growth factor-independent-1 transcription factor. *Journal of Biological Chemistry* **283**, 32056-32065 (2008).
71 Zeng, H., Yücel, R., Kosan, C., Klein-Hitpass, L. & Möröy, T. Transcription factor Gfi1 regulates self-renewal and engraftment of hematopoietic stem cells. *The EMBO journal* **23**, 4116-4125 (2004).
72 Hock, H. *et al.* Gfi-1 restricts proliferation and preserves functional integrity of haematopoietic stem cells. *Nature* **431**, 1002-1007 (2004).
73 Spooner, C. J., Cheng, J. X., Pujadas, E., Laslo, P. & Singh, H. A recurrent network involving the transcription factors PU. 1 and Gfi1 orchestrates innate and adaptive immune cell fates. *Immunity* **31**, 576-586 (2009).
74 Zhu, J., Jankovic, D., Grinberg, A., Guo, L. & Paul, W. E. Gfi-1 plays an important role in IL-2-mediated Th2 cell expansion. *Proceedings of the National Academy of Sciences* **103**, 18214-18219 (2006).
75 Ichiyama, K. *et al.* Gfi1 negatively regulates Th17 differentiation by inhibiting RORγt activity. *International immunology* **21**, 881-889 (2009).
76 Person, R. E. *et al.* Mutations in proto-oncogene GFI1 cause human neutropenia and target ELA2. *Nature genetics* **34**, 308-312 (2003).
77 Xia, J. *et al.* Prevalence of mutations in ELANE, GFI1, HAX1, SBDS, WAS and G6PC3 in patients with severe congenital neutropenia. *British journal of haematology* **147**, 535-542 (2009).
78 Adamik, J. *et al.* EZH2 or HDAC1 Inhibition Reverses Multiple Myeloma–Induced Epigenetic Suppression of Osteoblast Differentiation. *Molecular Cancer Research* **15**, 405-417 (2017).
79 Teramachi, J. *et al.* Blocking the ZZ domain of sequestosome1/p62 suppresses myeloma growth and osteoclast formation in vitro and induces dramatic bone formation in myeloma-bearing bones in vivo. *Leukemia* **30**, 390-398 (2016).
80 Otto, F. *et al.* Cbfa1, a candidate gene for cleidocranial dysplasia syndrome, is essential for osteoblast differentiation and bone development. *Cell* **89**, 765-771 (1997).
81 Nakashima, K. *et al.* The novel zinc finger-containing transcription factor osterix is required for osteoblast differentiation and bone formation. *Cell* **108**, 17-29 (2002).

82 Bernstein, B. E., Meissner, A. & Lander, E. S. The mammalian epigenome. *Cell* **128**, 669-681 (2007).
83 Struhl, K. Histone acetylation and transcriptional regulatory mechanisms. *Genes & development* **12**, 599-606 (1998).
84 De Ruijter, A. J., Van Gennip, A. H., Caron, H. N., Stephan, K. & Van Kuilenburg, A. B. Histone deacetylases (HDACs): characterization of the classical HDAC family. *Biochemical Journal* **370**, 737-749 (2003).
85 Fanti, L. & Pimpinelli, S. HP1: a functionally multifaceted protein. *Current opinion in genetics & development* **18**, 169-174 (2008).
86 Patel, D. J. & Wang, Z. Readout of epigenetic modifications. *Annual review of biochemistry* **82**, 81-118 (2013).
87 Probst, A. V., Dunleavy, E. & Almouzni, G. Epigenetic inheritance during the cell cycle. *Nature reviews Molecular cell biology* **10**, 192-206 (2009).
88 De Koning, L., Corpet, A., Haber, J. E. & Almouzni, G. Histone chaperones: an escort network regulating histone traffic. *Nature structural & molecular biology* **14**, 997-1007 (2007).
89 Stillman, B. Chromatin assembly during SV40 DNA replication in vitro. *Cell* **45**, 555-565 (1986).
90 Smith, S. & Stillman, B. Purification and characterization of CAF-I, a human cell factor required for chromatin assembly during DNA replication in vitro. *Cell* **58**, 15-25 (1989).
91 Groth, A. *et al.* Regulation of replication fork progression through histone supply and demand. *Science* **318**, 1928-1931 (2007).
92 Mello, J. A. *et al.* Human Asf1 and CAF-1 interact and synergize in a repair-coupled nucleosome assembly pathway. *EMBO reports* **3**, 329-334 (2002).
93 Trojer, P. & Reinberg, D. Histone lysine demethylases and their impact on epigenetics. *Cell* **125**, 213-217 (2006).
94 Hansen, K. H. *et al.* A model for transmission of the H3K27me3 epigenetic mark. *Nature cell biology* **10**, 1291-1300 (2008).
95 Bernstein, B. E. *et al.* A bivalent chromatin structure marks key developmental genes in embryonic stem cells. *Cell* **125**, 315-326 (2006).
96 Mikkelsen, T. S. *et al.* Genome-wide maps of chromatin state in pluripotent and lineage-committed cells. *Nature* **448**, 553-560 (2007).
97 Marks, H. *et al.* The transcriptional and epigenomic foundations of ground state pluripotency. *Cell* **149**, 590-604 (2012).
98 Brookes, E. *et al.* Polycomb associates genome-wide with a specific RNA polymerase II variant, and regulates metabolic genes in ESCs. *Cell stem cell* **10**, 157-170 (2012).
99 Roh, T.-Y., Cuddapah, S., Cui, K. & Zhao, K. The genomic landscape of histone modifications in human T cells. *Proceedings of the National Academy of Sciences* **103**, 15782-15787 (2006).
100 Pan, G. *et al.* Whole-genome analysis of histone H3 lysine 4 and lysine 27 methylation in human embryonic stem cells. *Cell stem cell* **1**, 299-312 (2007).

101 De Gobbi, M. *et al.* Generation of bivalent chromatin domains during cell fate decisions. *Epigenetics & chromatin* **4**, 9 (2011).
102 Alder, O. *et al.* Ring1B and Suv39h1 delineate distinct chromatin states at bivalent genes during early mouse lineage commitment. *Development* **137**, 2483-2492 (2010).
103 Young, N. L. *et al.* High throughput characterization of combinatorial histone codes. *Molecular & Cellular Proteomics* **8**, 2266-2284 (2009).
104 Voigt, P. *et al.* Asymmetrically modified nucleosomes. *Cell* **151**, 181-193 (2012).
105 Kim, D.-H. *et al.* Histone H3K27 trimethylation inhibits H3 binding and function of SET1-like H3K4 methyltransferase complexes. *Molecular and cellular biology* **33**, 4936-4946 (2013).
106 Pasini, D. *et al.* Coordinated regulation of transcriptional repression by the RBP2 H3K4 demethylase and Polycomb-Repressive Complex 2. *Genes & development* **22**, 1345-1355 (2008).
107 Schmitges, F. W. *et al.* Histone methylation by PRC2 is inhibited by active chromatin marks. *Molecular cell* **42**, 330-341 (2011).
108 Agger, K. *et al.* UTX and JMJD3 are histone H3K27 demethylases involved in HOX gene regulation and development. *Nature* **449**, 731-734 (2007).
109 Lee, M. G. *et al.* Demethylation of H3K27 regulates polycomb recruitment and H2A ubiquitination. *Science* **318**, 447-450 (2007).
110 Chen, S. *et al.* The histone H3 Lys 27 demethylase JMJD3 regulates gene expression by impacting transcriptional elongation. *Genes & development* **26**, 1364-1375 (2012).
111 Maherali, N. *et al.* Directly reprogrammed fibroblasts show global epigenetic remodeling and widespread tissue contribution. *Cell stem cell* **1**, 55-70 (2007).
112 Mikkelsen, T. S. *et al.* Dissecting direct reprogramming through integrative genomic analysis. *Nature* **454**, 49-55 (2008).
113 Guenther, M. G. *et al.* Chromatin structure and gene expression programs of human embryonic and induced pluripotent stem cells. *Cell stem cell* **7**, 249-257 (2010).
114 Wang, D. *et al.* Isolation and characterization of MC3T3-E1 preosteoblast subclones with distinct in vitro and in vivo differentiation/mineralization potential. *Journal of bone and mineral research : the official journal of the American Society for Bone and Mineral Research* **14**, 893-903, doi:10.1359/jbmr.1999.14.6.893 (1999).
115 Horwitz, E. M. *et al.* Clarification of the nomenclature for MSC: The International Society for Cellular Therapy position statement. *Cytotherapy* **7**, 393-395, doi:10.1080/14653240500319234 (2005).
116 Radl, J., De Glopper, E., Schuit, H. R. & Zurcher, C. Idiopathic Paraproteinemia. *The Journal of Immunology* **122**, 609-613 (1979).
117 Radl, J., Croese, J. W., Zurcher, C., Van den Enden-Vieveen, M. & de Leeuw, A. M. Animal model of human disease. Multiple myeloma. *The American journal of pathology* **132**, 593 (1988).

118 Radl, J. Age-related monoclonal gammapathies: clinical lessons from the aging C57BL mouse. *Immunology today* **11**, 234-236 (1990).
119 Vanderkerken, K. *et al.* Organ involvement and phenotypic adhesion profile of 5T2 and 5T33 myeloma cells in the C57BL/KaLwRij mouse. *British journal of cancer* **76**, 451-460 (1997).
120 Van Valckenborgh, E. *et al.* Murine 5T multiple myeloma cells induce angiogenesis in vitro and in vivo. *British journal of cancer* **86**, 796-802 (2002).
121 Dallas, S. L. *et al.* Ibandronate reduces osteolytic lesions but not tumor burden in a murine model of myeloma bone disease. *Blood* **93**, 1697-1706 (1999).
122 Oyajobi, B. O. *et al.* Detection of myeloma in skeleton of mice by whole-body optical fluorescence imaging. *Molecular cancer therapeutics* **6**, 1701-1708 (2007).
123 Fillat, C., Carrio, M., Cascante, A. & Sangro, B. Suicide gene therapy mediated by the Herpes Simplex virus thymidine kinase gene/Ganciclovir system: fifteen years of application. *Current gene therapy* **3**, 13-26 (2003).
124 Asosingh, K., Radl, J., Van Riet, I., Van Camp, B. & Vanderkerken, K. The 5TMM series: a useful in vivo mouse model of human multiple myeloma. *The hematology journal* **1**, 351-356 (2000).
125 Badeaux, A. I. & Shi, Y. Emerging roles for chromatin as a signal integration and storage platform. *Nature reviews Molecular cell biology* **14**, 211-224 (2013).
126 Sinha, K. M., Yasuda, H., Coombes, M. M., Dent, S. Y. & De Crombrugghe, B. Regulation of the osteoblast-specific transcription factor Osterix by NO66, a Jumonji family histone demethylase. *The EMBO journal* **29**, 68-79 (2010).
127 Ge, W. *et al.* Inhibition of Osteogenic Differentiation of Human Adipose-Derived Stromal Cells by Retinoblastoma Binding Protein 2 Repression of RUNX2-Activated Transcription. *Stem Cells* **29**, 1112-1125 (2011).
128 Hemming, S. *et al.* EZH2 and KDM6A act as an epigenetic switch to regulate mesenchymal stem cell lineage specification. *Stem cells* **32**, 802-815 (2014).
129 Komori, T. *et al.* Targeted disruption of Cbfa1results in a complete lack of bone formation owing to maturational arrest of osteoblasts. *cell* **89**, 755-764 (1997).
130 Ikeda, T. *et al.* The combination of SOX5, SOX6, and SOX9 (the SOX trio) provides signals sufficient for induction of permanent cartilage. *Arthritis & Rheumatology* **50**, 3561-3573 (2004).
131 Yang, H. N. *et al.* Chondrogenesis of mesenchymal stem cells and dedifferentiated chondrocytes by transfection with SOX Trio genes. *Biomaterials* **32**, 7695-7704 (2011).
132 Tontonoz, P., Hu, E. & Spiegelman, B. M. Stimulation of adipogenesis in fibroblasts by PPARγ2, a lipid-activated transcription factor. *Cell* **79**, 1147-1156 (1994).
133 Yeh, W.-C., Cao, Z., Classon, M. & McKnight, S. L. Cascade regulation of terminal adipocyte differentiation by three members of the C/EBP family of leucine zipper proteins. *Genes & development* **9**, 168-181 (1995).
134 Oishi, Y. *et al.* Krüppel-like transcription factor KLF5 is a key regulator of adipocyte differentiation. *Cell metabolism* **1**, 27-39 (2005).

135 Rudnicki, M. A. *et al.* MyoD or Myf-5 is required for the formation of skeletal muscle. *Cell* **75**, 1351-1359 (1993).
136 Wright, W. E., Sassoon, D. A. & Lin, V. K. Myogenin, a factor regulating myogenesis, has a domain homologous to MyoD. *Cell* **56**, 607-617 (1989).
137 Komori, T. Regulation of osteoblast differentiation by transcription factors. *Journal of cellular biochemistry* **99**, 1233-1239 (2006).
138 Ducy, P., Zhang, R., Geoffroy, V., Ridall, A. L. & Karsenty, G. Osf2/Cbfa1: a transcriptional activator of osteoblast differentiation. *cell* **89**, 747-754 (1997).
139 Kobayashi, H., Gao, Y.-h., Ueta, C., Yamaguchi, A. & Komori, T. Multilineage differentiation of Cbfa1-deficient calvarial cells in vitro. *Biochemical and biophysical research communications* **273**, 630-636 (2000).
140 Schroeder, T. M., Kahler, R. A., Li, X. & Westendorf, J. J. Histone deacetylase 3 interacts with runx2 to repress the osteocalcin promoter and regulate osteoblast differentiation. *Journal of biological Chemistry* **279**, 41998-42007 (2004).
141 Lee, H. W. *et al.* Histone deacetylase 1-mediated histone modification regulates osteoblast differentiation. *Molecular endocrinology* **20**, 2432-2443 (2006).
142 Shen, J. *et al.* Transcriptional induction of the osteocalcin gene during osteoblast differentiation involves acetylation of histones h3 and h4. *Molecular Endocrinology* **17**, 743-756 (2003).
143 Schroeder, T. M. & Westendorf, J. J. Histone deacetylase inhibitors promote osteoblast maturation. *Journal of Bone and Mineral Research* **20**, 2254-2263 (2005).
144 Zhu, L. & Xu, P.-C. Downregulated LncRNA-ANCR promotes osteoblast differentiation by targeting EZH2 and regulating Runx2 expression. *Biochemical and biophysical research communications* **432**, 612-617 (2013).
145 Schuettengruber, B., Chourrout, D., Vervoort, M., Leblanc, B. & Cavalli, G. Genome regulation by polycomb and trithorax proteins. *Cell* **128**, 735-745 (2007).
146 Vermeulen, M. *et al.* Selective anchoring of TFIID to nucleosomes by trimethylation of histone H3 lysine 4. *Cell* **131**, 58-69 (2007).
147 van Ingen, H. *et al.* Structural insight into the recognition of the H3K4me3 mark by the TFIID subunit TAF3. *Structure* **16**, 1245-1256 (2008).
148 Jiang, H. *et al.* Role for Dpy-30 in ES cell-fate specification by regulation of H3K4 methylation within bivalent domains. *Cell* **144**, 513-525 (2011).
149 Steward, M. M. *et al.* Molecular regulation of H3K4 trimethylation by ASH2L, a shared subunit of MLL complexes. *Nature structural & molecular biology* **13**, 852-854 (2006).
150 Dou, Y. *et al.* Regulation of MLL1 H3K4 methyltransferase activity by its core components. *Nature structural & molecular biology* **13**, 713-719 (2006).
151 Shilatifard, A. The COMPASS family of histone H3K4 methylases: mechanisms of regulation in development and disease pathogenesis. *Annual review of biochemistry* **81**, 65-95 (2012).
152 Thomson, J. P. *et al.* CpG islands influence chromatin structure via the CpG-binding protein Cfp1. *Nature* **464**, 1082-1086 (2010).

153 Eskeland, R. *et al.* Ring1B compacts chromatin structure and represses gene expression independent of histone ubiquitination. *Molecular cell* **38**, 452-464 (2010).
154 Simon, J. A. & Kingston, R. E. Mechanisms of polycomb gene silencing: knowns and unknowns. *Nature reviews Molecular cell biology* **10**, 697-708 (2009).
155 Margueron, R. & Reinberg, D. The Polycomb complex PRC2 and its mark in life. *Nature* **469**, 343-349 (2011).
156 Margueron, R. *et al.* Role of the polycomb protein EED in the propagation of repressive histone marks. *Nature* **461**, 762-767 (2009).
157 Song, J.-J., Garlick, J. D. & Kingston, R. E. Structural basis of histone H4 recognition by p55. *Genes & development* **22**, 1313-1318 (2008).
158 Swigut, T. & Wysocka, J. H3K27 demethylases, at long last. *Cell* **131**, 29-32 (2007).
159 Whetstine, J. R. *et al.* Reversal of histone lysine trimethylation by the JMJD2 family of histone demethylases. *Cell* **125**, 467-481 (2006).
160 Chen, Z. *et al.* Structural insights into histone demethylation by JMJD2 family members. *Cell* **125**, 691-702 (2006).
161 Huang, Y., Fang, J., Bedford, M. T., Zhang, Y. & Xu, R.-M. Recognition of histone H3 lysine-4 methylation by the double tudor domain of JMJD2A. *Science* **312**, 748-751 (2006).
162 Shi, Y. Histone lysine demethylases: emerging roles in development, physiology and disease. *Nature reviews genetics* **8**, 829-833 (2007).
163 De Santa, F. *et al.* The histone H3 lysine-27 demethylase Jmjd3 links inflammation to inhibition of polycomb-mediated gene silencing. *Cell* **130**, 1083-1094 (2007).
164 Lan, F. *et al.* A histone H3 lysine 27 demethylase regulates animal posterior development. *Nature* **449**, 689-694 (2007).
165 Yang, D., Okamura, H., Nakashima, Y. & Haneji, T. Histone demethylase Jmjd3 regulates osteoblast differentiation via transcription factors Runx2 and osterix. *Journal of Biological Chemistry* **288**, 33530-33541 (2013).
166 Zhang, F. *et al.* Histone demethylase JMJD3 is required for osteoblast differentiation in mice. *Scientific reports* **5** (2015).
167 Ohtani, K. *et al.* Jmjd3 controls mesodermal and cardiovascular differentiation of embryonic stem cells. *Circulation research*, CIRCRESAHA. 113.302035 (2013).
168 Burgold, T. *et al.* The histone H3 lysine 27-specific demethylase Jmjd3 is required for neural commitment. *PloS one* **3**, e3034 (2008).
169 Kartikasari, A. E. *et al.* The histone demethylase Jmjd3 sequentially associates with the transcription factors Tbx3 and Eomes to drive endoderm differentiation. *The EMBO journal* **32**, 1393-1408 (2013).
170 Przanowski, P. *et al.* The signal transducers Stat1 and Stat3 and their novel target Jmjd3 drive the expression of inflammatory genes in microglia. *Journal of Molecular Medicine* **92**, 239-254 (2014).
171 Shaw, T. & Martin, P. Epigenetic reprogramming during wound healing: loss of polycomb-mediated silencing may enable upregulation of repair genes. *EMBO reports* **10**, 881-886 (2009).

172 Na, J. *et al.* Histone H3K27 demethylase JMJD3 in cooperation with NF-κB regulates keratinocyte wound healing. *Journal of Investigative Dermatology* **136**, 847-858 (2016).
173 Pereira, F. *et al.* KDM6B/JMJD3 histone demethylase is induced by vitamin D and modulates its effects in colon cancer cells. *Human molecular genetics* **20**, 4655-4665 (2011).
174 Arcipowski, K. M., Martinez, C. A. & Ntziachristos, P. Histone demethylases in physiology and cancer: a tale of two enzymes, JMJD3 and UTX. *Current opinion in genetics & development* **36**, 59-67 (2016).
175 Perrigue, P. M., Najbauer, J. & Barciszewski, J. Histone demethylase JMJD3 at the intersection of cellular senescence and cancer. *Biochimica et Biophysica Acta (BBA)-Reviews on Cancer* **1865**, 237-244 (2016).
176 Ye, L. *et al.* Histone demethylases KDM4B and KDM6B promotes osteogenic differentiation of human MSCs. *Cell stem cell* **11**, 50-61 (2012).
177 Yang, D., Okamura, H., Teramachi, J. & Haneji, T. Histone demethylase Jmjd3 regulates osteoblast apoptosis through targeting anti-apoptotic protein Bcl-2 and pro-apoptotic protein Bim. *Biochimica et Biophysica Acta (BBA)-Molecular Cell Research* **1863**, 650-659 (2016).
178 Murry, C. E., Richard, V. J., Reimer, K. A. & Jennings, R. B. Ischemic preconditioning slows energy metabolism and delays ultrastructural damage during a sustained ischemic episode. *Circulation research* **66**, 913-931 (1990).
179 Shimazu, T. *et al.* Suppression of oxidative stress by β-hydroxybutyrate, an endogenous histone deacetylase inhibitor. *Science* **339**, 211-214 (2013).
180 Chowdhury, R. *et al.* The oncometabolite 2-hydroxyglutarate inhibits histone lysine demethylases. *EMBO reports* **12**, 463-469 (2011).
181 Lu, C. *et al.* IDH mutation impairs histone demethylation and results in a block to cell differentiation. *Nature* **483**, 474-478 (2012).
182 Cha, T.-L. *et al.* Akt-mediated phosphorylation of EZH2 suppresses methylation of lysine 27 in histone H3. *science* **310**, 306-310 (2005).
183 Nacerddine, K. *et al.* Akt-mediated phosphorylation of Bmi1 modulates its oncogenic potential, E3 ligase activity, and DNA damage repair activity in mouse prostate cancer. *The Journal of clinical investigation* **122**, 1920 (2012).
184 Huang, W.-C. & Chen, C.-C. Akt phosphorylation of p300 at Ser-1834 is essential for its histone acetyltransferase and transcriptional activity. *Molecular and cellular biology* **25**, 6592-6602 (2005).
185 Palacios, D. *et al.* TNF/p38α/polycomb signaling to Pax7 locus in satellite cells links inflammation to the epigenetic control of muscle regeneration. *Cell stem cell* **7**, 455-469 (2010).
186 Forcales, S. V. *et al.* Signal-dependent incorporation of MyoD–BAF60c into Brg1-based SWI/SNF chromatin-remodelling complex. *The EMBO journal* **31**, 301-316 (2012).

187 Levy, D. *et al.* Lysine methylation of the NF-κB subunit RelA by SETD6 couples activity of the histone methyltransferase GLP at chromatin to tonic repression of NF-κB signaling. *Nature immunology* **12**, 29 (2011).
188 Baba, A. *et al.* PKA-dependent regulation of the histone lysine demethylase complex PHF2-ARID5B. *Nature cell biology* **13**, 668-675 (2011).
189 Chi, Y. *et al.* Identification of CDK2 substrates in human cell lysates. *Genome biology* **9**, R149 (2008).
190 Wu, S. *et al.* Dynamic regulation of the PR-Set7 histone methyltransferase is required for normal cell cycle progression. *Genes & development* **24**, 2531-2542 (2010).
191 Chen, S. *et al.* Cyclin-dependent kinases regulate epigenetic gene silencing through phosphorylation of EZH2. *Nature cell biology* **12**, 1108-1114 (2010).
192 Liu, W. *et al.* PHF8 mediates histone H4 lysine 20 demethylation events involved in cell cycle progression. *Nature* **466**, 508-512 (2010).
193 Wei, Y. *et al.* CDK1-dependent phosphorylation of EZH2 suppresses methylation of H3K27 and promotes osteogenic differentiation of human mesenchymal stem cells. *Nature cell biology* **13**, 87-94 (2011).
194 Fei, T. *et al.* Genome-wide mapping of SMAD target genes reveals the role of BMP signaling in embryonic stem cell fate determination. *Genome research* **20**, 36-44 (2010).
195 Dahle, O., Kumar, A. & Kuehn, M. R. Nodal signaling recruits the histone demethylase Jmjd3 to counteract polycomb-mediated repression at target genes. *Sci Signal* **3**, ra48 (2010).
196 Estarás, C. *et al.* Genome-wide analysis reveals that Smad3 and JMJD3 HDM co-activate the neural developmental program. *Development* **139**, 2681-2691 (2012).
197 De Santa, F. *et al.* Jmjd3 contributes to the control of gene expression in LPS-activated macrophages. *The EMBO journal* **28**, 3341-3352 (2009).
198 Pereira, F. *et al.* Vitamin D has wide regulatory effects on histone demethylase genes. *Cell cycle* **11**, 1081-1089 (2012).
199 Osawa, Y. *et al.* TNF-α-induced sphingosine 1-phosphate inhibits apoptosis through a phosphatidylinositol 3-kinase/Akt pathway in human hepatocytes. *The Journal of Immunology* **167**, 173-180 (2001).
200 Guo, D., Dunbar, J. D., Yang, C. H., Pfeffer, L. M. & Donner, D. B. Induction of Jak/STAT signaling by activation of the type 1 TNF receptor. *The Journal of Immunology* **160**, 2742-2750 (1998).
201 Gilbert, L. C., Rubin, J. & Nanes, M. S. The p55 TNF receptor mediates TNF inhibition of osteoblast differentiation independently of apoptosis. *American Journal of Physiology-Endocrinology And Metabolism* **288**, E1011-E1018 (2005).
202 Klose, R. J., Kallin, E. M. & Zhang, Y. JmjC-domain-containing proteins and histone demethylation. *Nature Reviews Genetics* **7**, 715-727 (2006).
203 Croonquist, P. A. & Van Ness, B. The polycomb group protein enhancer of zeste homolog 2 (EZH2) is an oncogene that influences myeloma cell growth and the mutant ras phenotype. *Oncogene* **24**, 6269-6280 (2005).

204 Hernando, H. *et al.* EZH2 inhibition blocks multiple myeloma cell growth through upregulation of epithelial tumor suppressor genes. *Molecular cancer therapeutics* **15**, 287-298 (2016).
205 Agarwal, P. *et al.* Genome-wide profiling of histone H3 lysine 27 and lysine 4 trimethylation in multiple myeloma reveals the importance of Polycomb gene targeting and highlights EZH2 as a potential therapeutic target. *Oncotarget* **7**, 6809 (2016).
206 Kawano, M. *et al.* Interleukin-1 beta rather than lymphotoxin as the major bone resorbing activity in human multiple myeloma. *Blood* **73**, 1646-1649 (1989).
207 Moreaux, J. *et al.* BAFF and APRIL protect myeloma cells from apoptosis induced by interleukin 6 deprivation and dexamethasone. *Blood* **103**, 3148-3157 (2004).
208 Alexandrakis, M. G. *et al.* Relationship between circulating BAFF serum levels with proliferating markers in patients with multiple myeloma. *BioMed research international* **2013** (2013).
209 Garrett, I. R. *et al.* Production of lymphotoxin, a bone-resorbing cytokine, by cultured human myeloma cells. *New England Journal of Medicine* **317**, 526-532 (1987).
210 Yu, S. *et al.* The regulation of Jmjd3 upon the expression of NF-κB downstream inflammatory genes in LPS activated vascular endothelial cells. *Biochemical and Biophysical Research Communications* **485**, 62-68 (2017).
211 Bitzer, M. *et al.* A mechanism of suppression of TGF–β/SMAD signaling by NF-κB/RelA. *Genes & development* **14**, 187-197 (2000).
212 Gilbert, L. *et al.* Inhibition of osteoblast differentiation by tumor necrosis factor-alpha. *Endocrinology* **141**, 3956-3964, doi:10.1210/endo.141.11.7739 (2000).
213 Gilbert, L. *et al.* Expression of the osteoblast differentiation factor RUNX2 (Cbfa1/AML3/Pebp2alpha A) is inhibited by tumor necrosis factor-alpha. *The Journal of biological chemistry* **277**, 2695-2701, doi:10.1074/jbc.M106339200 (2002).
214 Kaneki, H. *et al.* Tumor necrosis factor promotes Runx2 degradation through up-regulation of Smurf1 and Smurf2 in osteoblasts. *The Journal of biological chemistry* **281**, 4326-4333, doi:10.1074/jbc.M509430200 (2006).
215 Lu, X. *et al.* Identification of the homeobox protein Prx1 (MHox, Prrx-1) as a regulator of osterix expression and mediator of tumor necrosis factor alpha action in osteoblast differentiation. *Journal of bone and mineral research : the official journal of the American Society for Bone and Mineral Research* **26**, 209-219, doi:10.1002/jbmr.203 (2011).
216 Mukai, T. *et al.* TNF-alpha inhibits BMP-induced osteoblast differentiation through activating SAPK/JNK signaling. *Biochem Biophys Res Commun* **356**, 1004-1010, doi:10.1016/j.bbrc.2007.03.099 (2007).
217 Yamazaki, M. *et al.* Tumor necrosis factor alpha represses bone morphogenetic protein (BMP) signaling by interfering with the DNA binding of Smads through the activation of NF-kappaB. *The Journal of biological chemistry* **284**, 35987-35995, doi:10.1074/jbc.M109.070540 (2009).

218 Lee, H. L. *et al.* Msx2 mediates the inhibitory action of TNF-alpha on osteoblast differentiation. *Experimental & molecular medicine* **42**, 437-445, doi:10.3858/emm.2010.42.6.045 (2010).
219 Osta, B., Benedetti, G. & Miossec, P. Classical and paradoxical effects of TNF-α on bone homeostasis. *Frontiers in immunology* **5** (2014).
220 Kokura, K., Sun, L. & Fang, J. In vitro histone demethylase assays. *Chromatin Protocols*, 109-122 (2015).
221 Zhao, W. *et al.* Jmjd3 inhibits reprogramming by upregulating expression of INK4a/Arf and targeting PHF20 for ubiquitination. *Cell* **152**, 1037-1050 (2013).
222 Méndez-Ferrer, S. *et al.* Mesenchymal and haematopoietic stem cells form a unique bone marrow niche. *nature* **466**, 829-834 (2010).
223 Bianco, P. "Mesenchymal" stem cells. *Annual review of cell and developmental biology* **30**, 677-704 (2014).
224 Houlihan, D. D. *et al.* Isolation of mouse mesenchymal stem cells on the basis of expression of Sca-1 and PDGFR-α. *Nature protocols* **7**, 2103-2111 (2012).
225 Xu, L. *et al.* Cell adhesion molecule CD166 drives malignant progression and osteolytic disease in multiple myeloma. *Cancer research* **76**, 6901-6910 (2016).
226 Kelly, T. K., De Carvalho, D. D. & Jones, P. A. Epigenetic modifications as therapeutic targets. *Nature biotechnology* **28**, 1069-1078 (2010).
227 Silverman, L. R. *et al.* Randomized controlled trial of azacitidine in patients with the myelodysplastic syndrome: a study of the cancer and leukemia group B. *Journal of Clinical oncology* **20**, 2429-2440 (2002).
228 Kantarjian, H. *et al.* Decitabine improves patient outcomes in myelodysplastic syndromes. *Cancer* **106**, 1794-1803 (2006).
229 Kaminskas, E., Farrell, A. T., Wang, Y. C., Sridhara, R. & Pazdur, R. FDA drug approval summary: azacitidine (5-azacytidine, Vidaza) for injectable suspension. *The oncologist* **10**, 176-182, doi:10.1634/theoncologist.10-3-176 (2005).
230 O'Connor, O. A. *et al.* (American Society of Clinical Oncology, 2013).
231 Morschhauser, F. *et al.* (American Society of Clinical Oncology, 2016).
232 Kruidenier, L. *et al.* A selective jumonji H3K27 demethylase inhibitor modulates the proinflammatory macrophage response. *Nature* **488**, 404-408 (2012).
233 Heinemann, B. *et al.* Inhibition of demethylases by GSK-J1/J4. *Nature* **514**, E1-E2 (2014).
234 Rathert, P. *et al.* Protein lysine methyltransferase G9a acts on non-histone targets. *Nature chemical biology* **4**, 344-346 (2008).
235 Pradhan, S., Chin, H. G., Estève, P.-O. & Jacobsen, S. E. SET7/9 mediated methylation of non-histone proteins in mammalian cells. *Epigenetics* **4**, 383-387 (2009).
236 Peng, L. & Seto, E. in *Histone Deacetylases: the Biology and Clinical Implication* 39-56 (Springer, 2011).
237 Miller, S. C. *et al.* Identification of known drugs that act as inhibitors of NF-κB signaling and their mechanism of action. *Biochemical pharmacology* **79**, 1272-1280 (2010).

CURRICULUM VITAE

Wei Zhao

EDUCATION:

2018 Ph.D. Indiana University, Indianapolis, Indiana
Department of Biochemistry and Molecular Biology
Dissertation: Decreased JMJD3 Expression in Mesenchymal Stem Cells Contributes to Long-term Suppression of Osteoblast Differentiation in Multiple Myeloma

2011 B.S. Southern Medical University, Guangzhou, China

RESEARCH EXPERIENCE:

2012-2017 Doctoral Research:
Defining the role of JMJD3 in resolving the bivalent domains at the transcriptional start sites of Runx2 and Osterix, and its contribution to multiple myeloma bone disease

Analyzing by microCT the effect of a novel sequestosome-1/p62 ZZ domain inhibitor XRK3F on bone parameters of multiple myeloma mouse models

Analyzing by microCT the effect of Gal-1 suppression in human myeloma cell lines on the bone parameters of multiple myeloma mouse models

Studying the role of serine 316 phosphorylation of p65 in differential gene regulation

2009-2012 Undergraduate Research:
Identifying HMGA1 as the transcription factor that induces microRNA-137 expression and defining its role as a tumor suppressor in colorectal carcinoma

Examining the expression of DAB2IP in hepatocellular carcinoma and its correlation with prognosis

PUBLICATIONS:

Zhao, W., Marino, S., Adamik, J., Galson, D. L., Roodman, G. D. Decreased JMJD3 Expression in Mesenchymal Stem Cells Contributes to Long-term Suppression of Osteoblast Differentiation in Multiple Myeloma. (Manuscript in preparation)

Storti, P., Marchica, V., Airoldi, I., Donofrio, G., Fiorini, E., Ferri, V., Guasco, D., Todoerti, K., Silbermann, R., Anderson, J. L., **Zhao, W.**, Agnelli, L., Bolzoni, M., Martella, E., Mancini, C., Campanini, N., Noonan, D. M., Petronini, P. G., Neri, A., Aversa, F., Roodman, G. D., Giuliani, N. (2016, December). Galectin-1 Suppression Delineates a New Strategy to Inhibit Myeloma-induced Angiogenesis and Tumoral Growth *in vivo*. *Leukemia*, 30(12): 2351-2363.

Teramachi, J., Silbermann, R., Yang, P., **Zhao, W.**, Mohammad, K. S., Guo, J., Anderson, J. L., Zhou, D., Feng, R., Myint, K. Z., Maertz, N., Beumer, J. H., Eiseman, J. L., Windle, J. J., Xie, X., Roodman, G. D., Kurihara, N. (2016, February). Blocking the ZZ Domain of Sequestosome 1/p62 Suppresses Myeloma Growth and Osteoclast Formation in vitro and Induces Dramatic Bone Formation in Myeloma-bearing Bones *in vivo*. *Leukemia*, 30 (2): 390-8.

Wang, B., Wei, H., Prabhu, L., **Zhao, W.**, Martin, M., Hartley, A. V., Lu, T. (2015, August). Role of Novel Serine 316 Phosphorylation of the p65 Subunit of NF-κB in Differential Gene Regulation. *J Biol Chem*, 290(33): 20336-47.

Liang, L., Li, X., Zhang, X., Lv, Z., He, G., **Zhao, W.**, Ren, X., Li, Y., Bian, X., Liao, W., Liu, W., Yang, G., Ding, Y. (2013, March) MicroRNA-137, an HMGA1 Target, Suppresses Colorectal Cancer Cell Invasion and Metastasis in Mice by Directly Targeting FMNL2. *Gastroenterology*, 144(3): 624-635.

Zhang, X., Li, N., Li, X., **Zhao, W.**, Qiao, Y., Liang, L., Ding, Y. (2012 June). Low Expression of DAB2IP Contributes to Malignant Development and Poor Prognosis in Hepatocellular Carcinoma. *J Gastroenterol Hepatol*, 27(6): 1117-25.

PROFESSIONAL PRESENTATIONS:

Zhao, W., Marino, S., Adamik, J., Galson, D. L., Roodman, G. D. *Decreased JMJD3 Expression in Mesenchymal Stem Cells Contributes to Long-term Suppression of Osteoblast Differentiation in Multiple Myeloma*. Oral and poster presentation at the annual meeting of the American Society for Bone and Mineral Research, Atlanta, GA.

Zhao, W., Marino, S., Adamik, J., Galson, D. L., Roodman, G. D. *Decreased JMJD3 Expression in Mesenchymal Stem Cells Contributes to Long-term Suppression of*

Osteoblast Differentiation in Multiple Myeloma. Oral and poster presentation at the annual meeting of the Cancer and Bone Society, Indianapolis, IN.

RESEARCH BASED SKILLS:

Mammalian Cell Culture
Transient Transfections using siRNA and gene-expressing plasmids
Stable Transfections using lentiviral system
Cloning/Subcloning using PCR
Chromatin Immunoprecipitation
RNA Extraction and qRT-PCR
Protein Extraction and Western blot
MicroCT
ALP, von Kossa and Alizarin Red S staining
MTT Assay
Flow Cytometry
Software: Word, Excel, Powerpoint, Photoshop and Prism